DYNAMIC SOIL WATER REPELLENCY

DYNAMIC SOIL WATER REPELLENCY IN HYDROLOGIC SYSTEMS

By SARAH M.B. BEATTY, M.Sc., B.Sc.

A Thesis Submitted to the School of Graduate Studies in Partial Fulfilment of the Requirements for the Degree Doctor of Philosophy

McMaster University

DOCTOR OF PHILOSOPHY (2016)

McMaster University, Hamilton, Ontario (Earth and Environmental Science)

TITLE: Dynamic soil water repellency in hydrologic systems

AUTHOR: Sarah Beatty, M.Sc. (McMaster University), B.Sc. (Brock University)

SUPERVISOR: Professor James E. Smith

NUMBER OF PAGES: xix, 213 p.

LAY ABSTRACT

Quantifying fluid behaviours in soils is important for a host of environmental, social, and economic reasons. Over the last 25+ years, one soil phenomenon has garnered increased attention because it interferes with our ability to carry out this work. Soils that are or become water repellent develop all over the world and where hydrophobic or non-wetting substances can enter soil and remain in pore spaces or as coatings on particles. To assist in the tracking and management of its complex effects on water storage and infiltration, the goals of this work were to develop fundamental insights into the manifestation and effects of this variable soil property on key hydrologic properties and processes. This work tests a new conceptual model for understanding these systems through both field and laboratory work and using a number of different technologies. These include X-ray microtomography (μXCT), tension infiltrometry, and more regularly applied techniques which are sensitive to changes in repellency. The works shows how combining fractional wettability and contact angle dynamics generates a stereoscopic conceptual framework which facilitates increased capacity for quantifying and understanding of soil systems expressing dynamic soil water repellency.

ABSTRACT

Dynamic soil water repellency is an important soil phenomenon in the vadose zone as it is now recognised that most soils in the world are likely to express some degree of reduced wettability and/or long term hydrophobicity. Fractional wettability and contact angles are, however, rarely discussed or quantified for natural systems. This is particularly the case in the presence of dynamic contact angles. Soil water repellency remains a persistent impediment and challenge to accurate conceptual and numerical models of flow and storage in the vadose zone. This dissertation addresses the opportunity and pressing need for contributions that develop better quantifiable definitions, descriptions, and understanding of soil water repellency. Using materials collected from post wildfire sites, this work employs water and ethanol to identify, isolate, and quantify contact angle dynamics and fractional wettability effects during infiltration. Varied concentrations of water and ethanol solutions were applied to soils and observed through X-ray microtomography, tension infiltration experiments, and moisture content measurements in the laboratory and field. Several analyses from lab and field investigations showed that applications of ethanol and specifically, water-ethanol aqueous solutions provide unique additional insights into proportions of media that remain non-wettable and how those proportions affect overall hydrologic processes, which are not readily observable through water infiltrations alone. Observations include the wetting up of microporous structures, reduced storage, and changes in unsaturated hydraulic conductivities. Challenges which develop as a consequence of variable fluid properties including changes to operational pore assemblages, slow down of wetting fronts, and non-uniqueness relative to infiltration responses are addressed. Important insights and contributions were developed through this approach and water-ethanol mixtures are valuable tools for developing greater quantification and mechanistic data to better inform our models and understanding of dynamic soil water repellency.

Keywords: dynamic soil water repellency, infiltration, sorptivity, ethanol, MED, molarity of ethanol drop, water drop penetration time, water repellency cessation time, time to first bubble, time to first five bubbles, fractional wettability, contact angle, contact angle dynamics, mixed wettability, μXCT, X-ray microtomography, tension infiltrometer

ACKNOWLEDGEMENTS

It is with great enthusiasm that I express thanks to the many people who helped bring this dissertation to fruition. First, I wish to thank my supervisory and comprehensive exam committees (Dr. Sarah Dickson, Dr. Emmanuel Arnaud, Dr. William Morris, and Dr. Altaf Arain) and external reviewer (Dr. Ty P.A. Ferre) for taking part in the development of this work. Their insights, comments, and suggestions have improved this dissertation and their support and guidance over the course of my study have been valued immensely.

The gratitude and respect I have for my supervisor, Dr. James E. Smith, cannot be overstated. He is, without doubt, one of the most supportive and creative individuals I have ever had the experience of knowing and working with. His knowledge, passion, and enthusiasm for hydrology and conducting scientific research is difficult to match and inspiring in countless ways. His humanity, compassion, and respect for the growth of developing scientists (and people in general), are however, I think, some of the things that set him apart as a potent collaborator, teacher, and guide. He has facilitated my development as a scientist in authentic and deeply personal ways and has helped me to see my strengths and grow beyond my limitations. I will forever be grateful for his patience, perspective, and mentorship.

I also wish to thank Dr. Dorthe Wildenschild at Oregon State University who made available the benchtop scanner system (housed at the School of Mechanical, Industrial, and Manufacturing Engineering) and associated technology and knowledges required for the X-ray microtomography portion of this work. Dr. Ryan Armstrong

trained me on all the equipment, reconstruction procedures, and analysis approaches all while nearing the completion of his own PhD. Anna Herring, Liz Harper, and Kendra Brown also helped in presence and made sure I got good data. One of the key observations of long-duration hydrophobicity in the μXCT portion of this dissertation could not have been done without the involvement of the late Chris Johnson. These materials were collected during a field sampling trip that he planned and executed. His curiosity, enthusiasm and willingness to assist this work as an MNR officer in Sudbury is difficult to find in strangers with busy lives and work schedules and I am fortunate for having had a chance to work with him and get to spend field hours him. I am thankful to the Sudbury MNR fire office and his supervisors for helping make that happen.

Colleagues come in all shapes and sizes, but I'm especially grateful for my lady crew of colleagues. Jennie Kirby is a lab tech to top all lab techs. She is an ace and a wonderful person to boot. Alyson Brown, Nagissa Mahmoudi, Lily Demiglio, Jen Hansen, Vicki Tschirhart, and Heather McLeod showed me how necessary and important it is to have women in science. Though conferences, stories, commiserations, questions, music, and late nights, I got to know these women as friends and the powerful scientists that they are.

Financial support is a critical element in generating new science. I am grateful to the R Edward Munn Graduate Scholarship, the Guelph Aquifer Ontario Research Fund Project (PI: Dr. Beth Parker), and NSERC Discovery Grant (PI: James E. Smith) for supporting this research, and especially while environmental science in Canada existed under scientifically hostile (Harper) government policies.

Creative work requires isolation. Fortunately for me, I'm surrounded by a substantial and powerful bunch of individuals who have not only kept loneliness at bay in such a creative pursuit, but watched with enthusiasm and helped me stay tuned into life as it exists outside the academy. It is with great pleasure that I get to give voice to the unsung heroes, anti-heroes, curious observers, and blind believers that have stood by with wonderment, respect and love to watch an initiation adventure and scientific work unfold. These people make up my non-biofamily and they are wild, eccentric, and strong as individuals. They are even stronger and more beautiful as a mass of humanity. They are artists, thinkers, tinkerers, music makers, parents, poets, chefs, scientists, circus performers, songwriters, counselors, world-class-huggers, teachers, radio show hosts, philosophers, engineers, and people who have dedicated their lives to learning, exploration, and new knowledge in their own ways. They are some of the smartest people I know and they teach me so many things about this world. So, thanks to them for being all they are and for the many undocumented ways they brought this dissertation into existence. Special thanks are in order for Roscoe and Marilyn Raby and the Raby's camp gang; Chris Lusty; Shari Dunn, Mary Simon and the Mississippi Bends residency gang; Christine Jackiw; Marianne King-Wilson and the late Dr. Roger Gould; the Balasak's & Theissen's.

My mom and late father nurtured in me a many great things that made this dissertation possible. A deep love of learning, curiosity, tenacity, a healthy work ethic, and a 'success comes in cans' attitude are some of the relevant highlights. My sister Rachel, and brothers John and Lincoln and my aunts, uncles and cousins have shown great pride and enthusiasm for me and this work. Special thanks to my cousin Katharine Beatty, Aunt Angela, and Aunt Bonnie for curious check-ins, question asking, and care packages. I am so fortunate to have the patient love and support my family sends from places near and far away.

TABLE OF CONTENTS

LIST OF FIGURES

LIST OF TABLES

DECLARATION OF ACADEMIC ACHIEVEMENT

This dissertation is comprised of four research papers and has been prepared according to McMaster University guidelines for the preparation of standard theses. Chapters 2, 4, and 5 have been previously published and/or submitted for peer review. Chapter 3 has not been submitted for peer review. This dissertation was completed in close consultation with Dr. James E. Smith who supervised the work contained herein and provided guidance and feedback on project scoping, experimental design, and framing and revision of manuscripts. Dr. Smith also provided lab facilities and technical support during field work and lab work. Contributions made by the dissertation author in relation to each of these articles are outlined below.

Chapter 2

Title: Dynamic soil water repellency and infiltration in post-wildfire soils.

Authors: Sarah M. Beatty and James E. Smith.

Published: (2013) *Geoderma*, 192:160-172.

The small scale conceptual model was conceived and illustrated by S.M. Beatty. The large scale conceptual model was conceived by S.M. Beatty (infiltration relationships, wettable network development and J.E. Smith (moisture content relationships). All graphical illustrations were designed by S.M Beatty and discussion in the manuscript around conceptual models was generated by S.M. Beatty. Column experiments were conceived, designed and apparatus' were built by J.E. Smith and S.M. Beatty in equal measure. S.M. Beatty and J.E. Smith sampled materials in equal measure. All experiments were prepared and conducted by S.M. Beatty with occasional assistance from J.E. Smith. Database development, data management, analysis, and interpretation were performed by S.M. Beatty with input from J.E. Smith. Chapter 2 is an extension of one contribution (of three unique contributions) from the dissertation author's MSc thesis and serves as a conceptual foundation for this dissertation. Figures and portions of text content (in theory, methodology and results sections) draw from work completed for and material presented in the MSc thesis. The peer-reviewed article was prepared by S.M. Beatty during the dissertation author's PhD program and presents new contributions made through a more sophisticated understanding and treatment of data in relation to traditional soil physics/hydrogeology and meaningful points of departure; this having developed after the MSc thesis. Most notably, this paper includes a discussion that generalizes the effects of a number of specific process-oriented implications for sorptivity, unsaturated hydraulic conductivity, and moisture content relationships as defined by dynamically repellent pore relationships.

Chapter 3

Title: X-ray computed tomography of dynamic soil water repellency: opportunities, challenges, and future directions.

Authors: Sarah M. Beatty

Field work and sampling were completed by the dissertation author with assistance from J.E. Smith and (late) Chris Johnson of the Ontario Ministry of Natural Resource fire office in Sudbury. Scans of sampled materials were completed by Sarah Beatty at Oregon State University in the School of Engineering. Scanning equipment was made available by Dorthe Wildenschilde to the dissertation for use. Scans were supervised and training was provided by Ryan Armstrong (primarily), Dorthe Wildenschilde, Anna Herring, Liz Harper. Experiments were designed by the dissertation author with advisement from J.E. Smith and in consideration of insights provided by Dorthe Wildenschilde and Ryan Armstrong on the scanner technology employed. All post-processing and image corrections were performed by the dissertation author in Dr. Wildenschilde's lab and using her facilities. Three-dimensional reconstructions were performed by the dissertation author at McMaster University using J.E. Smith's facilities. All image analysis was performed by the dissertation author. The manuscript and figures were generated by the dissertation author with J.E. Smith providing editorial feedback.

Chapter 4

Title: Infiltration of water and ethanol solutions in water repellent post wildfire soils.

Authors: Sarah M. Beatty and James E. Smith.

Published: (2014) *Journal of Hydrology*, 514: 233-248.

Field experimentation schemes and the MED-derived aqueous solution approach were devised by S.M. Beatty. So too was the time to first five bubbles method. Specific decisions regarding site selection, material selection, and research logistics were also carried out by S.M. Beatty. S.M. Beatty carried out all field experiments and sample collection work with technical assistance from J.E. Smith. Early-late time analysis approaches were designed by S.M. Beatty. S.M. Beatty performed all triangulations, mapping, and geodatabase development / maintenance related to figures drawn in the manuscript. The manuscript was otherwise written, and all figures drawn by S.M Beatty with J.E. Smith providing editorial feedback.

Chapter 5

Title: Dynamic soil water repellency: a primary driver during infiltration.

Authors: Sarah M. Beatty

Laboratory column experiments were designed by S.M. Beatty (materials and fluid combinations) and J.E. Smith (applied pressure steps, impermeable boundary apparatus). Sample and experimental preparation was done by S.M. Beatty and J.E. Smith. S.M. Beatty carried out the experiments and J.E. Smith provided technical support and assistance in the lab and logistics around infiltrometer customization for use with ethanol. S.M. Beatty performed all analyses, generated figures and wrote the manuscript. J.E. Smith provided editorial feedback on the manuscript.

CHAPTER 1 - AN INTRODUCTION TO DYNAMIC SOIL WATER REPELLENCY IN HYDROLOGIC SYSTEMS

1.1 Introduction

1.1.1 Problem Scope

The vadose zone is a critical interface where various physical, chemical and biological processes occur from ground surface to just below the water table. The vadose zone plays many complex hydro/bio/geo/chemical roles including the production of clean water and maintenance of resilient land resources. When it comes to global ecosystem services, these roles have even greater impact as increasing demand and stress is placed on existing land and water resources. Often treated as a ‘black box’ at large (watershed, catchment, aquifer) scales, vadose zone processes are complex and present many challenges in terms of mechanistic understanding. In a physical context, this often results from largely immeasurable pore-scale influences on storage and flux that manifest over larger spatial and temporal scales of social, political, and economic importance. For these reasons, adequately characterising and modelling pore-scale phenomena and their influence on moisture availability, groundwater fluxes, and recharge are powerful in various resource management contexts.

Over the last 20+ years, one soil phenomenon in particular has received increased attention for its ‘interference’ in the accurate quantification, assessment, and prediction of fluid behaviours in porous media. Soil water repellency / hydrophobicity / wettability studies target the origins, influence, and consequences of a reduced affinity for fluids (namely water) to soil surfaces. It has been discussed in the multiphase flow literature for some time, but traditionally regarded as an exceptional or niche topic in the context of soil systems. This, however, is changing as it is becoming more well known that soils all over the world exhibit reduced wettability, long duration hydrophobicity, or dynamic soil water repellency (Doerr et al., 2000). In Australia alone, it is estimated that over 10 million hectares of agricultural land are affected or at risk for developing soil water repellency (Roper et al., 2013).

In the presence of soil water repellency, resistance to wetting develops. This manifests in a variety of ways in a hydrologic context; most notably, infiltration is impeded. For climate sensitive landscapes and ecosystems in particular, this has profound implications on water quality, food production, erosion, and soil degradation. Increased overland flow, increased preferential flow, increased aquifer contamination risk, reduced interception, limited seed germination, and impaired agronomic activity are regularly attributed to soil water repellency effects on infiltration processes in the vadose zone (Roper et al., 2013). Even still, key relationships between soil water repellency and fundamental hydrologic processes are poorly understood as the quantification and comparative assessment of soil water repellency in relation to other mechanistic drivers of infiltration remains a great challenge. Indeed, isolating the effects of soil water repellency in vadose systems is not straightforward.

As a relatively young research subject that spans many geoscience, material science, and biologically-based disciplines, it has become clear that systems expressing reduced wettability present unique challenges for researchers. Many of our existing numerical tools and conceptual approaches are outmatched, having been largely developed for and in relation to fully wettable (idealized) systems. Consequently, there is a substantial need and opportunity for integrated approaches that develop points of connection between existing approaches/understanding and new science knowledge in the hydrologic sciences relative to variable wettability.

1.1.2 Soil water repellency

Soil water repellency is a near surface soil phenomena that develops where hydrophobic compounds are able to enter the soil matrix and remain either as interstitial matter or as coatings on particle surfaces (Bisdom et al., 1993; Franco et al., 1995). The sources of these hydrophobic compounds are generally associated with microbial inputs, interstitial or volatilized organic matter, and contamination sources (Mataix-Solera et al., 2007; Schaumann et al., 2007; Doerr et al., 2000). Different microbial (bacteria and fungi) populations and their repellency characteristics as they relate to in sand dunes, golf greens have been explored by Lichner at al. (2013) among others. Naturally occurring organic sources of repellency are also commonly associated with leaf litter and decomposing nearby plant material (Doerr et al. 2000). In more mineral based substrates, it is well established that Mediterranean climates and coniferous landscapes are particularly suited for expressing repellency given the presence of fatty waxes and oils in plant material which can be integrated through natural soil profile development processes. This can be enhanced during a fire where volatilized waxes and oils in plant material, as hypothesized, move along steep temperature gradients deeper into the soil profile coalescing onto soil particles themselves at depths a few cm from the surface (DeBano et al., 2003). This is not a prerequisite, however, as repellency can be found in organic soils with low mineral content and in the absence of waxy substances as is the case for peats and where under dry conditions, repellency can be expressed well into the soil profile (Doerr et al., 2000). Repellency was found in Dutch sand dunes up to 50 cm by Dekker and Ritsema (1994). Clay soils appear to mitigate the presence of repellency and can be used as a soil amending agent to lessen the effects of repellency. While numerous other environmental factors can variably affect the expression of repellency, these factors alone cannot generate it as a chemical input source is required such that the surface energy of the substrate is sufficiently low compared to the surface tension of water such that water will preferentially bead up vs. spread across a surface (e.g. time, pH, temperature, relative humidity, texture, moisture, fire) (Bisdom et al., 1993; Debano, 2003; MacDonald and Huffman, 2004; Bayer and Schaumann, 2007; Diehl, 2013). Repellency can occur within the top few

At the material scale, as shown in Figure 1.1, hydrophobic and hydrophilic surfaces are defined as having contact angles greater than 90^0 and less than 90^0, respectively. The force balance that arises at the three phase contact between a liquid (water), gas (air), and solid (soil particle) is described in theoretical terms by Young's (1805) equation:

$$\sigma_{LV}\cos(\theta) = \sigma_{SV} - \sigma_{SL} \qquad \text{(eq 1.1)}$$

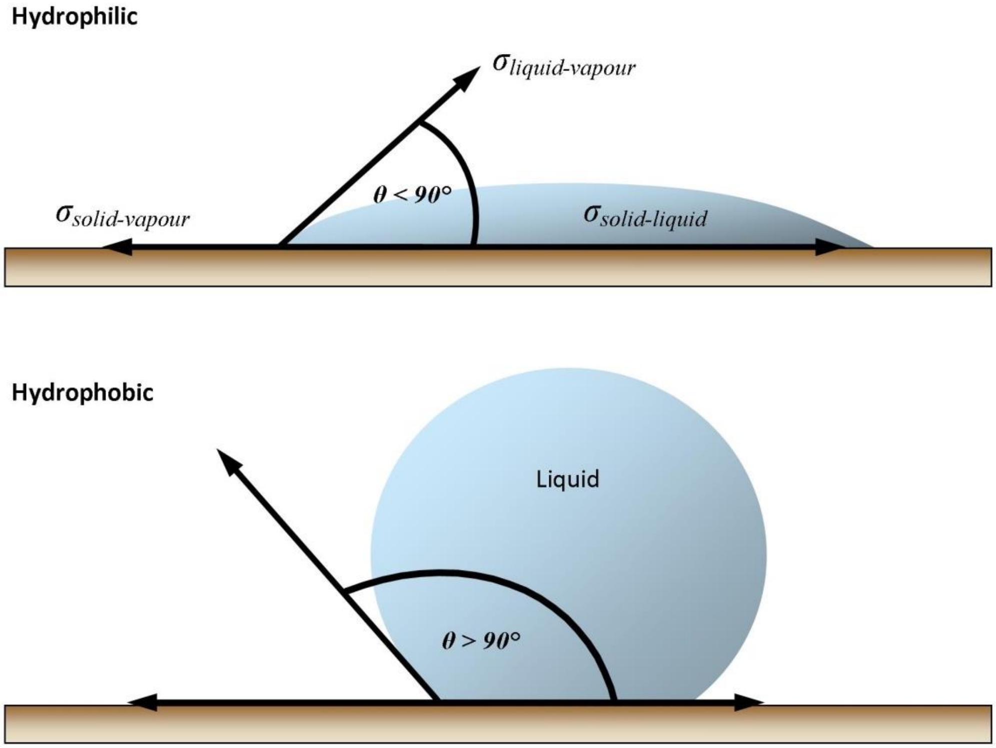

Figure 1.1 Hydrophilic and hydrophobic conceptual diagram describing equation 1.1

The tendency for water to bead up or spread across a material surface is determined by the surface energy of the substrate in relation to the cohesive forces of water (i.e. surface tension) (Douglas et al., 2007; Roy and McGill, 2002). In materials where the surface energy (σ_{SV}) of the substrate is lower than that of water (σ_{LV}), water will not spontaneously spread across the surface. At the molecular level, this is being driven primarily by 1) the spatial arrangement of functional groups and supramolecular makeup of the substrate, and 2) the chemistry of the applied fluid (e.g. water, soil solution, etc.) (Diehl, 2013).

Contact angles are functionally difficult to measure in soils; chiefly because, even in the laboratory, soils do not generally satisfy the conditions of Young's equation (i.e. where surfaces are smooth, flat, rigid, chemically homogeneous, non-reactive and insoluble (de Gennes, 1985), and where fluids are pure and adsorption to the substrate is negligible (Chibowski, 2007)). Consequently, apparent contact angles are often reported. Nevertheless, significant contributions have been made through laboratory studies measuring contact angles through a variety of both static and dynamic measurement techniques to get at this material scale information (Beatty and Smith, 2010; Bachmann et al., 2000; Goebel et al., 2007; Czachor et al., 2010).

Outside of the laboratory, contact angle information is even more challenging to obtain. As a result, secondary measures of repellency / wettability are regularly employed to characterize repellency both quantitatively and qualitatively in systematic ways; the most common approaches are drop penetration tests. Water Drop Penetration Time (WDPT) tests and variable aqueous ethanol solutions as used in Molarity of Ethanol Drop (MED) / Critical Surface Tension (CST) / Aqueous Ethanol Percentage (AEP) tests are regularly reported upon because of their relative simplicity and utility in a variety of applications. Frequent in the literature though they may be, they are able to supply only limited spatial information on wetting in repellent soils.

While accurately quantifying and characterizing repellency at the material scale is fundamental to most studies on hydrophobicity and repellency, studies on the impact of soil water repellency on the landscape and its effects on soil moisture, erosion, degradation, contamination, agronomy, etc. have been critical in advancing the science in an applied context. For example, Ebel and Moody (2013) point out that in post-wildfire environments, water repellent soils can act as near-impermeable surfaces with infiltration rates near zero; they go on to say that this could help explain why catastrophic flooding is a regular occurrence at the first rain following a fire event. Various infiltration- based techniques, both in the laboratory and field, have been useful in showing the complex nature of infiltration in water repellent media and documenting the limitations of these techniques when there is a resistance to wetting. The outcome of that has been an increased widening of measurement and analysis approaches to characterize repellency and its effects on infiltration over a variety of scales. Still, there remain significant gaps in our ability to characterize and understand repellency as a soil phenomenon and its pore to watershed scale impacts on a number of hydrologic variables and processes.

1.1.3 Fractional wettability and contact angle dynamics

Water repellent soils can be comprised of materials that exist over a continuum of possible contact angles. Figure 1.2 was developed based on classifications regularly employed in the multiphase flow literature, which has been instrumental in developing our understanding of wettability and fractional wettability in hydrologic systems. This model of wettability is employed throughout this work and provides a more sophisticated framework for conceptualizing soil water repellency in a range of porous media conditions. While repellent materials can sometimes be considered synonymous with

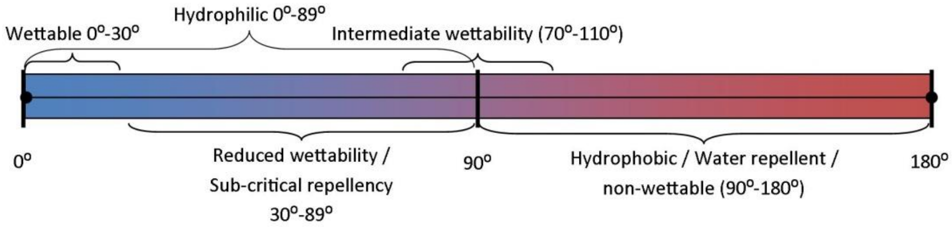

Figure 1.2 Contact angle continuum of wettability / repellency classifications over 180^0

hydrophobicity and wettable materials synonymous with hydrophilicity, much more is happening in water repellent systems than is describable using a hydrophobic / hydrophobic binary conceptualization of repellency based around a singular 90^{o} contact angle threshold. Hydrophobic/hydrophilic language limits our ability to discuss complexity in soil systems.

Fractional wettability, as it is often defined within the multiphase flow literature, is a term that describes a porous media where some portion of the bulk media (i.e. particle surfaces and/or pore spaces) is wettable, and some portion exhibits a resistance to wetting. It describes the spatial heterogeneity of repellency in porous media and is often reported upon using percentages (e.g. 25% hydrophobic + 75% wettable) or proportional representations (e.g. 1:6) in controlled laboratory investigations that use synthetically hydrophobized and homogenized materials (e.g. Bradford et al., 1997; O`Carroll et al., 2005).

In most soils, however, fractional wettability is largely unknown / not well studied or characterized as such. This is problematic, since for most natural soil materials, especially in post-wildfire soils as discussed throughout this work, fractional wettability is likely to be the norm (Beatty and Smith, 2010). Fractional wettability and the spatial heterogeneity in repellency it imposes has far reaching implications on moisture contents, moisture distributions, unsaturated hydraulic conductivities, and various hydrologic and hydrologically-driven environmental processes (e.g. erosion, degradation, aquifer contamination). There is an opportunity and critical need for contributions that serve to better define, describe, and understand fractional wettability in natural porous media.

In addition to expressing variability in contact angles in space, soils can also express contact angle dynamics. The dynamic change of contact angles over time is, indeed, one of the primary mechanisms by which water eventually can enter an initially water repellent pore. The rate at which this occurs is of critical importance and remains challenging to determine. Nevertheless, numerous water repellency studies have documented the dynamic behaviour of water repellent soils through one of the most commonly used tests in water repellency investigations, WDPT tests. This has established the significance of contact angle dynamics in water repellent media and reduced wettability hydrologic processes at the small scale. Still, great unknowns remain around the nature of changes in water repellent soils such as temporal rates of meaningful change (e.g. seconds, minutes, weeks, months, years), what specific drivers cause change at the molecular level, and most importantly in the context of this work, how those dynamic changes are affecting larger scale hydrologic process and parameters as well as when/where they are quantifiable. Admittedly, quantifying dynamic changes is challenging for both intrinsic and extrinsic reasons. Non-uniqueness (multiple parameters inducing similar changes) and a limited conceptual/mathematical understanding of how these hydrologic systems operate and differ in relation to wettable media are major challenges to overcome.

1.1.4 Hydrologic processes in water repellent capillaries

While there is much to be gained in measuring wettability at the material scale in water repellent media, the scale of greatest practical importance in most hydrologic studies on soil water repellency lies at the pore scale. The influence of repellency on moisture distributions and infiltration in unsaturated media is shrouded in non-uniqueness, uncertainty, and complexity. In the presence of water repellent soils, much of that develops out of the violation of two key simplifying assumptions that are regularly employed in hydrologic conceptual (and numerical) models. The Modified Laplace Equation for Capillarity describes the height of rise or the relationship between wettability and fluid pressure in a cylindrical capillary as shown in eq. 1.2,

$$h_p = \frac{2\sigma\cos(\beta)}{r\rho g} \qquad \text{(eq. 1.2)}$$

where h_p is the pressure of the wetting fluid in head units, σ is the interfacial tension of the two fluids (e.g. water and air), β is the contact angle through the wetting fluid, r is the effective physical radius of the pore (with $r/(\cos\beta)$ expressing the effective radius of the air-water interface), ρ is the density of the fluid, and g the gravitational constant (Bear, 1988).

One assumption is designed to generate an understanding of pore size distributions based on fluid pressures. It replaces θ with 0° and is technically only valid in fully (perfectly) wettable, homogenous capillary as represented in Figure 1.3. While replacing the curvature of the interface with an equivalent pore size can be valid in fully wettable homogeneous media, this assumed pore size – pressure head relationship does not hold in many repellent materials. In most repellent soils, contact angles can exist across a range of possible contact angles between 0° and 180^{0} and express fractional wettability.

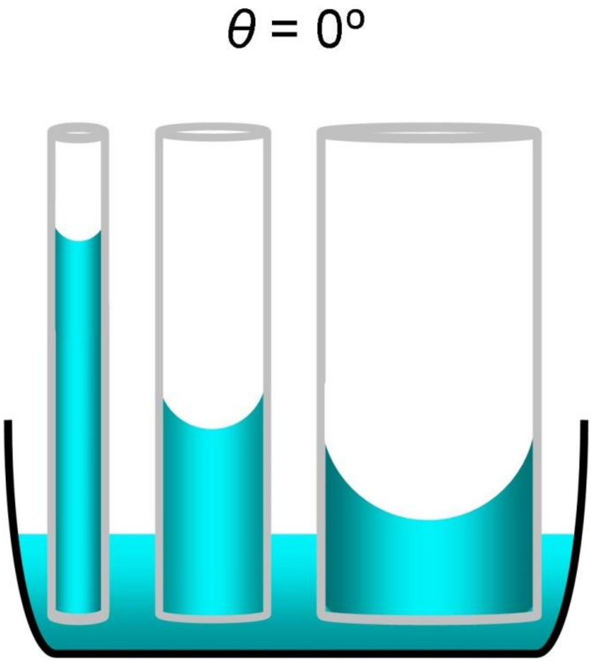

Figure 1.3 Conceptual model: Static, homogeneous wetting in a capillary tube

The second common simplifying assumption is that these contact angles are static. The reality is that contact angles express dynamic/time-dependent behaviours in soils and strongly in water repellent soils over variable time scales that measurement techniques are sometimes unknowably sensitive to. Water repellency is a dynamic phenomenon in a dynamic environment. This means that given pore sizes can exhibit a range of pressures over time, and that at a given pressure, a widening and/or narrowing range of pore sizes may be activated and/or deactivated over time (Figure1.4). Consequently, conceptual and methodological approaches that employ static, homogeneous, and/or wettable contact

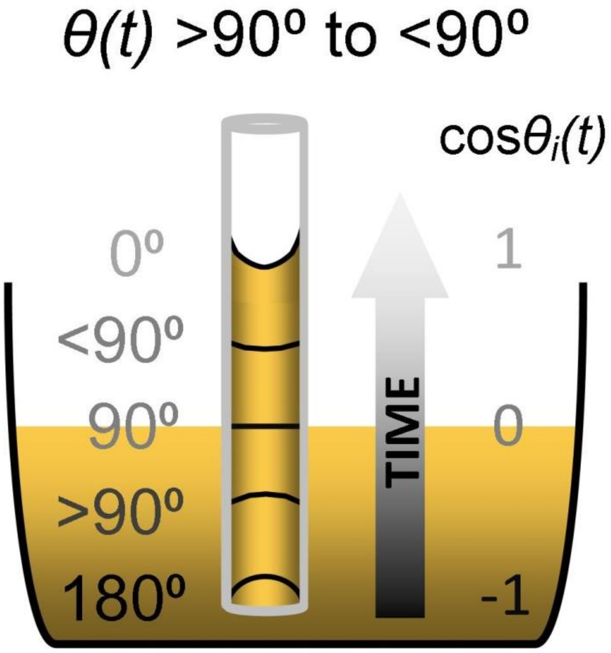

Figure 1.4 Conceptual Model: Dynamic wettability in an initially repellent capillary tube

angle assumptions provide only limited and uncertain insights on storage and conductivity in systems expressing soil water repellency. Indeed, water repellent soils often generate results apparently inconsistent with fundamental theories when such assumptions and approaches are employed. Examples include negative hydraulic conductivities (Moody et al., 2009), distorted capillary pressure – saturation curves (Bauters et al., 2000), curved cumultive infiltration vs. square root of time plots (Wallach and Graber, 2007), and unusually low hydraulic diffusivities (Beatty and Smith, 2010; Wallis and Horne, 1992).

1.2 Research Objectives

Significant opportunities for new insights and knowledge exist at the interface between the multiphase flow literature and the soils literature. To move both these sciences forward and address persisting gaps in our knowledge, this dissertation reports upon an investigation into dynamic soil water repellency through the combined lenses of fractional wettability and contact angle dynamics. This research is aimed at developing insights to understand the contribution of water repellency during infiltration events such that quantifying, assessing, and understanding its overall effect on storage and fluxes can be considered in different kinds of analyses and land resource management applications. While there is some understanding of coarse differences between idealized or characteristic wettable and non-wettable infiltration behaviours, soils exhibiting dynamic soil water repellency generate infiltration behaviours that are not readily explainable using traditional and static soil physics theory concepts. Consequently, this work also aims to develop a stronger mechanistic (conceptual and experimental) framework for understanding systems expressing dynamic soil water repellency that is flexible, robust, and applicable in a range of dynamic soil water repellency scenarios.

1.3 Thesis Overview

This thesis documents new insights on dynamic soil water repellency generated via a combination of field and laboratory experimental work using post-wildfire materials studied and/or sampled in Northern Ontario, Canada. Through a large number of tension infiltration experiments and X-ray microtomography (μXCT), the work employs water and various concentrations of aqueous ethanol solutions to better isolate and contrast the effects of dynamic soil water repellency from wettable hydrologic behaviours. This experimental work is the first to directly assert and show that dynamic contact angles and changes in fractional wettability are primary drivers of infiltration in reduced wettability systems and that measurement techniques which are sensitive to these parameters are the path to a more robust assessment of their combined impact on hydrologic and hydrologic-dependent processes.

Chapter 2 presents a series of laboratory column experiments using variably fractionally wettable and dynamically repellent post-wildfire materials to develop mechanistic understanding of the roles of capillarity and gravity during infiltration. The significant contributions of this chapter are new pore scale and column scale conceptual models that integrate and describe wetting, moisture content relationships, and infiltration behaviours in soils with different levels of fractionally wettability and contact angle dynamics. This lays the conceptual foundation for the thesis.

Chapter 3 presents X-ray microtomographic (μXCT) images and discussion of fractional wettability and dynamic soil water repellency in the context of water and ethanol infiltration. Paired dry/wet scans are analysed qualitatively and are the first to show proof-of-concept information of fractionally wettable/dynamic wetting in natural materials at the pore scale. Here, ethanol, as is commonly used in small scale drop tests and infiltration tests, is first introduced into this work as a means to better understand pore scale behaviours of a fully wetting fluid in relation to non-wetting fluids (i.e. water).

Chapter 4 describes a large number of *in situ* infiltration experiments carried out at a post-wildfire site and presents new insights gained when different concentrations of ethanol are employed during infiltration. It examines how soil wettability is expressed/modified in the presence of different fluid wettabilities over cm scales of infiltration and shows for the first time how variable concentrations of ethanol can be used to systematically draw out fractional wettability information in natural soil materials using tension infiltrometers. It also evaluates the limitations of using tension infiltrometer data to derive unsaturated hydraulic conductivities and sorptivities in dynamically repellent and fractionally wettable soils.

Chapter 5 utilizes tension disc infiltrometry and controlled laboratory column experiments with field sampled homogenized materials in which moisture content and infiltration rates are measured. Through variable concentrations of ethanol, this work shows for the first time how, for dynamically repellent soils, the relationship between moisture content and hydraulic conductivity is far less well related than is commonly conceptualized and discusses opportunities and challenges in using wettable system analogues to generate insights in reduced wettability systems.

Chapter 6 presents overall conclusions and contributions.

References

Bachmann, J., A. Ellies, and K.H. Hartge. 2000. Development and Application of a New Sessile Drop Contact Angle Method to Assess Soil Water Repellency. Journal of Hydrology 231-232:66-75.

Bauters, T.W.J., T.S. Steenhuis, D.A. DiCarlo, J.L. Nieber, L.W. Dekker, C.J. Ritsema, J.-. Parlange and R. Haverkamp. 2000. Physics of water repellent soils. J. Hydrol. 231-232:233-243.

Bayer, J. and G. Schaumann. 2007. Development of Soil Water Repellency in the Course of iIsothermal Drying and Upon pH Changes in Two Urban Soils. Hydrological Processes 21:2266-2275.

Bisdom, E.B.A., Dekker, L.W., Schoute, J.F.T. 1993. Water repellency of sieve fractions from sandy soils and relationships with organic material and soil structure. Geoderma 56:105-118.

Bear, J. 1988. Dynamics of Fluids in Porous Media. American Elsevier Publishing Company, Inc. Mineola, N.Y.

Beatty, S.M., Smith, J.E. 2010. Fractional wettability and contact angle dynamics in burned water repellent soils. J. Hydrol. 391:99-110.

Bradford, S. a., Abriola, L. M., & Leij, F. J. (1997). Wettability effects on two- and three-fluid relative permeabilities. *Journal of Contaminant Hydrology*, *28*(97), 171–191. doi:10.1016/S0169-7722(97)00024-7

Czachor, H., Doerr, S. H., Lichner, L. 2010. Water retention of repellent and subcritical repellent soils: New insights from model and experimental investigations. Journal of Hydrology, 380(1-2), 104–111. doi:10.1016/j.jhydrol.2009.10.027

Chibowski, E. 2007. On Some Relations Between Advancing, Receding and Young's Contact Angles. Advances in Colloid and Interface Science 133:51-59.

DeBano, L.F. 2003. The Role of Fire and Soil Heating on Water Repellency in Wildland Environments: A review. In: Soil Water Repellency: Occurrence, Consequences, and Amelioration. 2003. Eds: C.j. Ritsema and L.W. Dekker. Elsevier. Wageningen, Netherlands.

Dekker, L.W. and C.J. Ritsema. 1994. How water moves in a water repellent sandy soil 1. Potential and actual water repellency. Water Resour. Res. 30:2507-2517.

de Gennes, P.G. 1985. Wetting: Statics and Dynamics. Reviews of Modern Physics 57(3):827-863.

Diehl, D. 2013. Soil water repellency: Dynamics of heterogeneous surfaces. Colloids Surf. Physicochem. Eng. Aspects 432:8-18.

Doerr, S.H., R.A. Shakesby and R.P.D. Walsh. 2000. Soil Water Repellency: Its Causes, Characteristics and Hydro-Geomorphological Significance. Earth-Science Reviews 51:33-65.

Douglas, P., K. Mainwaring, C. Morley and S. Doerr. 2007. The Kinetics and Energetics of Transitions Between Water Repellent and Wettable Soil Conditions: A Linear Free Energy Analysis of the Relationship Between WDPT and MED/CST. Hydrological Processes 21:2248-2254.

Ebel, B. A., & Moody, J. A. 2013. Rethinking infiltration in wildfire-affected soils. Hydrological Processes, 27(10), 1510–1514. doi:10.1002/hyp.9696

Franco, C.M.M., M. E. Tate, Oades, J. M.. 1995. Studies on non-Wetting Sands. I. The Role of Intrinsic Particulate Organic Matter in the development of Water Repellency in non-Wetting Sands. Australian Journal of Soil Research 33:253-263.

Goebel, M., Woche, S.K., Bachmann, J., Lamparter, A., Fischer, W.R.. 2007. Significance of Wettability-Induced Changes in Microscopic Water Distribution for Soil Organic Matter Decomposition. Soil Science Society of America Journal 71:1593-1599.

Lichner, L., Hallett, P.D., Drongova, Z., Czachor, H., Kovacik, L., Mataix-Solera, J., Homolak, M. 2013. Algae influence the hydrophysical parameters of a sandy soil. Catena 108:58-68.

MacDonald, L.H. and Huffman, E. L.. 2004. Post-fire Soil Water Repellency: Persistence and Soil Moisture Thresholds. Soil Science Society of America Journal 68:1729-1734.

Mataix-Solera, J., V. Arcenegui, C. Guerrero, A.M. Mayoral, J. Morales, J. González, F. García-Orenes and I. Gómez. 2007. Water Repellency Under Different Plant Species in a Calcareous Forest Soil in a Semiarid Mediterranean Environment. Hydrological Processes 21:2300-2309.

Moody, J.A., D.A. Kinner and X. Úbeda. 2009. Linking hydraulic properties of fire-affected soils to infiltration and water repellency. J. Hydrol. 379:291-303.

O'Carroll, D. M., Abriola, L. M., Polityka, C. a., Bradford, S. a., & Demond, A. H. (2005). Prediction of two-phase capillary pressure–saturation relationships in fractional wettability systems. *Journal of Contaminant Hydrology*, *77*(4), 247–270. doi:10.1016/j.jconhyd.2005.01.004

Roper, M. M., Ward, P. R., Keulen, a. F., & Hill, J. R. (2013). Under no-tillage and stubble retention, soil water content and crop growth are poorly related to soil water repellency. Soil and Tillage Research, 126, 143–150. doi:10.1016/j.still.2012.09.006

Roy, J.L. and W.B. McGill. 2002. Assessing soil water repellency using the molarity of ethanol droplet (med) test. Soil Sci. 167:83-97.

Schaumann, G., Braun, B., Kirchner, D., Rotard, W., Szewzyk, U., Grohmann, E.. 2007. Influence of Biofilms on the Water Repellency of Urban Soil Samples. Hydrological Processes 21:2276-2284.

Wallach, R. and Graber, E.R. 2007. Infiltration into effluent irrigation-induced repellent soils and the dependence of repellency on ambient relative humidity. Hydrol. Process. 21:2346-2355.

Wallis, M.G., Horne, D.J. 1992. Soil water repellency. Adv. Soil S. 20:91-146.

Young, T. 1805. An Essay on the Cohesion of Fluids. Philosophical Transactions of the Royal Society of London 95:65-87.

CHAPTER 2 - DYNAMIC SOIL WATER REPELLENCY AND INFILTRATION IN POST-WILDFIRE SOILS*

Sarah M. Beatty[a] and James E. Smith[a]

[a] School of Geography and Earth Sciences, McMaster University, 1280 Main St. West.

Hamilton, Ontario, Canada L8S 4L8

*Reproduced with permission from Beatty, S.M and Smith, J.E (2013). Dynamic soil water repellency and infiltration in post-wildfire soils. *Geoderma*, 192: 160-172.

Abstract

The changing nature of soil water repellency and its apparent effect on hydrologic processes in the vadose zone are regularly reported upon, yet the fundamental mechanisms governing these changes over time and how they are manifested during infiltration are poorly understood. To address this knowledge gap, we investigate dynamic soil water repellency and report upon the concerted roles of contact angle dynamics and fractional wettability in post-wildfire materials collected approximately 1.5 years post-fire. A term commonly used in the multiphase flow literature, fractional wettability describes proportional spatial variability in contact angles in bulk media. Twenty two laboratory column experiments were used to measure 1D infiltration rates and moisture contents over time. Tension infiltrometers were used to mechanically maintain a negative pressure throughout water repellent layers. Those data were analysed in conjunction with advancing contact angle data to better understand infiltration processes in these materials and the propensity for them to change with time. The hydrophobic materials expressing low fractional wettability experienced the longest delays in infiltration which we attribute to slow contact angle dynamics. Materials with greater fractional wettability expressed faster rates of contact angle change through much shorter delays in infiltration and unique infiltration rate behaviours. These findings were used to develop a conceptual model that integrates contact angle dynamics and fractional wettability and explains their combined effect on soil-water processes in complex water repellent media.

Keywords: soil water repellence, dynamic, infiltration, contact angle, fractional wettability, wildfire, tension infiltrometer

2.1 Introduction

Soil water repellency is regularly identified as a dynamic soil property (Doerr et al., 2000; Beatty and Smith, 2010; Lamparter et al., 2010) where changes in particular materials can be linked to the origin of hydrophobic substances and the environmental conditions under which they form and exist in the soil (DeBano, 2000; Doerr and Thomas, 2000; Quyum et al., 2002). However, the formative and functional complexities of these systems present unique challenges during hydrologic investigations. For example, most of our understanding of dynamic behaviours in water repellent media has come from the most widely-applied test in water repellency investigations, the Water Drop Penetration Time test (Letey, 2001). While being informative measures for characterization purposes, these small spatial and temporal scale tests have numerous unknowns related to larger temporal and scalar dependencies of water repellency in general (Orfanus et al., 2008), and infiltration processes in particular (Doerr and Thomas, 2000; Cerda and Doerr, 2007). Also impeding our ability to effectively isolate and track the critical mechanisms at play in water repellent media during infiltration is the inability to identify wettable-system analogs that can reflect the complex spatial and/or temporal characteristics of these systems (see, for example, Leighton-Boyce et al. (2007) or Wallach and Graber (2007)). As these systems garner more attention in the literature, what is becoming clear is that (1) a number of interconnected mechanisms are likely to have primary roles during infiltration in water repellent media and (2), the systematic detection and investigation of these mechanisms is difficult. Approaches that more effectively isolate these mechanisms yet preserve sufficient complexity are desirable.

For our purposes herein, we conceptually define a fractionally wettable system as one in which some proportion of the particles or particle surfaces are water wettable (with contact angles < 90°) while the other particles or particle surfaces are water repellent (with contact angles > 90°). Both bulk media and individual pores with greater proportions of wettable surfaces are considered more fractionally wettable than those with fewer wettable surfaces, respectively. Beatty and Smith (2010) observed that statistical variability in contact angle measures provides useful indications of the relative wettability of materials, with more fractionally wettable materials tending to express larger ranges and variances. A definition based on a theoretical 90° threshold, however, only holds rigorously for infiltration into cylindrical capillaries. In porous media, the interaction between contact angles and complex pore geometries result in lower required contact angles before spontaneous infiltration occurs (Czachor et al., 2010).

To evaluate the effect of fractional wettability, more reductionist approaches often simplify air-water multiphase flow systems by using various fractions of synthetically hydrophobized sands in ponded infiltration experiments (e.g. Bauters et al., 2000; Carrillo et al., 2000; Feng et al., 2001). While synthetic systems are useful in providing information related to the effects of static fractional wettability, forced imbibition or infiltration under a positive applied water pressure is largely controlled by the magnitude of water pressure applied, and not by the system's changing properties. Consequently, such tests are unable to inform us on temporal changes in water repellency and fractional wettability (Bauters et al., 2000; Feng et al., 2001). Alternatively, tension infiltrometers or tension disc permeameters are being more seriously considered as a means to observe hydraulic properties or time dependent changes in naturally water repellent materials (e.g. Tillman et al., 1989; Clothier et al., 2000; Doerr and Thomas, 2000; Hallet et al., 2004; Bens et al., 2007; Lichner et al., 2007; Lewis et al., 2008). In contrast to ponded infiltration techniques, tension infiltrometers facilitate more direct observations of time dependent changes in repellency since pore water pressures need to be or become negative before infiltration occurs. Given that repellent materials are regularly characterized by initial positive pore water pressures and air-entry pressures, changes in the rate of discharge from tension infiltration instruments express and can provide useful indications of contact angle change and associated changes in fractional wettability as time of exposure to water increases.

In this paper we report upon the concerted roles of contact angle dynamics and fractional wettability during bulk-scale (cm) infiltration in post-wildfire materials using infiltration experiments and a conceptual model. These post-fire materials exhibited dynamic changes in repellency at the material (mm) scale in earlier work (see Beatty and Smith, 2010) and are evaluated here through the use of tension infiltrometers that maintained a negative pressure head through water repellent layers. We hypothesised that maintaining a constant small negative pressure at the surface of dynamically repellent materials would generate more informative data and provide better insight into the controls and processes governing infiltration behaviour in complex systems. Specifically, we hypothesised that infiltration rates would be notably sensitive to changes in fractionally wettable materials through the associated changes in unsaturated hydraulic conductivies. We also hypothesised that higher contact angle materials found beneath surface wettable materials (as reported in Beatty and Smith (2010)) would have longer transitions between non-wetting and wetting angles and experience slower changes in infiltration rate behaviours than lower initial contact angle materials that exhibited more consistently hydrophobic contact angles at the surface and near-surface. This is consistent with the simplifying assumption that the *rates* of contact angle change for all non-wetting materials investigated would be similar and act independently of fractional wettability. Our final analysis examines the effect of both *a priori* material characteristics (initial fractional wettability) and temporal dependencies (contact angle dynamics) in relation to real time *in situ* moisture content information collected during experiments via moisture sensors. Through this integrated approach, we not only shed light on important and complex infiltration behaviours in repellent materials, but also reveal an interdependency of contact angle dynamics and fractional wettability, which we suspect is a primary control of soil water behaviour in such systems.

2.2 Theory and small scale conceptual model

In any pore space, the tendency to imbibe water is determined by the pore water pressure and can be defined by the Young-Laplace equation for capillary pressure. Expressed in water pressure head units using (Bear, 1972):

$$h_p = \frac{-2\sigma \cos\theta}{r\rho g} \quad \text{(eq. 2.1)}$$

h_p is the water pressure head in the pores, σ is the air-water surface tension , θ is the effective water-solid contact angle (as measured through the water phase), r is the effective radius of the pore at the location of the air-water interface, ρ is water density, and g is the gravitational constant. While this relationship is unable to accurately express larger scale and complex phenomena such as flow through tortuous and/or fractionally wettable pore spaces (Czachor et al., 2010), microscopic relationships provide a useful starting point / benchmark for our understanding (Letey, 2001; Bachmann et al., 2007).

According to Eq. 2.1, for systems where the wetting fluid experiences no changes in surface tension, water pressure head is determined by the pore radius and the contact angle between the porous media and two immiscible fluids (i.e. water and air). In a completely hydrophilic (homogeneous) soil where there is no resistance to wetting (i.e. all particle surface contact angles are 0°), water supplied at the surface under a small negative constant pressure head will spontaneously infiltrate due to the capillary component of the hydraulic gradient. Pores will preferentially fill according to size, such that all pores smaller than those in equilibrium with the applied pressure will fill with water. This concept is well documented and long established within the literature. For homogeneous, *non-wettable* materials where contact angles are greater than 90° (i.e. $\cos(\theta) < 0$), the tendency will be to resist infiltration or repel water by the same relative magnitudes.

Because of this fundamental relationship, the tendency in water repellency literature has been to attribute the majority of flow in water repellent systems to the weakest capillaries: large pores (e.g. Bauters et al., 2000; Carrillo et al., 2000; Feng et al., 2001). While this may be true in static and homogeneous scenarios, it is prudent to question the validity of this assumed wettability-pore size distribution relationship in the presence of dynamic contact angles and fractionally wettable media. It is important to consider that any and all size pores, depending on their wettability, may or may not contain water at any given pressure. Specifically, the convention in static homogeneous porous media of replacing the curvature of the air-water interface with $r/(\cos\theta)$ and extending that simply by conceptualising a water pressure as an associated pore size lacks sufficient utility in these more complex wetting / non-wetting scenarios and can literally be an obstacle to fuller understanding.

To illustrate this disconnection between pore-size and water pressure, Figure 2.1 depicts two contrasting *fractional wettability* scenarios subject to contact angle dynamics and their related implications on infiltration processes at the pore scale. It is our view that fractional wettability and contact angle dynamics work in concert with one another and are the norm in water repellent media. We assert that this union of ideas is the key to a better understanding of these complex hydrologic systems.

Consider a pore that is bordered by both wettable (<90°) and non-wettable soil particles (>90°) where each soil particle has a singular surface chemistry and value of contact angle that is either wetting or non-wetting prior to the introduction of water, and the pore space contained within is dry. Upon the introduction of water supplied at a small negative pressure head, one of two spontaneous things will occur. If the wettable fraction is playing a dominant role (WD – left side in Figure 2.1), water will enter the pore (WD-

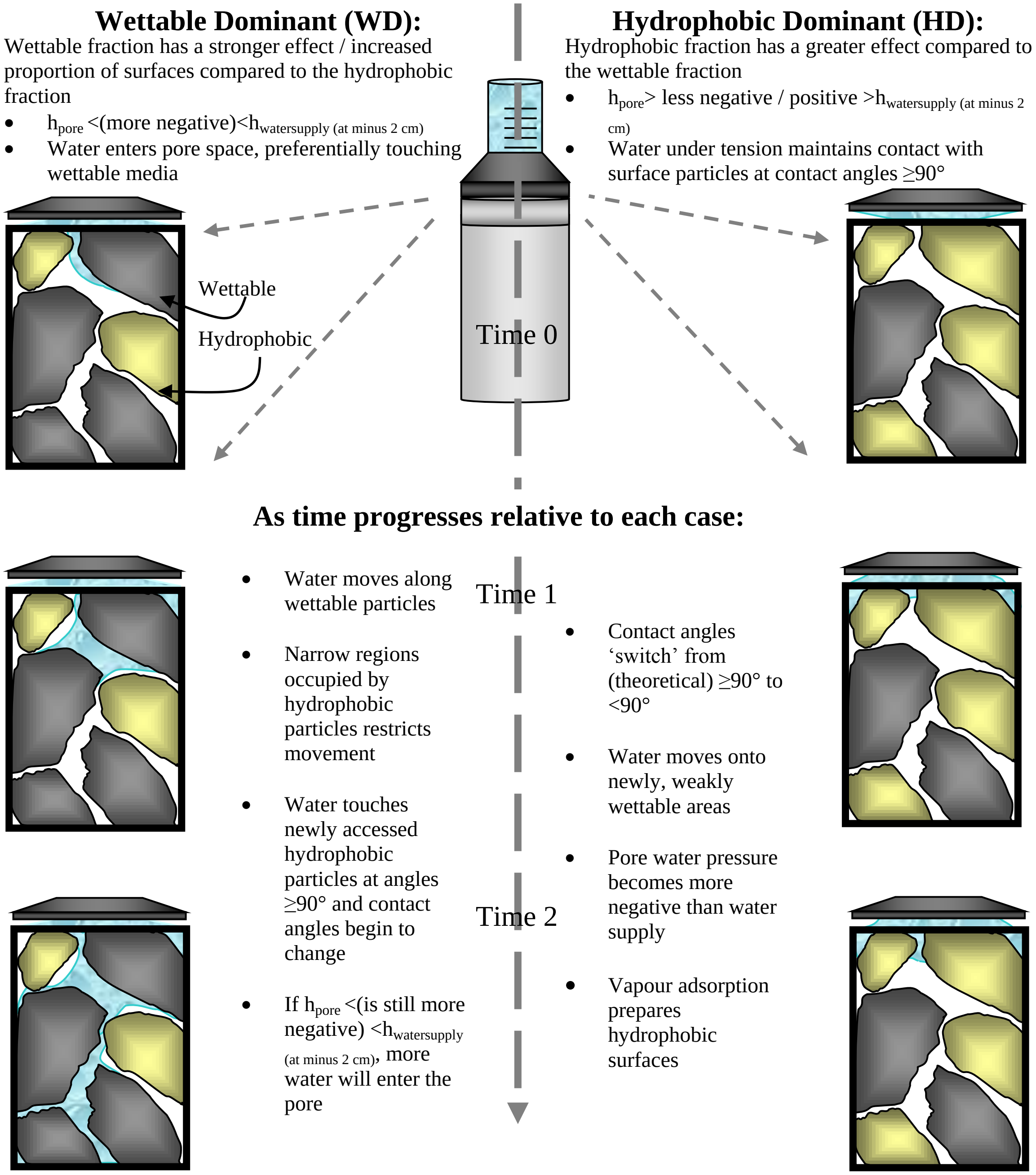

Wettable Dominant (WD):
Wettable fraction has a stronger effect / increased proportion of surfaces compared to the hydrophobic fraction

- h_{pore} <(more negative)< $h_{watersupply\ (at\ minus\ 2\ cm)}$
- Water enters pore space, preferentially touching wettable media

Hydrophobic Dominant (HD):
Hydrophobic fraction has a greater effect compared to the wettable fraction

- h_{pore}> less negative / positive >$h_{watersupply\ (at\ minus\ 2\ cm)}$
- Water under tension maintains contact with surface particles at contact angles ≥90°

As time progresses relative to each case:

- Water moves along wettable particles
- Narrow regions occupied by hydrophobic particles restricts movement
- Water touches newly accessed hydrophobic particles at angles ≥90° and contact angles begin to change
- If h_{pore} <(is still more negative) <$h_{watersupply\ (at\ minus\ 2\ cm)}$, more water will enter the pore

- Contact angles 'switch' from (theoretical) ≥90° to <90°
- Water moves onto newly, weakly wettable areas
- Pore water pressure becomes more negative than water supply
- Vapour adsorption prepares hydrophobic surfaces

Figure 2.1 Pore scale schematic of infiltration into two contrasting fractional wettability scenarios.

Time 0). Conversely, if the non-wettable fraction is playing a dominant role (HD – right side in Figure 2.1), water will *not* enter the pore, but will maintain contact with surface materials at some contact angle greater than (theoretically) 90° (Letey, 2001).

Under a spontaneous wetting condition (WD), water entering the pore will preferentially adsorb to wettable particles and remain in narrower regions until the pore water pressure is at equilibrium with the supply pressure. This is consistent with traditional theory describing the distribution of wetting fluids in variable pore spaces. However, non-wetting particles bordering the pore can contribute to an increased resistance to wetting overall (i.e. a less negative pore pressure head); particularly so if non-wetting particles border regions where water has the greatest tendency to situate. The presence of non-wettable pore walls may even result in larger physical regions of the pore filling prior to narrow regions (WD-Time 1). While water may only be adsorbed to wettable materials initially, as time progresses and the pore continues to fill (WD-Time 2), water will begin to contact the non-wetting fraction of particles at some angle between 90° and 180°. This physical contact provides a means by which contact angle dynamics can now readily take place. Flow of water *between* fractionally wettable pores will also be governed by these same conditions (WD – Time 2).

In contrast, for initially non-wetting pores with a sufficiently large proportion of non-wettable pore walls (HD), increased exposure of water repellent materials to water held at the surface is likely to contribute to conformational changes as described by Bayer and Schaumann (2007) and eventual changes in contact angle with time (Rodríguez-Valverde et al., 2002; Diehl and Schaumann, 2007). The initial contact angle and its rate of change are largely dependent on the origin of non-wettable materials and the resistance of surface chemistries and physical properties to surface energy changes with increased exposure to water (Diehl and Schaumann, 2007). While water may not enter the pore for some time, changes in contact angle will occur as time of contact with water increases for these surface materials (HD – Time 0). Only once initially non-wetting surface materials become wettable and/or the surface tension of the infiltrating fluid decreases substantially, will water begin to enter the initially hydrophobic pore (HD – Time 1). That is to say, when water is *not* being forced into this media through the application of positive pressures, the tendency to fill a water repellent pore (at any particular point in space) will be governed *first* by (dynamic) wettability and orientation of surfaces and secondarily by pore size. In terms of storage in dynamically repellent materials, this means that under a given moisture content, not only can particular pore pressures be represented in a widening and/or narrowing range of pore sizes (at any particular time), but also that particular pore sizes may exhibit a large and variable range of pore water pressures over time. This could help to explain why multiple and highly complex water repellency – moisture content relationships exist in the literature (e.g. see, for example, Taumer et al., 2005; Bayer and Schaumann, 2007; Verheijen and Cammeraat, 2007), and why water repellency investigations that employ conventional techniques based on static, idealized, hydrophilic pore sizes often produce results apparently markedly inconsistent with fundamental theories. Examples include negative hydraulic conductivity (K) values (Moody et al., 2009), heavily skewed or distorted CPS curves (Bauters et al., 2000), curved cumulative infiltration vs. square root of time plots (Wallach and Graber, 2007), and diffusivities much lower than wettable counterparts (Wallis and Horne, 1992). We suspect that these inconsistencies arise due to highly variable pores scale wettability dynamics throughout the medium which impede/delay the development of connected films and interconnected pathways between pore bodies. Consequently, until pore throat displacement pressures are exceeded by positive local water pressures or local contact angles become wettable, both large and small pores may remain unable to transmit water and participate in increases in K in ways as anticipated in wettable systems under similar increases in moisture content. That is, unsaturated hydraulic conductivity may have a substantially weaker relation to water content in dynamic fractionally wettable media than commonly conceptualised.

2.3 Material and Methods

Twenty-two 1D (vertical) tension infiltration tests were carried out using fire affected materials collected from Halfway Lake Provincial Park 1.5 - 2 years post-fire. All experiments tested layered systems consisting of a wettable, loam textured, mineral B Horizon soil overlain by subsampled intact duff-layer organic materials with different repellency characteristics. The mineral soil collected from the site was a Podzolic B horizon, the colour of which was consistent with iron enrichment; for further site/fire details we refer the reader to Beatty and Smith (2010). Replicate tests used two experimental column set ups: non-instrumented and instrumented with moisture sensors (Figure 2.2). For all tests, tension infiltrometers (filled to capacity with deionized water) were used as constant head devices to maintain a small, negative pressure head condition throughout water repellent layers. This experimental design was favoured over positive

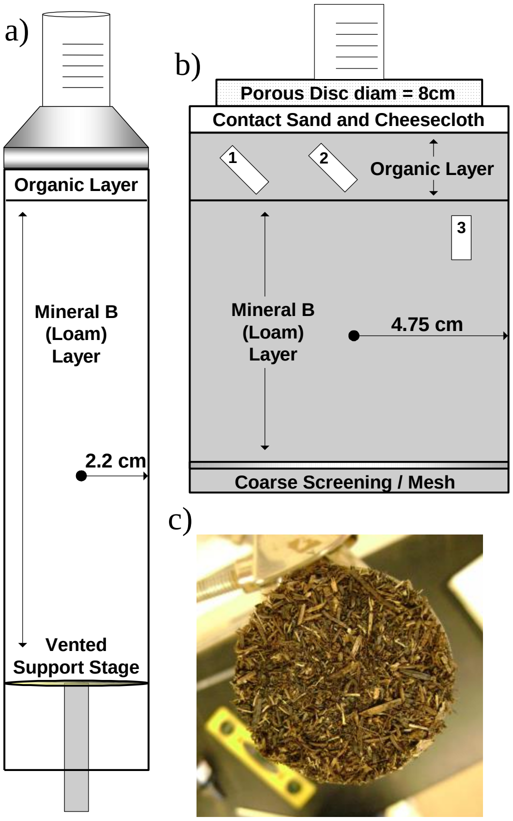

Figure 2.2 a) Experimental apparatus for non-instrumented test b) set-up for instrumented tests showing moisture sensor insertion locations and orientation (1, 2, and 3). Moisture sensors were inserted approximately normal to the curvature of the column wall towards the centre of the cross-sectional area, c) top-view example of subsampled Brown organic materials fitted to non-instrumented infiltration column (4.8 cm across).

pressure tests as it would remove the influence of macropore related flow phenomena resulting from topographic differences and/or pressure build up in water repellent layers. This provided the means to identify / measure changing hydrophobic behaviour (i.e. from non-wetting to wetting) using time of exposure to water as a key determinant of overall system behaviour. It was *not* our intent to measure hydraulic conductivity, matric flux potential, or sorptivity using soil water infiltration theories commonly applied and appropriate for hydrophilic soils.

All columns were packed similar to / based on the specific material configurations and orientation of materials in the field. For all experiments, air-dried mineral soil was first packed via a continuous pour method to field comparable bulk densities (i.e. 1.1g/cm^3 average bulk density (range: 1.0-1.2 g/cm^3)). Before use, this B Horizon soil material was prepared by removing cobbles and stones by hand. Peds and small cohesive units in the remaining material were broken up by hand and passed through a 2mm mesh (U.S.A. Standard stainless steel sieve, A.S.T.M. E-11 Specifications). The < 2mm sieve fraction was mixed and split (Versa-Splitter, model no. SP-2.5, Gilson Co., Inc. Worthington, OH) to avoid particle / sample bias. Textural properties of B horizon material were analysed using the mechanical sieving technique outlined in Carter (1993) and found to belong to the Loam textural classification. All the mineral B horizon material was hydrophilic in WDPT tests (<5s to drop disappearance). The thickness of this layer varied (i.e. 9.5 – 25cm) by design depending on the water repellency of the overlying organic material to ensure that, in all cases, wetting fronts never reached the bottom of the column. Newly subsampled materials were used for each test; no materials were re-used.

Subsequent to the packing of mineral B materials in the column, organic duff layers of similar origin, but variable burn conditions were packed and/or placed above. This resulted in four testing (layer) configurations: Mineral only (MO), Char over mineral (COM), Brown over mineral (BOM), Mixed over mineral (MOM). Material properties and repellency characteristics for these configurations appear in Table 2.1 and Table 2.2. Mineral only tests consisted only of a layer of the Podzolic B horizon material. For Mineral Only column experiments, soil at the top of each of the columns was levelled approximately 1mm above the surface of the apparatus to ensure good contact of the infiltrometer disc to the surface of the mineral soil throughout the test. Char materials (used in COM tests) were scraped from the soil surface *in situ* as composite samples*;* they showed significant signs of consumption by fire. To prepare for infiltration tests, these materials were packed into stainless-steel rings the same diameter as the column apparatus and then allowed to air-dry. Brown materials (used in BOM tests) showed minimal signs of surface scorching and no present evidence of char at the surface 1.5 years post-fire. They were sampled in the field in larger 30cm x 30cm slabs to maintain their natural integrity and structure. For use in column experiments, these materials were subsampled using a stainless steel insertion ring with a bevelled edge and cut with a box-cutter blade to maintain the internal structure of the material. The subsampled organic “puck” was then weighed and placed on top of the mineral–packed column; additional

Table 2.1 Material properties and repellency characteristics for non-instrumented tests.

Material Configuration	Organic layer thickness as tested in non-instrumented columns	Organic layer bulk density (g/cm^3)	Mineral layer bulk density (g/cm^3)	Binary drop test at surface/2 cm depth[a]	Representative advancing contact angles[a] 0 cm depth (mean°/std.dev)	2 cm depth (mean°/ std.dev)
Mineral Only (MO)	0 cm	n/a	1.0-1.2	wettable/wettable	n/a	n/a
Char over Mineral (COM)	1.0 - 1.1 cm	0.23-0.28	1.0-1.2	wettable/wettable	79°/10.13	n/a
Mixed over Mineral (MOM)	1.3 - 1.7 cm	0.19-0.25	1.0-1.1	wettable/non-wettable	77°/13.65	113°/5.95
Brown over Mineral (BOM)	1.2 - 1.6 cm	0.14-0.20	1.1-1.2	non-wettable/non-wettable	96°/12.11	105°/6.90

[a] Data from drop tests and/or contact angle measures of Char, Mixed, and Brown materials in earlier work (Beatty and Smith, 2010).

Table 2.2 Experimental conditions and material properties of instrumented tests.

Instrumented Test ID	Symbol	Organic layer thickness as tested in instrumented columns (cm)	Organic layer bulk density (g/cm^3)	Mineral layer bulk density (g/cm^3)	Pressure at organic surface (cm)	Calculated pressure at organic-mineral interface (cm)	Sensor Location Codes[a] (see Figure 2b) 1	2	3
INST-1 (Mixed over Mineral (MOM))	+	3.5	0.16	1.05	-4.0	-0.5	OM-17	OM-20	MIN-40
INST-2 (Mixed over Mineral (MOM))	~~x~~	3.3	0.18	1.05	-3.9	-0.6	OM-P3	OM-P4	MIN-40

[a] OM-17 and OM-20 are positioned 1.7cm and 2.0cm below the top of the column / organic surface, respectively. OM-P3 and OM-P4 are both positioned 1.3cm below the top of the column / organic surface. MIN-40 is positioned 0.5cm below the organic-mineral interface in both INST-1 and INST-2.

gentle force was applied at the organic surface to ensure good contact at the organic-mineral interface across the diameter of columns. Mixed materials (used in MOM tests) were more complex materials that exhibited characteristics of each of the previously mentioned materials, i.e. having visible signs of burning / charring in the top ≤0.5cm with Brown material characteristics below. These were field-sampled in large, structurally preserved blocks and subsampled and prepared for use in column experiments similarly to Brown materials.

In all tests, the infiltrometer was secured with sufficient force to ensure good secure contact across the disc diameter. The resultant compression of the organic surface was between 0.1 and 0.5cm for all tests. Infiltrometers were checked / adjusted during tests to ensure good contact with the surface. Tests were conducted until the entire infiltrometer was emptied (approx. 85ml in non-instrumented tests and 300ml in instrumented tests), and during which time water volume information was continually collected. Upon completion, columns were immediately turned horizontal and sectioned at 2cm intervals via a combination of excavation and extrusion. The post-infiltration material collection process lasted between three and five minutes. Following excavation / extrusion, samples were then weighed and dried to constant weight in a 40-60 °C oven to avoid any burning off of organic materials. Weights were used in conjunction with bulk densities to construct end-of-test volumetric moisture content profiles.

2.3.1 Non-Instrumented Columns

In non-instrumented tests, a Mini Disk Infiltrometer (Decagon Devices, Pullman, WA) was used with an applied pressure head of -2cm. The thickness of the organic pucks used in these tests was variable (see Table 2.1), and as such, would result in small differences in the (tension) boundary condition at the mineral-organic interface. However, assuming the extreme situation of static equilibrium conditions, because organic layers in the non-instrumented column experiments were less than 2cm thick, a negative pressure head condition existed throughout the organic layers and at the organic-mineral boundary at all times. Twenty of 22 total experiments were conducted using this set-up.

2.3.2 Instrumented Columns

The only meaningful difference between the instrumented and non-instrumented column designs is the inclusion of 5cm long moisture sensor blades (model: ECH$_2$0 EC-5 Moisture Sensors, Decagon Devices, Pullman, WA), which necessitated the use of thicker organic “pucks”, a larger-diameter (9.5 cm diameter) column, and a larger tension infiltrometer (8cm diameter porous disc, Soil Measurement Systems, U.S. patent no. 4884436) in instrumented tests. Tensions and other details of the experimental conditions of the instrumented tests appear in Table 2.2. For the instrumented experiments, moisture content data were collected over one minute intervals which were then automatically averaged and stored in a data logger (model: Em 5b, Decagon Devices, Pullman, WA). Consistent with recommendations of the manufacturer (Cobos, 2009), the moisture probes were specifically calibrated for each of our experiments *in situ* using measured initial and final (post-infiltration) volumetric moisture contents in the column. In addition, to ensure good hydraulic connection with the soil surface, this set-up incorporated a poured layer (approx. 1.2 cm) of contact sand (Ricci Brothers: 56-3-10) over draped cheesecloth (Reynolds, 2006; Soil Measurement Systems, 2006).

Two of 22 total experiments were conducted using this larger column and infiltrometer set-up. Only Mixed material pucks were used in instrumented tests. Charring at the surface of Mixed materials used in the first instrumented experiment (Inst-1) was significantly less than the approximately 0.5cm wettable char layer present in the second instrumented experiment (Inst-2). Similar to non-instrumented tests, the pressure head throughout the duff (organic) materials was mechanically maintained under tension according to the assigned values of the infiltrometer disc. Tensions for each of these instrumented experiments were calculated based on a static equilibrium assumption – which places an upper boundary on the possible strength of the tensions. This resulted in applied tensions more negative than the sum of the: 1) thicknesses of the contact sand (~1cm) and 2) the organic layer (~3 cm), i.e. applied tension = thickness of contact sand + thickness of organic layer + <1cm. This ensured that no ponding would occur.

Prior to experimentation, the amount of water necessary to saturate the cheesecloth and contact sand was determined (approx. 30ml). The sand contact layer was fitted to the diameter of the column (9.5 cm) and not the diameter of the porous disc (8cm). While this would result in a small amount of divergent flow in the contact layer, it would be limited to a fraction of the time required to fill the contact sand layer with water (< 15 seconds).

2.4 Results and Discussion

2.4.1 Cumulative Infiltration

Cumulative Infiltration for Mineral Only (MO), Char over Mineral (COM), Mixed over Mineral (MOM) and Brown over Mineral (BOM) tests are expressed in two related ways in Figure 2.3: a) vs. time$^{1/2}$ and b) vs. time. Mineral Only tests provide a valuable reference case respective of the other material configuration tests; these replicates exhibit classic hydrophilic infiltration. Char over Mineral columns have a slight increase in overall infiltration such that tests tend to reach 5cm of cumulative infiltration a few minutes before the majority of Mineral Only columns, however the overall behaviour is consistent with hydrophilic infiltration. Mixed over Mineral data exhibit a general convex shape, i.e. a trend to increasing slope with time under the same constant tension used in the MO and COM tests. Brown over Mineral data exhibit significant and long delays in infiltration not observed in any of the other tests. Two of the five replicates reached 4cm of cumulative infiltration before 12 min$^{1/2}$ (~140 minutes) and appear to behave similarly to MOM tests, while the three other replicates did not reach 4cm until after 20 min$^{1/2}$ (~400 minutes). Both the Mixed material and the Brown material tests exhibit convex cumulative infiltration (vs. time$^{1/2}$). Since the thickness of the hydrophobic layers were less than the magnitude of the applied tensions (see Table 2.1 and 2.2), we attribute this behaviour to hydrophobicity in materials and their expression of dynamic wettability (contact angle dynamics). Similar convex infiltration behaviours have been observed elsewhere (e.g. Wallach and Graber, 2007), having been attributed to positive pressure build-up in the wetting front, which as stated above, is not a condition that exists within

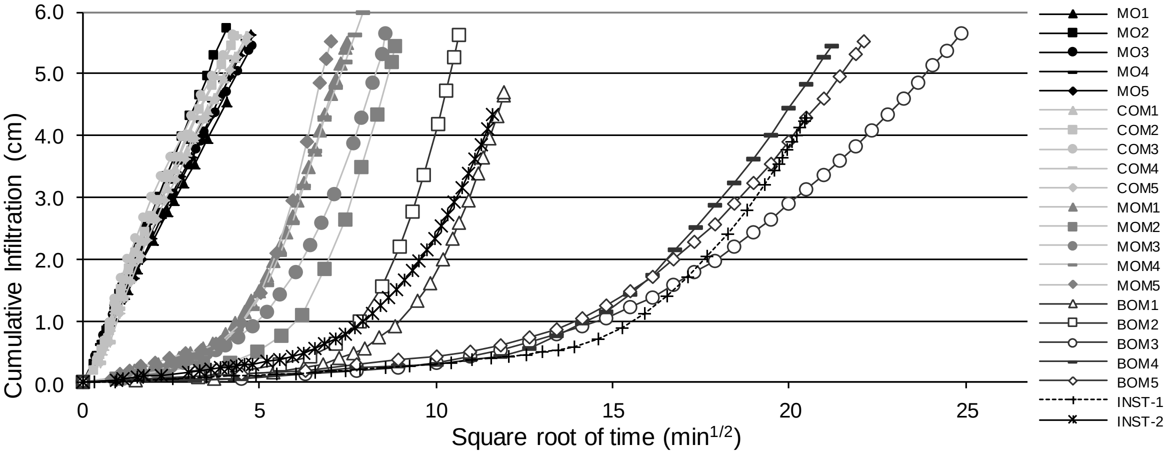

(a)

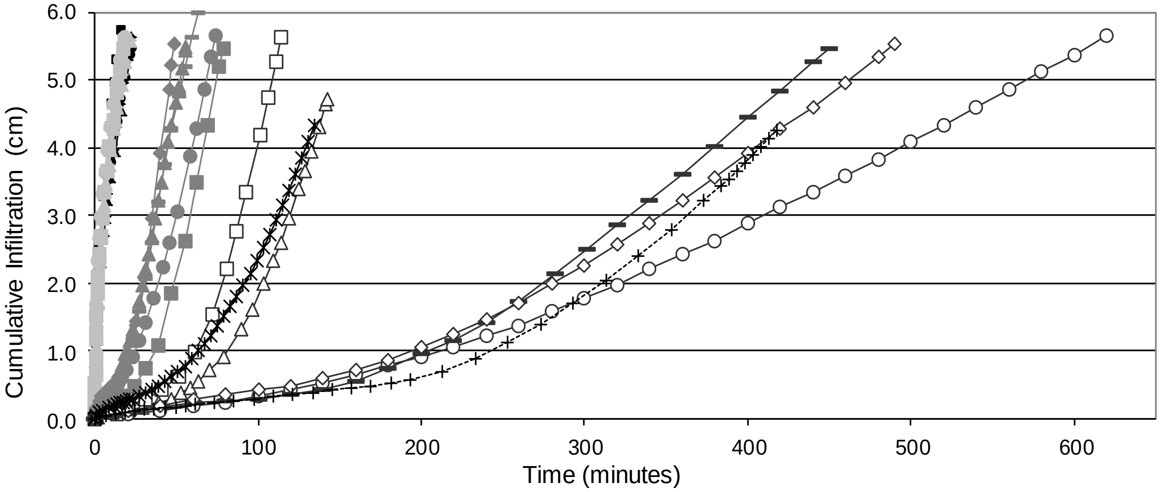

(b)

Figure 2.3 Cumulative Infiltration vs. a.) Time^{½} and b.) Time plots for instrumented and non-instrumented replicate column experiments. Replicate symbologies are as follows: Rep 1 - ▲; Rep 2 -■; Rep 3 - ●; Rep 4 - ▬ ; Rep 5 -◆. Inst-1 - + and Inst-2 – x are the instrumented column results and have been shown here for comparison. Colourings correspond to those used in Figure 4: Mineral only = black; Char over mineral = Light grey; Mixed over mineral = medium grey; Brown over mineral = dark grey and white fill.

our experiments. Water repellent materials in instrumented columns exhibit the same kind of convex infiltration behaviour observed in the non-instrumented column experiments. Inst-1 behaves more similarly to Brown material cases that have lower fractional wettability surface materials and Inst-2 behaves more similarly to Mixed material cases which have higher fractionally wettable surface materials. This is consistent with the larger portion of charred wettable materials at the surface in Inst-2. While tensions at the organic material surface were slightly higher (by ~3cm) for Inst-1 and Inst-2 than those in non-instrumented tests (-2cm in all cases), these small differences elicited essentially undetectable differences in infiltration behaviours between the two set ups. The major difference between the instrumented tests is that Inst-1 data are near-linear up to ~13.5 min$^{1/2}$ (~180 minutes) and Inst-2 data is linear only for the first 6.25 min$^{1/2}$ (~40 minutes) of testing.

While there is variability among tests as shown in Figure 2.3, the relative magnitudes of dynamic repellency are well expressed visually and numerically (e.g. BOM tests had the longest overall delays in infiltration). When the water supply is maintained at a negative pressure head throughout the hydrophobic layer, the increasing slope with time can only be attributed to the breakdown of repellency with time and not because pressure build-up at the wetting front or hydrophobic-hydrophilic material interface (e.g. Feng et al., 2001; Wallach and Graber, 2007).

2.4.2 Infiltration rates (non-instrumented columns)

Infiltration Rate vs. Time data for all non-instrumented test replicates appears in Figure 2.4. *Mineral Only (MO)* B horizon materials (Figure 2.4a) follow curves typically

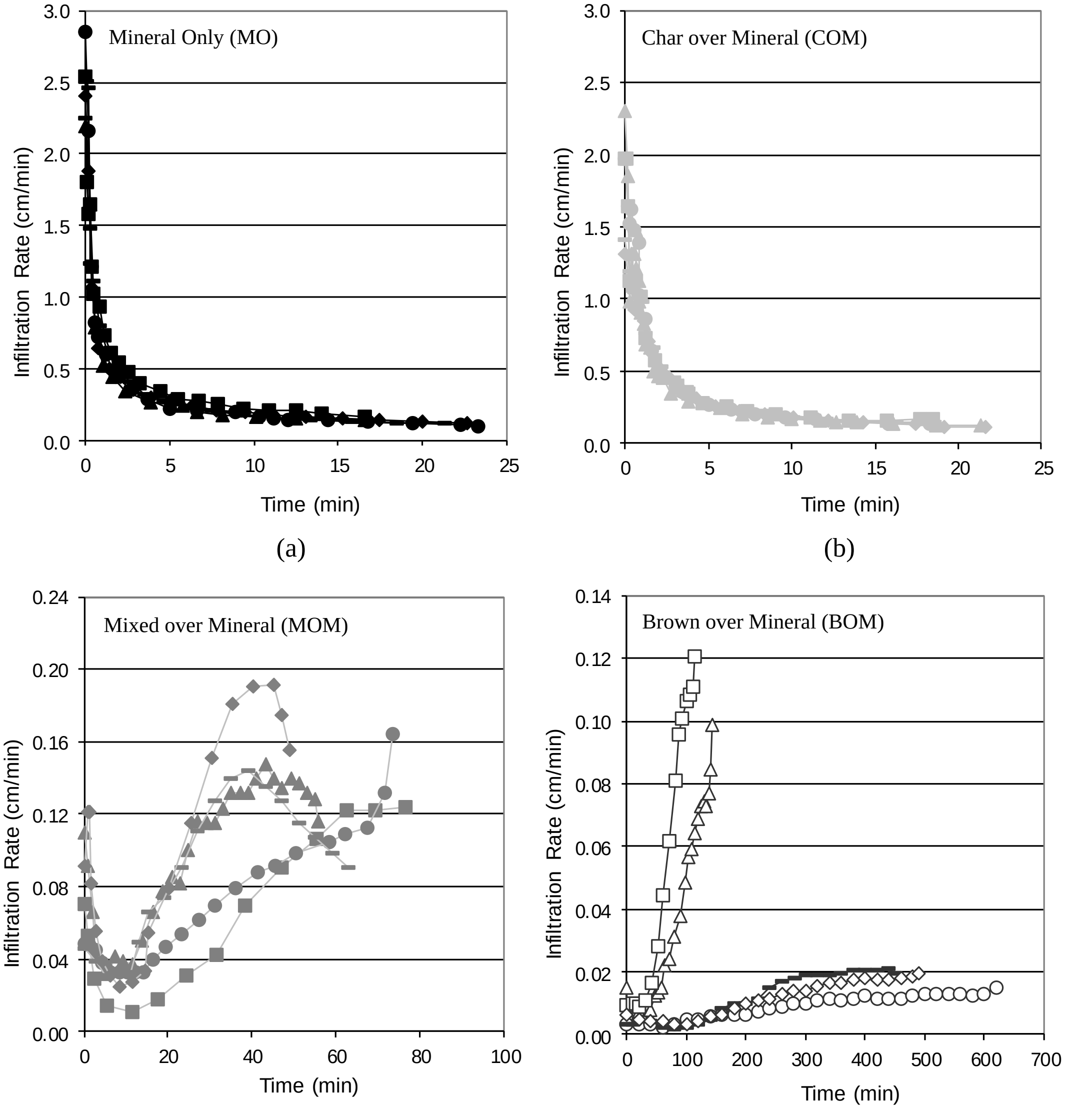

(a) (b)

(c) (d)

Figure 2.4 Showing infiltration rate behaviour as a function of time for 20 non-instrumented one-dimensional infiltration column experiments. Replicates are shown for (a) Mineral Only, (b) Char over Mineral, (c) Mixed over Mineral, and (d) Brown over Mineral material configurations. Replicate symbologies are as follows: Rep 1 - ▲; Rep 2 -■; Rep 3 - ●; Rep 4 - ▬ ; Rep 5 -◆.

observed in hydrophilic soils. The near-exponential drop in infiltration rate is due to the decreasing contribution of the capillary (or pressure head) driven component of the hydraulic gradient that develops as the wetting front moves further away from surface where the porous disc maintains a constant negative pressure head. At late time the infiltration rate approaches a value equal to the prevailing hydraulic conductivity since the capillary (pressure head) component of the hydraulic gradient approaches zero and the gravity driven component of the hydraulic gradient becomes the remaining driving force (dh/dz=1). The MO data serve as a valuable reference case for direct comparison to the behaviour of later experiments that include hydrophobic materials and shows that approximately 80 ml of water infiltrated in 17-24 minutes for the 5 replicates.

The *Char over Mineral (COM)* material configuration (Figure 2.4b) behaves similarly to the Mineral Only (MO) infiltration data, with tests lasting 19 to 23 minutes and exhibiting minor (secondary) differences. Early time data show that infiltration into COM columns was marginally slower than in MO columns in the first minute of infiltration. This small difference is likely attributable to a slightly weaker initial capillary component of the hydraulic gradient within the coarser aggregated Char material and/or an initial resistance to wetting caused by an imperfectly wetting fraction. This indicates that the Char material is behaving as a bulk hydrophilic material with slight and/or indiscernible changes in contact angles (wettability) over the duration of the test. This behaviour is consistent with rapidly changing contact angles measured on 0 cm Char Surface Materials in Beatty and Smith (2010).

Mixed over Mineral (MOM) tests (Figure 2.4c) exhibit complex, variable, and distinct behaviours that are readily distinguishable from the MO and COM hydrophilic material configurations. At early times (up to 10 minutes across the 5 replicates) MOM infiltration shows decreasing infiltration rates similar to typical hydrophilic systems. This behaviour can be attributed to the sorption of water into fractionally wettable surface (0cm) materials (DeBano, 2000) in the material "puck." Initial differences in fractionally wettable surfaces plays an important role in the noted variability in infiltration rate between tests by making different contributions to this initial wicking behaviour and later time changes in contact angle. After 10 minutes, the infiltration rates across the 5 replicates increase substantially with time. This type of increasing infiltration rate with time has been observed elsewhere in hydrophobic media (e.g. Imeson et al., 1992; Clothier et al., 2000; Feng et al., 2001; Pierson et al., 2008) under different experimental conditions. Where highest infiltration rates for MO and COM tests occur at the beginning of tests, the highest infiltration rates for MOM tests are observed at late time. In three of the five replicates, infiltration rates reach a maximum infiltration rate between minutes 37 and 47, after which time infiltration rates decrease for the remainder of the test. These maxima can be interpreted as indicating a transition between *primarily* hydrophobic and *primarily* hydrophilic states (i.e. fractional wettability still exists in these materials and they remain imperfectly wetting). If water repellent media are largely identified as having increasing infiltration rates and hydrophilic media are characterized by monotonically decreasing infiltration rates, then it would appear that these materials started to become hydrophilic during the course of testing. More specifically, this behaviour can be explained by a competition that is occurring between 1) a hydraulic gradient that is approaching unity and causing the infiltration rate to decrease with time and 2) contact angles that are becoming more wettable and contributing to increases in the wettability of the bulk material with prolonged exposure to water – which leads to increases in the infiltration rate over time. Changes in the wettability of initially non-wettable surfaces can lead to higher moisture contents that can increase connectivity between wettable pore networks and result in higher unsaturated hydraulic conductivities. Consequently, at any particular point in time, the infiltration rate is a function of these two primary mechanisms (i.e. contact angles becoming wettable and the hydraulic gradient); and its direction (i.e. increasing or decreasing) indicates which mechanism is winning. This means that contact angle dynamics are a primary mechanism during infiltration for a length of time that is largely influenced by the fraction of initially wettable materials and the rate at which the initially non-wettable fraction becomes wettable, i.e. contact angle dynamics. The observance of decreasing rates at multiple time points indicates that the behaviour is not random. It is important to note, however, that the Mixed materials were not completely wettable since infiltration rates were still decelerating at the ends of these replicate tests. However, rates at this point *were* close to end-of-test rates observed in hydrophilic material tests (e.g. Mineral Only and Char over Mineral). Even still, because of the nature of infiltration using the tension infiltrometer (i.e. with the tension infiltrometer pores must ‘switch’ to a negative pore water pressure for infiltration to occur), a possible time stamp for when dynamically changing contact angles approach wettable conditions may now be more systematically identifiable.

The other two (of five) MOM replicates have increasing infiltration rates from ~10 minutes onward. These tests, which are about three times longer than the hydrophilic tests discussed earlier, exhibit lower and more variable rates that also approach late-time values similar to gravity driven infiltration through the Mineral Only and Char over Mineral tests. In spite of differences between individual tests, these data indicate that over time 1) increased portions of the bulk hydrophobic media are becoming more wettable via dynamic contact angles and are being expressed as such via increased infiltration rates, and 2) complex water repellent materials can reach sustained rates of flow comparable to wettable materials within an hour. These results suggest that hydrophilic-hydrophobic layered materials play an important role during infiltration into these systems. While geomorphological processes such as erosion and degradation are commonly reported in water repellent systems and could remove this wettable fraction under high-magnitude, low frequency rain events, it is important that test methods (e.g. surface preparation) consider fractionally wettable surface materials as a key determinant of the persistence of repellency (contact angle change) in the overall soil profile; particularly for low-magnitude, high frequency rainfall events.

Similar to MOM tests, *Brown over Mineral (BOM)* (Figure 2.4d) tests exhibit decreasing infiltration rates at early time in 4 of 5 replicates (i.e. <100 minutes in 3 of 5 replicates and < 30 minutes in 1 replicate) vs. 10 minutes in MOM), however, initial and average minimum rates are an order of magnitude lower for BOM materials. These lower initial rates in BOM tests can be largely attributed to a smaller wettable fraction at the surface. In the longest tests (i.e. BOM replicates 3-5), rates remain low and essentially constant until ~ 100 minutes, after which time, slow increases occur over the remainder of the tests. Clothier et al. (2000) observed similar behaviour in silt loam, which they attribute to the breakdown of repellency. Here, we interpret this rate behaviour as a kind of barometer of the initially wettable fraction at the surface, and how it influences contact angle changes in subsurface materials and/or the wettability of the bulk media over time. The other two replicates (BOM1 and BOM2) exhibit much quicker increases in infiltration rate beginning around 25 minutes. These two replicates express intermediate behaviour which lies between the longest Brown over Mineral tests and the MOM tests and show a possible lower range for the repellency persistence in the Brown materials. Overall, these tests show that water repellent materials with a smaller fraction of wettable materials at the surface exhibit slower contact angle dynamics as expressed through slower and smaller increases in infiltration rates with time.

2.4.3 Infiltration rates and real time moisture content (instrumented columns)

Infiltration rate data for instrumented experiments (Inst-1 and Inst-2) are presented with corresponding real time volumetric moisture content data collected and logged with in situ moisture sensors in Figure 2.5. Infiltration into the contact sand is not shown in the infiltration plots for the instrumented column experiments since it is an artefact of the method and over rapidly. Also, consistent with the negative applied pressures, no ponding was observed at any time.

From early time in Inst-1, small and consistent increases in moisture content are observed in the shallowest sensor (i.e. 1.7 cm from top of column), OM-17 (Figure 2.5a). At 50 minutes, however, a steepening in moisture content occurs; this also corresponds

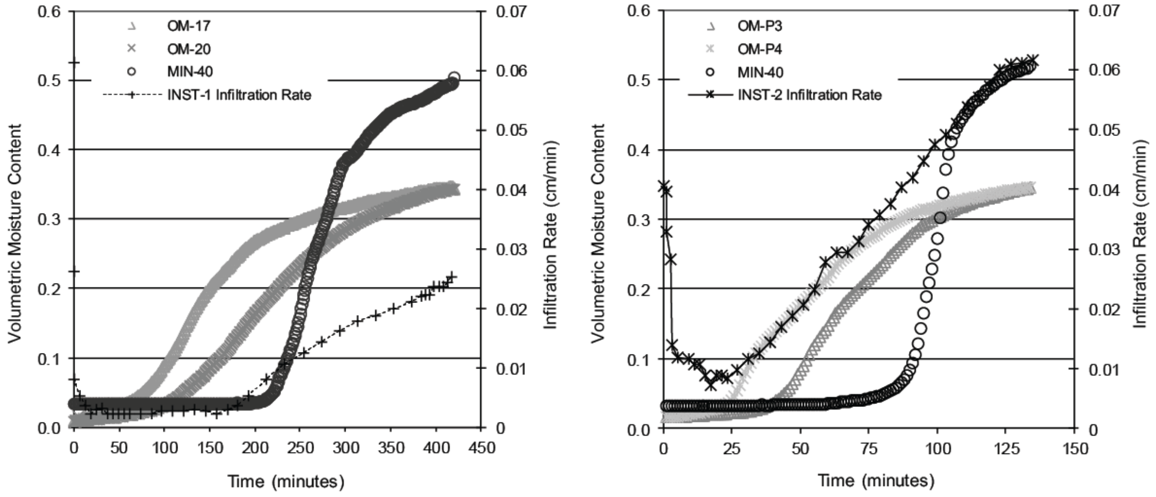

Figure 2.5 Infiltration rate and real-time moisture content plots for a) Inst-1 and b) Inst-2.

with increased moisture contents being detected in OM-20. Infiltration rates do not change over this interval. In this test, OM-20 exhibits a distinctively dampened and more gradual response to the advancing front relative to OM-17 (the shallower of the two by 0.3cm). However, the shape of both dispersed fronts indicate that wetting in these materials is not akin to the sharp wetting fronts often identified in hydrophilic materials of similar texture.

What is most notable in these data, is that for materials with a smaller portion of initially wettable materials at the surface (Inst-1), the infiltration rate decreases initially and remains low and essentially constant between minutes 35 and 175, after which time more gradual and consistent increases in infiltration rate are observed. Breakthrough past the organic-mineral interface was observed visually at 190 minutes however, MIN-40 (the B Horizon material moisture sensor positioned) did not detect increases in moisture content until 195 minutes; this difference can be attributed to its position 0.5cm below the organic-mineral interface. The lack of a sharp (steep slope) wetting front in MIN-40 is an expression of the complex nature of infiltration through the hydrophobic organic layer.

No significant increases in infiltration rate were observed before visual observations of breakthrough into B Horizon materials; during this time moisture contents increased substantially in organic puck materials (i.e. up to 0.24). This means that water was infiltrating and being stored in this relatively thin (~3cm) organic layer for nearly 3 hours. It is only after this long period of time that water entered the underlying mineral layer and infiltration rates began to increase. The majority of increases in moisture content of shallow organic materials (OM-17) occurred in the period before breakthrough. Slightly deeper organic materials (OM-20) saw the majority of increases in moisture content following breakthrough.

Immediately following the onset of an increasing infiltration rate, breakthrough of multiple preferential flow paths into mineral B horizon materials was observed. Given that the water supply pressure remained negative throughout the organic layer, we attribute increases in infiltration rate to the combined effects of the changing wettability and connectivity of pore networks within the organic layer and the number of breakthrough points into the mineral layer. At 350 minutes however, when a uniform front wetted the mineral layer across the entire cross sectional area of the column, any additional increases in infiltration rate can then be solely attributable to changes in the wettability of pore networks of the organic layer. While the capacity of the infiltrometer (approx. 300ml) limits the extent to which changes in moisture contents and infiltration rates can be observed beyond 350 minutes, we can see that infiltration rates and moisture contents in these layered hydrophobic systems do not behave like layered hydrophilic systems do. The texture and apparent pore size distribution of the organic layer is such that its unsaturated hydraulic conductivity (under completely wettable conditions at the applied tension) can be assumed to be equal to or greater than that of the mineral soil. This means that the effective infiltration rate (i.e. the one measured via the infiltrometer) is a combination of the hydraulic properties of the sub-layer hydrophilic media and the overlying hydrophobic media (whose conductivity is changing with time as greater fractions of materials become wettable via contact angle change). So, while subsurface B Horizon materials can influence infiltration behaviour in these types of systems, late time and overall changes in infiltration rate are most substantially affected by the changing and/or static properties of overlying hydrophobic materials.

In the second instrumented experiment (Inst-2) (Figure 2.5b), behaviour of OM-P4 over the course of the test can be characterized by a sharp increase at 25 minutes which is preceded by small and gradual increases in moisture content. For the remainder of the test, the curve follows a concave curvilinear trend with a gradually decreasing slope to the end of the test. Sensor 3 (OM-P3) exhibits similar behaviour, although 40 minutes pass before substantial increases in moisture content occur. This provides a temporal measure of preferential wetting since both OM-P3 and OM-P4 are positioned at the same height in the column. MIN-40, which is embedded in B Horizon material, does not show any noticeable change in moisture content until 85 minutes. Similar to the previous case, B horizon material exhibits the greatest rate and amount of moisture content change over the duration of the test. However, moisture contents increase much more steeply in Inst-2 B Horizon materials. This steepening is directly related to the water supply rate, which is being controlled by the overlying hydrophobic organic materials. If supply was not impeded at all, a steeper moisture profile would be observed (in MIN-40). Since a severely sharp front occurs neither in Inst-1 nor in Inst-2, we can therefore conclude that moisture content changes in the hydrophilic material are flux limited and reflect the gradual change of contact angles and wettability of the organic layer as time of water exposure increases.

Similar to the other experiments on hydrophobic materials, Inst-2 exhibits a decreasing infiltration rate at early time and increasing rate at later time. In contrast to Inst-1, Inst-2 experiences a quick rebound in infiltration rate with no significant increases in moisture content. Subsequent increases in infiltration rate can be attributed to the combined effects of increases in the number and size of fingers breaking through into the hydrophilic mineral layer and the changing wettability of pore networks within the organic layer, albeit at a faster rate than observed in Inst-1. These mechanisms generate strong linear increases in infiltration rate which are approximately three times faster than in the less heavily charred materials (Inst-1). The small perturbation in this trend at 60 minutes is an artefact of re-securing the infiltrometer in response to sample compression.

2.4.4 Post-Infiltration moisture content profiles

The moisture content profile at the end of each infiltration test appear in Figure 2.6. Initial volumetric moisture contents for air dry B Horizon materials were between 0.01 and 0.04 for all tests. Mineral Only (MO) moisture profiles are presented with the

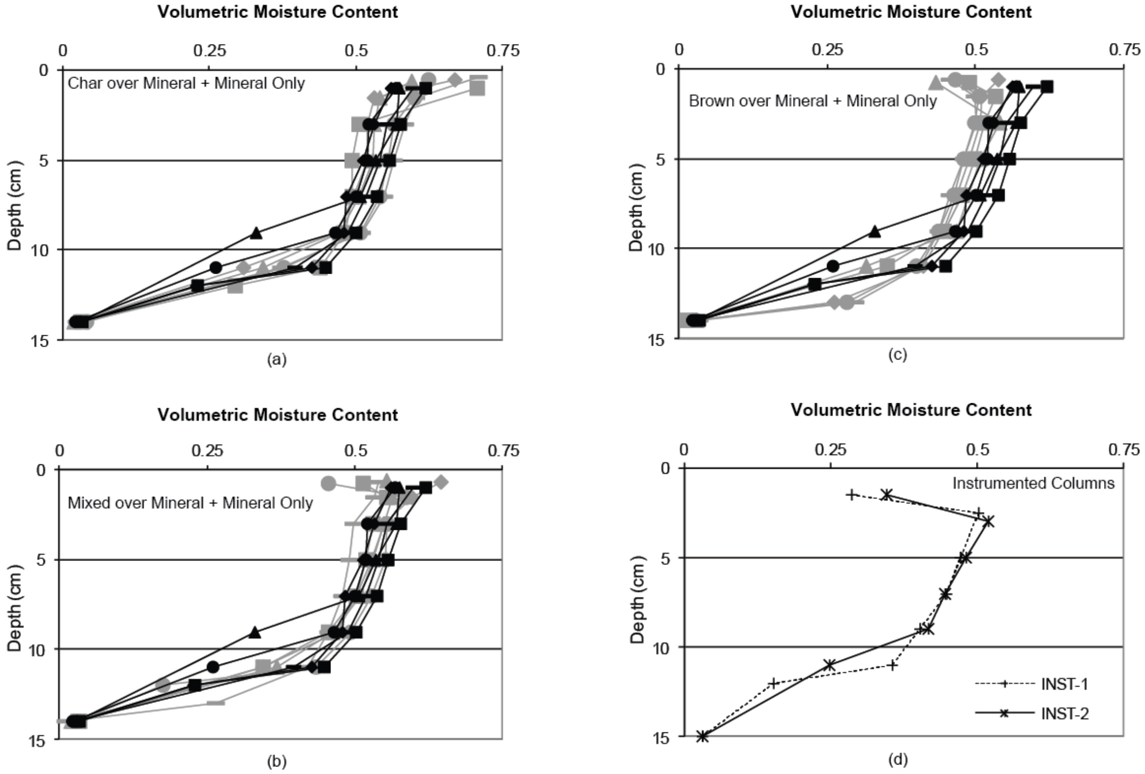

Figure 2.6 Post infiltration volumetric water content profiles for 1D column experiments, using replicate symbologies found in Figure 3 and Figure 4. Mineral only replicate tests use black symbologies in non-instrumented profiles (a, b, and c).

other material configurations' moisture data to provide a reference for profile comparisons (Figure 2.6). Instrumented column data appear in Figure 6d. Data points are centered at each 2cm sample interval (i.e. 2-4cm interval assigned 3cm). Organic "puck" points and immediately adjacent mineral materials fall at the centre depth relative to each material thickness since there was some small variability in the thickness of pucks between tests (see Table 2.1).

Organic material moisture contents tend to exhibit an indirect, but variable relationship with water repellency i.e. more persistently hydrophobic and less fractionally wettable materials have lower end-of-test moisture contents (see Figure 2.6a, 2.6b, 2.6c). Moisture contents and the depth of wetting in mineral materials across the non-instrumented columns are similar for all tests. The most hydrophobic material tests (Brown over Mineral) exhibit lower moisture contents overall and marginally deeper profile wetting compared to other materials – which reflects the similar applied volume but longer duration of these tests. Differences between instrumented and non-instrumented organic layers can be explained, at least in part, by the slightly more negative pressure heads in Inst-1 and Inst-2.

2.4.5 Conceptual model of dynamic soil water repellency in bulk media

Fractional wettability and contact angle dynamics are the key to understanding dynamic soil water repellency. The current state of knowledge is such that there are no mechanistic models of the wetting mechanism (Diehl and Schaumann, 2007). Here we discuss the wetting mechanism through the combined effects of contact angle dynamics and fractional wettability. While fractional wettability and contact angle dynamics are normally studied separately, as a consequence of the work conducted here and in Beatty and Smith (2010), we find it necessary and advantageous to consider them as inextricably linked. Bayer and Schaumann (2007) discuss that (temporal) differences between water wettable and water repellent states are controlled by 1) the thickness of the layers of water molecules on hydrophobic materials and 2) heterogeneity in soil surface characteristics. Using a conceptual model to express the nature of repellency in response to increasing moisture, they note that slow changes in water repellency can occur even after constant moisture contents are reached. From this fundamental understanding of sub-porescale relationships and behaviours, here we explain wetting in water repellent soils at the bulk scale so that the roles of fractional wettability and contact angle dynamics can be better understood relative to more observable hydrologic processes.

The process of wetting in complex water repellent media and the relationship between moisture contents and infiltration rates with time are presented in the following conceptual diagram (Figure 2.7). In case A, we consider hydrophilic mineral materials overlain by hydrophobic dominant (HD) organic materials that consist of a very small fraction of wettable materials at the surface, and low-angle hydrophobic materials subsurface (e.g. with contact angles 95-110°). Upon the introduction of water supplied at a constant and negative pressure head, the small wettable surface fraction will contribute to the sorption of water into the surface matrix and result in an initial decrease in infiltration rate; this elicits movement along an initial pore water pressure head curve (i.e. case A: from CI0 to CI1). The size of this initial volume of water is a key determinant of the (rate of) subsequent contact angle dynamics in adjacent near-surface materials and overall changes in the fractional wettability of the bulk media.

Following the initial decrease in infiltration rate, moisture contents increase while the infiltration rate remains low and unchanging. Beyond CI1, contact angles in the (organic) hydrophobic porous media are continually decreasing which shifts the capillary – pressure head relationship as shown by Bradford et al. (1997) in proportion to *cos(θ)* (as found by Arye et al. (2007)). These continual decreases in contact angle also affect the

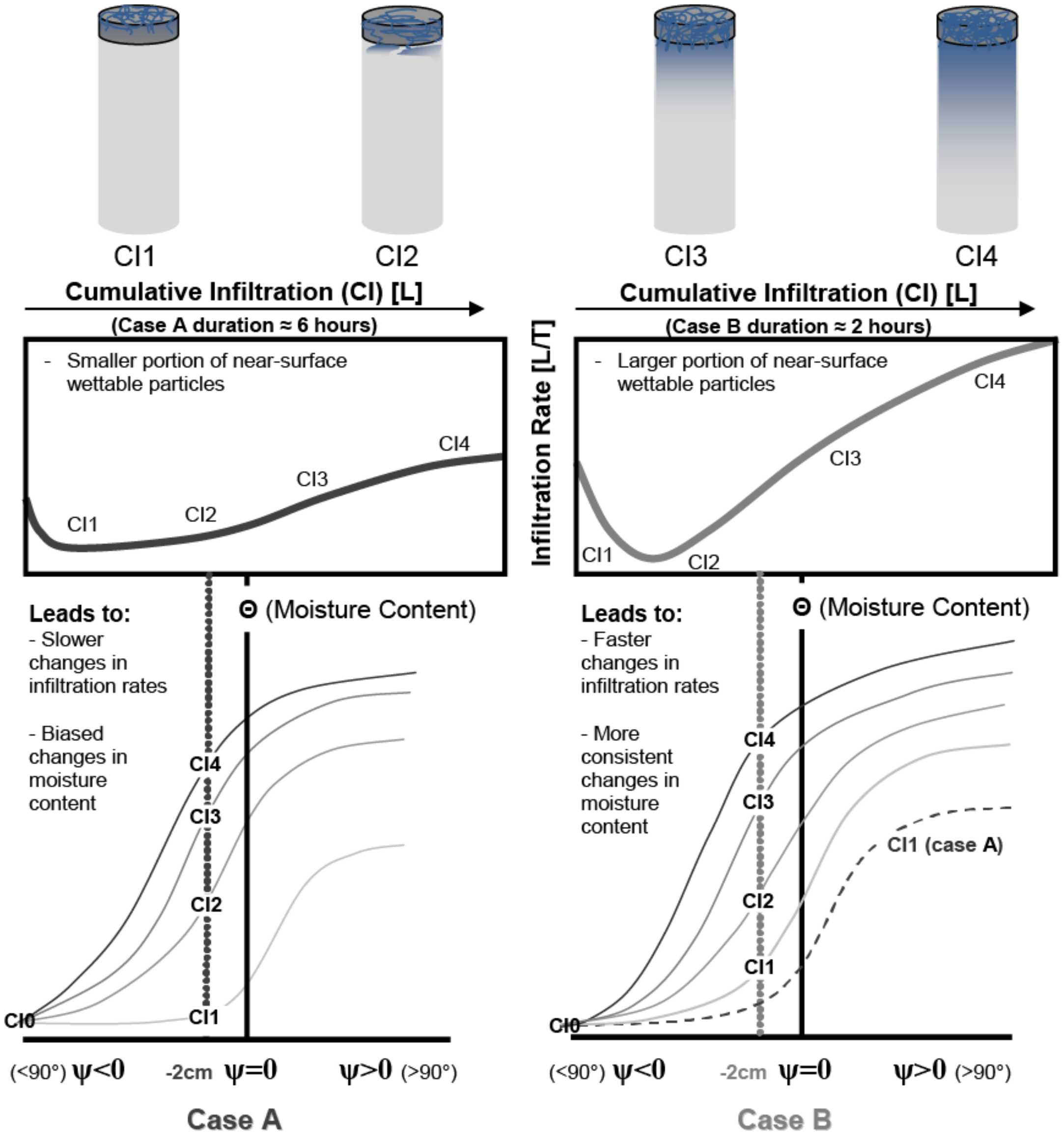

Figure 2.7 Conceptual model of fractional wetting and dynamic contact angle change in two different cases. Case A (green) describes a system with a small (initially) wettable fraction such that the role of contact angle change is the dominant process throughout an infiltration event. Case B (yellow) describes a system with a large (initially) wettable fraction such that the role of fractional wettability is the dominant control on infiltration. Graphs on lower half of the figure represent hypothesised pressurehead - moisture content relationships for Cases A and B with pressurehead (*ψ)* appearing on x-axes and moisture content (θ) appearing on y-axes.

fractional wettability of the bulk media such that greater fractions are becoming more wettable. At this time, possible increases in infiltration rate are proportionally equal to or less than the effect of a decreasing gradient caused by the slow advance of a discontinuous wetting ‘front’. That is, from CI1 to CI2, increases in fractional wettability allow variable pore networks to grow deeper into the soil profile. These pore networks may increase the conductivity of the material via connected pathways or may only contribute to increases in storage in the form of (temporary) dead-end zones. Changes in moisture contents at early time that do not result in proportional increases in infiltration rate are an indication of the presence of these temporarily disconnected pore networks within the medium.

At breakthrough past organic materials (case A: CI2), infiltration rates begin to increase noticeably. At the first breakthrough location, local changes in the wettability of adjacent organic materials occur, ever increasing the rate of delivery to hydrophilic subsurface materials from this entry point. At the same time, additional points of entry into subsurface hydrophilic materials develop as moisture contents increase in hydrophobic materials; this also contributes to an increasing infiltration rate. Throughout, shifts in the pore water pressure head relationship occur as moisture contents increase (CI3). When the pressure head condition is held constant at the surface and negative throughout the hydrophobic layer, increases in moisture content can only occur when water is drawn into pores. Increased moisture contents can therefore only be attributed to two things: 1) increased access to fractionally wettable particles via connected pathways and/or, 2) changes in contact angle. The first case elicits movement along existing curves, while the second results in small shifts in the pore water pressure head curve. Throughout the medium, it is likely that both of these processes are happening concurrently. At later time (case A: CI4), no further increases should be observed in infiltration rate if a static wettable fraction was affecting infiltration since rates are being increasingly dampened as gradients approach one (i.e. dh/dz →1). However, increases in infiltration rate still occur even after this point (CI4). This flux-limited behaviour can only be attributed to slow, but consistent changes in contact angles and the increasing fraction of materials that are gradually becoming more wettable with prolonged exposure to water.

In case B, we consider media where there is a greater fraction of wettable materials, and as a consequence, experiences faster contact angle dynamics. Relative to the materials discussed previously (case A), consider hydrophilic mineral materials overlain by wettable dominant (WD) hydrophobic organic materials that consist of a larger fraction of wettable materials at the surface, and with higher contact angle hydrophobic materials (e.g. CA=115-130°) subsurface. Overall, the conceptual model behaves similarly in case B to case A, except that fractional wettability changes the nature of the shifting pore water pressure head relationship in an infiltration event. Similar to case A, an initial decrease in infiltration rate can be attributed to the sorption of water in hydrophilic surface media, or movement *along* an initial capillary-pressure head curve (i.e. case B: from CI0 to CI1). The higher relative position of the curve in case B (compared to case A), is resultant of the 1) the larger proportion of wettable surfaces and 2) the initial magnitude of contact angles in hydrophobic media. This concept is consistent with research on synthetically hydrophobised granular materials (e.g. Bradford et al., 1997; O'Carroll et al., 2005; Hwang et al., 2006; Bachmann et al., 2007).

In case B, the rate of supply (under the same negative pressure head condition) is much quicker than in case A, but the overall response of the system is not as dependent on the supply since 1) supply is not being restricted and 2) the greater fraction of wettable particles facilitates transport through wettable pore networks without the requisite of changing contact angles. The first case may appear as somewhat of a self-referential statement, but for hydrophobic materials whose rates of contact angle change are largely dependent on the thickness of the film of water, when water is freely available, rates are then only subject to the temporal constraints of the physicochemical structure of solid surfaces. In the previous case (i.e. case A), these factors (i.e. changing contact angles, moisture content, and supply) were inextricably linked to one another because moisture content governed contact angle dynamics and contact angle dynamics governed supply. In this case however, the rate of supply is less associated with moisture content (and contact angle dynamics) because there is an increased wettable fraction that does not need to wet-up and undergo contact angle changes in order to transmit water. This means that water gets to non-wettable regions more quickly and that contact angle changes are accelerated in those regions.

As a result of these effects, wettable pore networks develop more quickly such that much shorter time intervals are required before 1) infiltration rates quickly rebound and begin to increase steeply, 2) there are steep increases in moisture content, and 3) breakthrough into underlying hydrophilic materials occurs (CI2). The rate of rebound will be substantially quicker than in the previous case because connected wettable pore networks across the entire medium are developing in quick succession and breaking through into underlying hydrophilic materials. Similar to the previous case (A), entry points and materials adjacent to entry points are undergoing changes in contact angle with time, albeit at a much faster rate. This means that the capillary-pressure head curve of case B is shifting more quickly as contact angles change more readily. We suspect that the increased influence (dominance) of the initially wettable fraction amplifies the magnitude of these shifts; which is why increases in infiltration rate occur faster in these materials (CI3).

Similar to case A, infiltration rates continue to increase at later time, even while infiltration rates would normally be dampened by a decreasing hydraulic gradient approaching unity (CI4). This late time behaviour reinforces the conclusion that the magnitude and rate of change of contact angles is a dominant mechanism during infiltration into fractionally wettable and dynamically changing materials.

2.5 Summary and conclusions

For greater understanding and insight into hydrologic processes in water repellent media, combining the concepts of contact angle dynamics and fractional wettability is an essential union of ideas. Considering either fractional wettability or dynamic contact angles alone is insufficient. We conclude that the complex interplay between the relative fractions of wettable and non-wettable materials and how those proportions shift over time with dynamic contact angles is the fundamental nature of these systems. The investigative approach presented here facilitated the systematic observance of this relationship and its dominant role during infiltration.

Our works shows that tension infiltrometers are sensitive to fundamental differences in fractional wettability and contact angle dynamics in hydrophobic materials. We utilized the ability of the tension disc infiltrometer to maintain a negative pressure head condition throughout repellent layers rather than use it for its intended purposes of measuring conductivity and sorptivity values. When negative pore water pressure heads are mechanically maintained throughout a repellent layer, behavioural trends in infiltration rate and the acceleration of rates over time provide direct information about the nature of changes in contact angles and fractionally wettability within hydrophobic materials. This is particularly powerful information when coupled with initial measures of contact angle. For example, in layered, non-wetting systems, hydrophobic materials overlain by increased fractions of wettable (charred / combusted) surface materials can experience quicker and more consistent increases in infiltration rate, which can in-turn contribute to system feedback loops that cause greater fractions of materials to become more wettable via contact angle change.

The conceptual summary presented here is based on experiments using fire affected soils. However, its fundamental concepts are relevant and transferrable to other hydrophobic systems. While data captured in some repellent systems can be coarsely approximated using traditional hydrophilic infiltration theories, dynamically repellent materials, such as this, do not lend themselves to meaningful interpretation using those approaches. By moving away from static pore–size distribution concepts, there is great potential for a more comprehensive and advanced understanding of these kinds of systems across scales. In order to move forward in our ability to simulate, quantify and predict the hydrology of hydrophobic systems accurately, it is essential that greater consideration be given to dynamic measures of water repellency over time scales that express the interconnectedness of properties within these uniquely challenging systems.

Acknowledgements

This research was financially supported by the Ontario Graduate Scholarship program and Natural Sciences Engineering Research Council of Canada (NSERC) Discovery Grant program. We would like to express our sincere thanks to Jennie Kirby of McMaster University for her curiosity, willingness to help, and invaluable assistance in the lab.

References

Arye, G., I. Nadav and Y. Chen. 2007. Short-term reestablishment of soil water repellency after wetting: Effect on capillary pressure-saturation relationship. Soil Sci. Soc. Am. J. 71:692-702.

Bachmann, J., M. Deurer and G. Arye. 2007. Modeling water movement in heterogeneous water-repellent soil: 1. development of a contact angle dependent water-retention model. Vadose Zone J 6:436-445.

Bauters, T.W.J., T.S. Steenhuis, D.A. DiCarlo, J.L. Nieber, L.W. Dekker, C.J. Ritsema, J.-. Parlange and R. Haverkamp. 2000. Physics of water repellent soils. J. Hydrol. 231-232:233-243.

Bayer, J. and G. Schaumann. 2007. Development of soil water repellency in the course of isothermal drying and upon pH changes in two urban soils. Hydrol. Process. 21:2266-2275.

Bear, J. 1972. Dynamics of fluids in porous media. Dover Publications, Inc., New York.

Beatty, S.M. and J.E. Smith. 2010. Fractional wettability and contact angle dynamics in burned water repellent soils. J. Hydrol. 391: 99-101

Bens, O., N. Wahl, H. Fischer and R. Hüttl. 2007. Water infiltration and hydraulic conductivity in sandy cambisols: Impacts of forest transformation on soil hydrological properties. Euro. J. Forest Res. 126:101-109.

Bradford, S.A., L.M. Abriola and F.J. Leij. 1997. Wettability effects on two- and three-fluid relative permeabilities. J. Contam. Hydrol. 28:171-191.

Carrillo, M.L.K., J. Letey and S.R. Yates. 2000. Unstable water flow in a layered soil: I. effects of a stable water-repellent layer. Soil Sci. Soc. Am. J. 64:450-455.

Carter, M.R. 1993. Soil sampling and methods of analysis. Canadian Society of Soil Science, Lewis Publishers, Boca Raton, FL.

Cerdà, A. and S. Doerr. 2007. Soil wettability, runoff and erodibility of major dry-mediterranean land use types on calcareous soils. Hydrol. Process. 21:2325-2336.

Clothier, B.E., I. Vogeler and G.N. Magesan. 2000. The breakdown of water repellency and solute transport through a hydrophobic soil. J. Hydrol. 231-232:255-264.

Cobos, D.R. 2009. Calibrating ECH20 soil moisture sensors. Available: www.decagon.com/pdfs/app_notes/CalibratingECH20SoilMoistureProbes.pdf (Accessed: August, 2009).

Czachor, H., S.H. Doerr, and L Lichner. 2010. Water retention of repellent and subcritical repellent soils: New insights from model and experimental investigations. J. Hydrol. 380: 104-111.

DeBano, L.F. 2000. The Role of Fire and Soil Heating on Water Repellency in Wildland Environments: A review. J. Hydrol. 231-232:195-206.

Diehl, D. and G. Schaumann. 2007. The nature of wetting on urban soil samples: Wetting kinetics and evaporation assessed from sessile drop shape. Hydrol. Process. 21:2255-2265.

Doerr, S.H. and A.D. Thomas. 2000. The role of soil moisture in controlling water repellency: New evidence from forest soils in Portugal. J. Hydrol. 231-232:134-147.

Doerr, S.H., R.A. Shakesby and R.P.D. Walsh. 2000. Soil Water Repellency: Its Causes, Characteristics and Hydro-Geomorphological Significance. Earth Sci.Rev. 51:33-65.

Feng, G.L., J. Letey and L. Wu. 2001. Water ponding depths affect temporal infiltration rates in a water-repellent sand. Soil Sci. Soc. Am. J. 65:315-320.

Hallet, P.D., N. Nunam, J.T. Douglas, and I.M. Young. 2004. Millimeter-scale spatial variability in soil water sorptivity: Scale, surface elevation and subcritical repellency effects. Soil Sci. Soc. Am. J. 68:352-358.

Hwang, S.I., K.P. Lee, D.S. Lee and S.E. Powers. 2006. Effects of fractional wettability on capillary pressure-saturation-relative permeability relations of two-fluid systems. Adv. Water Resour. 29:212-226.

Imeson, A.C., J.M. Verstraten, E.J. van Mulligen and J. Sevink. 1992. The effects of fire and water repellency on infiltration and runoff under mediterranean type forest. Catena 19:345-361.

Lamparter, A., J. Bachmann, M. Deurer, S.K. Woche. 2010. Applicability of ethanol for measuring intrinsic hydraulic properties of sand with various water repellency levels. Vadose Zone J. 9:445-450.

Leighton-Boyce, G., S.H. Doerr, R.A. Shakesby and R.P.D. Walsh. 2007. Quantifying the impact of soil water repellency on overland flow generation and erosion: A new approach using rainfall simulation and wetting agent on *in situ* soil. Hydrol. Process. 21:2337-2345.

Letey, J. 2001. Causes and consequences of fire-induced soil water repellency. Hydrol. Process. 15:2867-2875.

Lewis, S.A., P.R. Robichaud, B.E. Frazier, J.Q. Wu and D.Y.M. Laes. 2008. Using hyperspectral imagery to predict post-wildfire soil water repellency. Geomorphology 95:192-205.

Lichner, L., P. Hallett, D. Feeney, O. Ďugová, M. Šír and M. Tesař. 2007. Field measurement of soil water repellency and its impact on water flow under different vegetation. Biologia 62:537-541.

Moody, J. D.A. Kinner, and X. Úbeda. 2009. Linking hydraulic properties of fire-affected soils to infiltration and water repellency. J. Hydrol. 379: 291-303.

O'Carroll, D.M., L.M. Abriola, C.A. Polityka, S.A. Bradford and A.H. Demond. 2005. Prediction of two-phase capillary pressure-saturation relationships in fractional wettability systems. J. Contam. Hydrol. 77:247-270.

Orfanus, T., Z. Bedrna, L. Lichner, P.D. Hallet, K. Kňava and M. Sebíň. 2008. Spatial variability of water repellency in pine forest soil. Soil Water Res. 3:123-129.

Pierson, F.B., P.R. Robichaud, C.A. Moffet, K.E. Spaeth, C.J. Williams, S.P. Hardegree and P.E. Clark. 2008. Soil water repellency and infiltration in coarse-textured soils of burned and unburned sagebrush ecosystems. Catena 74:98-108.

Quyum, A., G. Achari, and R.H. Goodman. 2002. Effect of Wetting and Drying and Dilution on Moisture Migration Through Oil Contaminated Hydrophobic Soils. Sci Total Environ. 296:77-87.

Reynolds, W.D. 2006. Tension infiltrometer measurements: Implications of pressure head offset due to contact sand. Vadose Zone J 5:1287-1292.

Rodríguez-Valverde, M.A., M.A. Cabrerizo-Vílchez, P. Rosales-López, A. Páez-Dueñas and R. Hidalgo-Álvarez. 2002. Contact angle measurements on two (wood and stone) non-ideal surfaces. Colloids Surf. Physicochem. Eng. Aspects 206:485-495.

Soil Moisture Systems (SMS). 2006. Tension Infiltrometer. [online] Available: http://www.soilmeasurement.com/tension_infil.html. (Accessed: May, 2009).

Taumer, K., H. Stoffregen and G. Wessolek. 2005. Determination of Repellency Distribution Using Soil Organic Matter and Water Content. Geoderma 125:107-115.

Tillman, R.W., D.R. Scotter, M.G. Wallis and B.E. Clothier. 1989. Water repellency and its measurement by using intrinsic sorptivity. Aust. J. Soil Res. 27:637-644.

Verheijen, F.G.A. and L.H. Cammeraat. 2007. The Association Between Three Dominant Shrub Species and Water Repellent Soils along a Range of Soil Moisture Contents in Semi-Arid Spain. Hydrol. Process. 21:2310-2316.

Wallach, R. and E.R. Graber. 2007. Infiltration into effluent irrigation-induced repellent soils and the dependence of repellency on ambient relative humidity. Hydrol. Process. 21:2346-2355.

Wallis, M.G. and D.J. Horne (1992). Soil water repellency. Adv. in Soil Sci. 20, 91-146.

CHAPTER 3 - X-RAY COMPUTED TOMOGRAPHY OF DYNAMIC SOIL WATER REPELLENCY: OPPORTUNITIES, CHALLENGES, AND FUTURE DIRECTIONS

3.1 Introduction

Many pore scale phenomena are largely difficult to observe and measure. When dynamic, these phenomena present even greater challenges to developing mechanistic linkages and insights. Understanding these pore scale phenomena and being able to make direct observations at that scale, are however, important for gaining insight into complex and dynamically wettable pore spaces and effects on infiltration over larger scales. Internal examination of how complex pore scale processes align with and diverge from traditional conceptual models of fluid flow and wetting behaviours in porous media can help to inform on processes across a much larger range of scales.

As a non-destructive tool for observations of soil structure, pore connectivity, tortuosity, and other pore scale phenomena, x-ray microtomography (μXCT) has gained substantial ground in recent years through work using monochromatic synchrotron μXCT found in national laboratories and polychromatic light source bench top scanners (Mooney, 2002; Helliwell et al., 2013; Armstrong et al., 2015; Taina et al., 2008; Ketcham and Carlson, 2001). While synchrotron sources are fast and generate high resolution scans (<1 μm resolution), access is limited (Helliwell et al., 2013). Bench top scanner systems are a more accessible alternative with increasing usage in a variety of institutional research settings. This has facilitated a large expansion of research and insights into scanning a variety of geomaterials in fluid resource applications that include oil & gas and the hydrologic sciences (e.g. Taina et al., 2008; Al-Raoush and Wilson, 2005; Wildenschild and Hopmans, 2005; Herring et al., 2013; Brown et al., 2014; Armstrong et al., 2015; Wang et al., 2011).

What is most unique regarding scanning near surface geomaterials (soils) is the complex nature of their physical/chemical/biological makeup. A range of materials with significant differences in atomic densities can occur within a given sample. Atomic number is a primary determinant of contrast between different scanned features as it defines the attenuation coefficient (of x-rays) in any particular scan as described by (eq 3.1):

$$\mu = 5\rho N_A 10^{-28}\left\{0.587\exp[-0.028(E-30)\} + 1.25\frac{Z_{ef}^{2.0}}{E^{1.9}} + 9.8\frac{Z_{ef}^{3.8}}{E^{3.2}}\right\} \qquad \text{(eq. 3.1)}$$

where μ is the attenuation coefficient, ρ is the density of the investigated object, N_A is Avogadro's number; E is the X-ray energy in keV, Z_{ef} is the effective atomic number of the sample, f_i is the electron concentration of the ith component of the sample (Duliu, 1999). It describes that for heterogeneous media, attenuation coefficient can be variable within a sample depending on both atomic number and the density of the investigated material (Duliu, 1999).

Beer's Law describes how incident x-rays on a scanned object are attenuated before detection on a scintillator (detector) as:

$$I = I_0\exp(-\mu x) \qquad \text{(eq. 3.2)}$$

where I_0 is the integral current of incident X photons (at a detecting source), I is the integral current transmitted by the sample, μ is the linear attenuation coefficient of the sample, and x is the sample width (Duliu, 1999).

Multiple scans at different energies can be additionally useful for isolating particular materials or mineral differences (Helliwell et al., 2013). This is especially the case when organic (low atomic density) and mineral (relatively higher atomic density) exist within a single sample, as would be in the case for peds, aggregates and/or unconsolidated near surface soils with significant organic content (Taina et al., 2008; Wang et al., 2011).

Scanning in primarily organic soils, which express less sample composition heterogeneity, also present challenges in scanning environments because of low or largely quantitatively indistinguishable differences in atomic density. Atomic density is based most substantially on the molecular weight of elements that are found within a given material; with organic, air, and water existing within a similar range of atomic densities given their high elemental position (makeup) on the periodic table. This generates significant overlap in resultant intensity values (often measured in Hounsfield Units) between air, water, and OM (litter, duff, humus) in generated scans (Helliwell et al., 2013). Medical scanning has a longer history of dealing with phase contrast in multi-low-density-feature environments, however, scan resolutions in those applications provide more macroscopic visualizations of target features / materials (Ketcham and Carlson, 2001). Generating high resolution scans at the pore scale across variable materials, is thus, a pending challenge in soils research with significant opportunity to generate complex insights. Consequently, few existing approaches that facilitate quantitative analysis via segmentation methods are available for soil materials with a significant organic component.

Significant differences in attenuation coefficients (a.k.a. phase contrast) are what allow researchers to computationally quantify a range of pore scale phenomena that include pore/particle size distributions, water distribution, macropore structures, wettability characteristics, interfacial tension properties (curvatures), and biofilms (Wildenschild and Hopman, 2005; Helliwell et al., 2013; Taina et al., 2008;). In the presence of significant overlap in x-ray attenuation between phases in water, air, and soils, the primary approach to facilitate computational phase determination and achieve good phase contrast is to chemically increase the electron density in one of the phases (Helliwell et al., 2013). Contrast agents that increase the attenuation of infiltrating fluids are favoured, though it is not clear whether these approaches alter wettability and/or affect the behaviour of infiltrating fluids on non-wettable surfaces and/or in microporous organic soils which are apt to absorb fluids. Recent work has shown the advantages of metal based staining agents such as those used in medical sciences (Van Loo et al., 2014), however in dynamic wettability studies, the staining process (of soil particles) itself imposes a potentially biased response to the introduction of water by changing the surface properties of the hydrophobic media. For example, Brown et al. (2014) showed changes in wettability of glass beads at the introduction of an oil based solution into sintered columns over multiple scans in a μXCT environment. It is therefore important to identify opportunities for scanning in the presence of dynamically wettable media with complex and largely unobserved pore scale wetting behaviours. To our knowledge, there are no papers in the peer-reviewed scientific literature that report on three-dimensional imaging of dynamically wettable natural soil materials.

This chapter presents a visual, qualitative inquiry into physical pore scale wetting phenomena in complex dynamically repellent materials and provides observations on materials and fluid behaviours while evaluating opportunities and limitations of μXCT approaches in these media. The work presented here is the first of its kind and constitutes a significant move forward including unique proof of concept images of fluid behaviours in such systems.

3.2 Materials & Methods

3.2.1 Materials

Materials used in this study were collected from post-wildfire sites in Northern Ontario, Canada. Five different samples from three different fires were used. Sample collection and preparation methods of (two) samples collected from Halfway Lake Provincial Park (HLPP) are described in detail in Chapter 2. Two key materials from HLPP were targeted during this scanning work, Char and Brown materials exhibited significantly different repellency properties. Char materials were identified as being hydrophilic or wettable, with essentially undetectable differences in infiltration behaviours compared to wettable mineral soil behaviours (collected at the same site). In contrast, Brown materials were identified as exhibiting long duration dynamic soil water repellency and low fractional wettability. Three additional materials were collected from two Sudbury fires (SUD1 and SUD2) that burned in 2011. Sampling for SUD1 and SUD2 occurred (Oct 2-5, 2011). The SUD1 fire burned on a rocky outcrop hilltop area outside of the city of Sudbury (on Aug. 28-30, 2011). SUD2 was an active fire at the time of the sampling trip (Oct. 2-5, 2011) and was sampled on the same day the fire was considered out and the site accessible. SUD1 sampled materials were mineral in nature, having been sampled in small amounts by hand from an A/B Horizon; it was repellent in binary water drop penetration tests performed *in situ*. While the fire area was small, <0.1 ha, nearly 20cm of duff (LFH) consumption was observed at this fire site. The SUD2 fire, in contrast, burned in a relatively low lying area, on Oct. 3-5, 2011 within city limits. It was a low to moderate intensity fire having burned an area <.1 ha and the duff (LFH) layer remained largely intact. Vegetation consisted of suckering shrubs, trembling aspen, and juniper. Two charred materials (SUD2Phobic and SUD2Philic) were collected from SUD2. They were organic, surface duff materials and showed signs of varying combustion and repellency during binary water drop infiltration tests. One of the two charred materials (SUD2Phobic) at this site, in contrast to all charred materials collected at HLPP exhibited strong signs of repellency. MNR staff noted that this is common on fire sites in Ontario (Chris Johnson, personal communication). Photos of materials collected from SUD1 and SUD2 prior to column packing are shown in Figure 3.1 a-b.

All samples were air-dried prior to scanning, with Sudbury fire samples being allowed to air dry for approximately one month. No other material preparations were made prior to column packing. Materials were dry packed by hand into columns (6.42mm ID x 20 mm length) which was fitted to the support stage used for the µXCT scanner.

Samples were spooned into the column and the sides of the column were tamped to increase bulk density inside the column. Large organic materials present in the majority of samples underwent some destruction during the packing process.

Figure 3.1 a-b showing a) Mineral A/B materials from SUD1 b) PhobicChar materials from SUD2

3.2.2 μXCT Scanning and Image Processing

Twelve scans were carried out using the benchtop μXCT housed in and maintained by the School of Mechanical, Industrial, and Manufacturing Engineering at Oregon State University in Corvallis, OR. The benchtop system is comprised of a polychromatic cone-beam FeinFocus FXE-160.20 X-ray source and 16-bit (2448 x 2084 pixel resolution) CCD camera (Point Grey Research, GRAS-50s5 M-C) which is coupled to an intensifier (Medelex Model HXS-93/P5) (Herring et al., 2013). A machined support stage and fitted socket secures samples during scanning. Applied scan energies were 26 and 32 kV / 269 and 244 μA and generated a scan resolution of 13 μm. Taina et al. (2008) compiled instrumentation parameters for visualization of organics using CT. The energies used in this study are lower than commonly observed for lower resolution scanners and were selected for each sample when contrast / histogram spread were maximized, with samples having a greater mineral content using the higher energy, and organic based materials using the lower. This is advantageous since low-energy x-rays are more sensitive to differences in composition (Ketcham and Carlson, 2001). Each sample scan underwent 360^0 of rotation in 1440 increments. Four images (looks) were averaged at each increment to reduce noise and enhance image quality. Scan times lasted approximately 1.5 hours.

All columns were scanned under dry conditions and then followed by scans under wet conditions. A 10% (w/w) KI and water solution was used in all wet columns except for the SUD2Phobic column which was scanned using deionized water and ethanol. For wet scan sequences, a small volume of fluid (DI water: 0.2 ml for SUD2Phobic, KI water:

0.4 ml for SUD1 materials, and 0.3 ml for all others) was placed at the top of the column and allowed to infiltrate for two hours prior to the wet scan (Figure 3.2). For the SUD2Phobic column, an additional small volume (0.1 ml) of 95% denatured ethanol was applied after the wet scan and allowed to equilibrate for five minutes before a third scan was conducted on this sample. Given that ethanol is considered a wetting fluid in hydrophobic materials, five minutes of wait time was used before the water + ethanol scan began. It was assumed that this would be sufficient time for the fluid in the column to mix and equilibrate with water in the column. A slowdown at the wetting front caused by the mixing of water and ethanol were not considered at this point in the experimental design.

Raw sinograms generated by the μXCT were distortion corrected using a grid based algorithm in ImageJ (freeware). Corrected sinograms were then normalized for beam intensity fluctuations to light and dark flat-field images and reconstructed into stacks of (approximately 1,200) 2D slices using Octopus 8.5 software (inCT, Ghent, Belgium). No corrections were made for ring artefacts or beam hardening, which generated higher values (of approximately 30 intensity units of 255 total) at the column wall compared to the interior zones of the column in materials with the same composition. All subsequent image processing and 3D visualizations were performed using ImageJ. For our purposes, 2D image slices were enhanced using the Enhance Contrast feature in ImageJ and a median filter with a 1 pixel resolution. Brightness and Contrast were also adjusted (though this did not change pixel values) prior to conversion from 16-bit (65,536 greyscale values) to 8-bit (256 greyscale values) which were required for 3D visualizations. Three-dimensional projections were then generated using (required) 8-bit converted images. These processes decreased noise and increased the visual distinction of resolvable features.

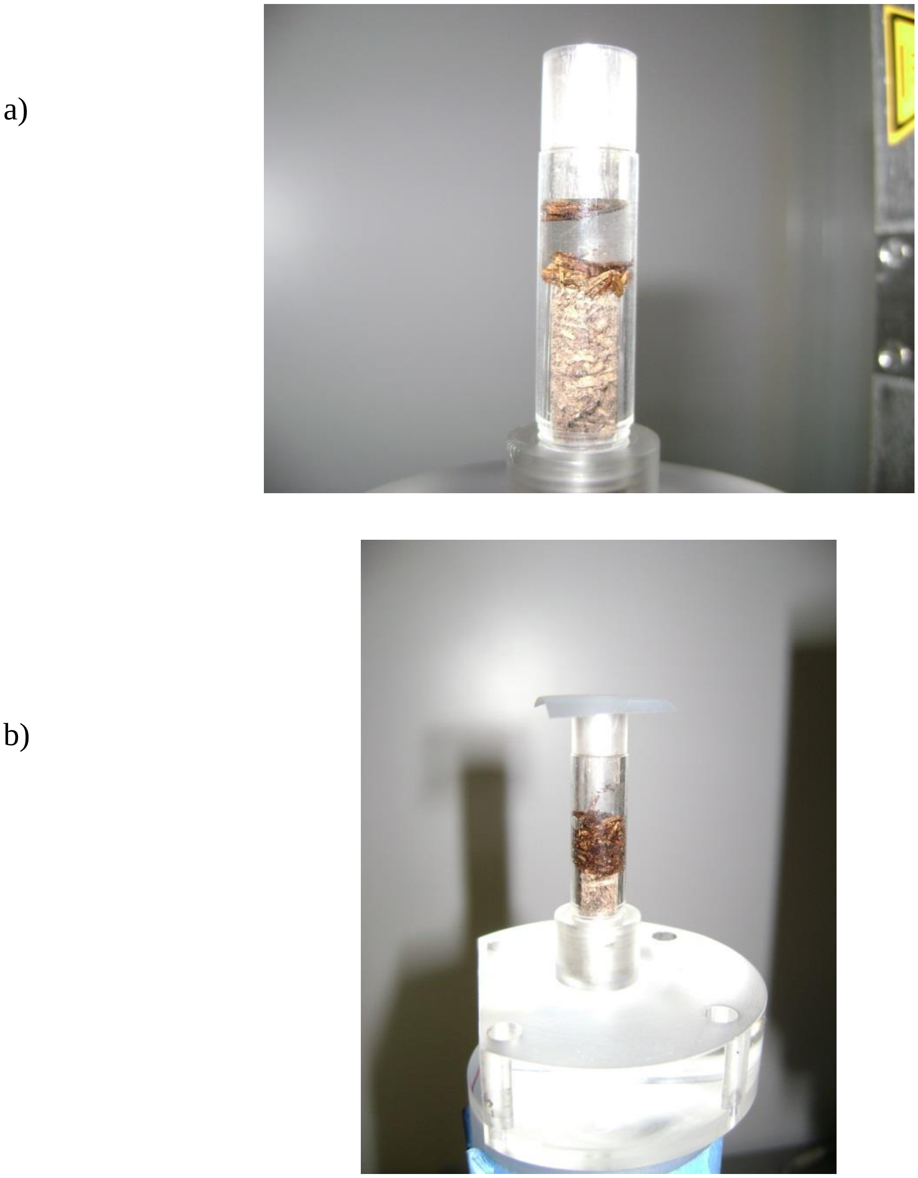

Figure 3.2 a) Showing prepared column shortly after 0.3 ml of KI doped water applied to the top of the column and b) showing same column 10 minutes later. Brown (hydrophobic) HLPP materials are featured. Column ID: 6.42mm

3.3 Results and Discussion

Much information can be gained through an interior examination of the three-dimensional visualization of structural features found in scanned columns. Quantitative analysis in a 3D scanning environment is typically based on the separation of features found in the intensity value histogram for given scans (Ketcham and Carlson, 2001). To accurately and reliably distinguish features, multiple and separate peaks need to be present in the intensity histogram (Helliwell et al., 2013). For these columns, a unimodal, or slightly bimodal histogram was generated in all cases, which means that the distribution of intensity values for air, material, and water overlapped significantly, and thusly, were not quantitatively segmentable.

To facilitate visualization of the interior of the column, a ~90° wedge was removed computationally from the stack of images within a given scan prior to the generation of 3D projections in post-processing. The first image in each figure for a given material/fluid combination is centred on the rotation axis of the wedge. Subsequent images show the exterior extent of soil materials at the column wall interface. A vertical line has been drawn to distinguish the 45° faces on either side of the wedge. Additional lines have been included to demarcate the column wall interface at that (wedge) rotation. Each subsequent image represents a ~90° clockwise rotation around the centre line to present the 360° rotation of scanned columns. To facilitate qualitative analysis, certain structural features within paired scans are visible in these rotations between dry and wet scans. These appear in fixed 2D images of 3D reconstructed projections in this section. Animated gifs, which show continuous and full rotations at 12 frames/s are available through the McMaster University Open Access Dissertations and Theses collection and can be located by searching for this dissertation document by the author's last name or document title (https://macsphere.mcmaster.ca/).

Figures 3.3 and 3.4 show Halfway Lake Provincial Park dry and wet Brown materials (HLPPBrown), respectively. These materials were identified as having relatively slow dynamics and low (repellent) fractional wettability in previous work (Beatty, 2009). Most notably, there is good structural information available in the dry scan. This comes as a consequence of the scanner resolution in relation to the resolvable features within the soil column such that partial volume effects do not interfere with the generation of visibly identifiable interfaces between air and individual soil particles. While air is not completely resolved across the full length of the column (i.e. it should have a value of 0 and appear as completely black within scans), there is still good delineation between air and structural elements in the soil. Binary segmentation was evaluated for its utility in these materials and found not useful in isolating organic material from air in a consistent manner and was abandoned as an analysis technique early on.

The wet column (Figure 3.4), which includes 0.3 ml of water doped with a 10% (w/w) KI solution shows enhanced contrast in water, individual soil particles, and void space. Void spaces generate visibly transparent (value <10) zones in 3D projections, whereas in the dry columns, voids register with values ~50. It is interesting to note that water is the most well resolved feature, exhibiting relatively high intensity values (130+).

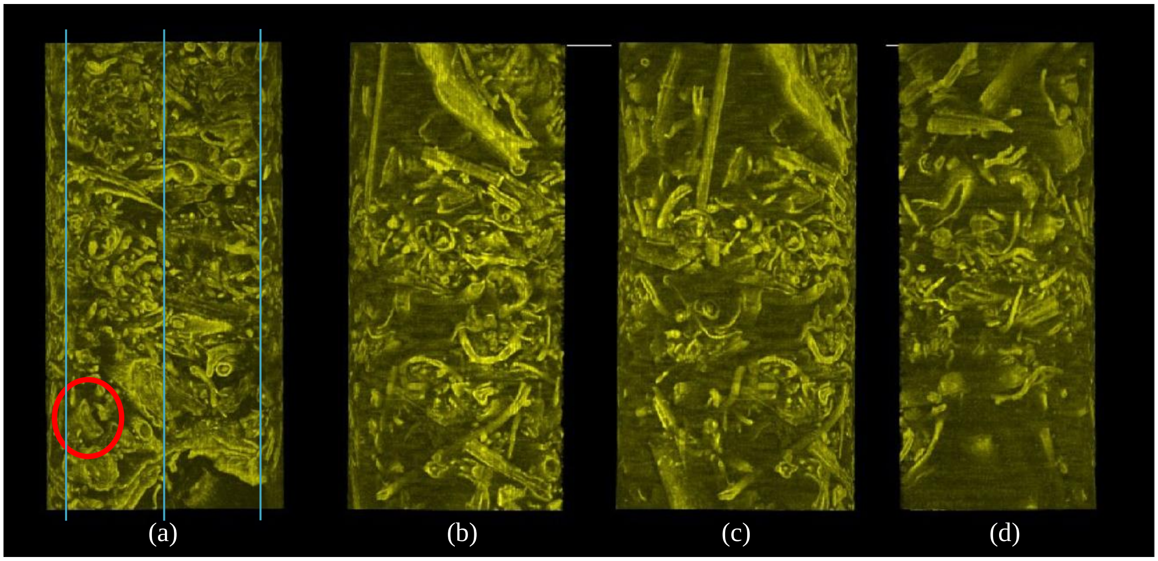

Figure 3.3 HLPPBrown hydrophobic material (dry scan), a-d represent 90^0 clockwise rotations (for 360^0). Brighter zones represent more attenuating materials and darker zones are less attenuating. Red circle referenced as microporous zones in the column. Blue vertical line represents the centre of the wedge cut and edge of column.

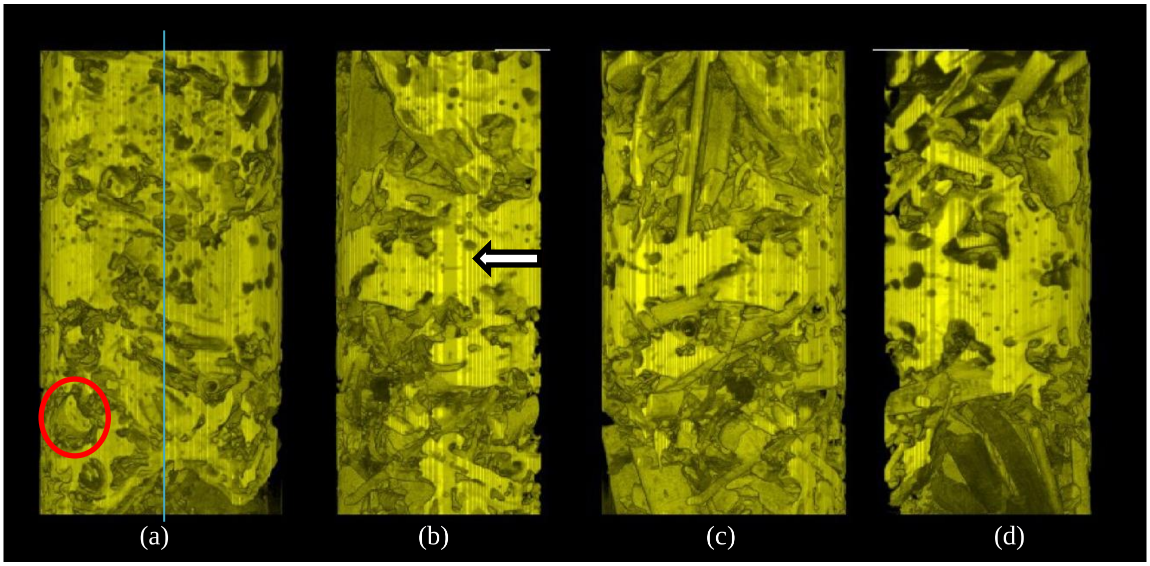

Figure 3.4 HLPPBrown hydrophobic material (wet scan) with 0.3 ml of water doped with a 10% (w/w) KI solution after two hours of equilibration time. Red circle indicates wetted microporous zone in the column. Presence of vertical lines generated in 3D projections indicated by arrow.

Small amounts of entrapped air are visible throughout the column, both within the wedge face (Figure 3.4a) and at the column wall (Figure 3.4a-d). Comparatively, soil structural elements exhibit slightly lower values (60-170) overall, but within the ranges observed for water. In addition to wetting on the bodies of soil particles, it is interesting to note that these scans show direct evidence for the uptake of water into microporous structures within individual OM particles. This is most readily observable in, for example 1) the wedge image where linear features are cut as indicated by the red circles and 2) the overall marked enhancement of resolved boundaries between individual soil particles and pore space in Figure 3.4 b-d.

In terms of fluid behaviours, after 2 hours of wetting and 1.5 hours of scan time, water is distributed in two primary zones. At the column wall, while wetting is visible along the length of the column (Figure 3.4b), water is primarily located between more closely compact, and smaller particles at the centre of the column. Vertical lines through the water blobs are an artefact of the 3D reconstruction / projection generation and are visible in greater or lesser degrees in nearly all figures, but most visible in wet areas. The interior of the column (Figure 3.4a) reveals that wetting is most often associated with clusters of particles, and structural features. This reflects and may indicate a preference towards film flow type wetting over the course of ~3.5 hours.

Actual wetting processes are difficult to detect in these series of images. Recall that these materials were identified had low fractional wettability with slow dynamics in earlier work. Large unfilled zones are visible in these scans and there is a tendency for wetting in small pore spaces and along particle surfaces in the interior of the column

(Figure 3.4a). This indicates that these materials are wetting up within a few hours' time in a manner consistent with dynamic fractional wettability observed in earlier infiltration testing work. The small volume of water applied at the surface prior to scanning may not have exceeded displacement pressures of larger pores, which would have filled the largest pores first. It is possible that these larger void zones were filled first (due to initial positive pressures of the applied fluid), and then subsequently emptied over time as water moved along particle interfaces and into smaller microporous zones that became wettable over time.

Figures 3.5 and 3.6 show scan rotations for Char materials from Halfway Lake Provincial Park (HLPPChar). These materials were identified as hydrophilic in drop tests in earlier work (Beatty, 2009). Like HLPPBrown dry columns (Figure 3.3), void space is not transparent throughout the column. The greatest contrast occurs in the middle section of the column, which may be related to the nature of the cone beam and interactions with air/organic materials at the periphery of the beam along the length of the column, with the centre generating the greatest resolution and fewer scanning artefacts.

Overall, HLPPChar columns contain a larger portion of (apparently) mineral soil materials with higher attenuation properties that absorb more X-rays which yield brighter zones. In HLPPBrown columns (Figure. 3.3 and Figure. 3.4), soil particles tended to have a sinuous or linear characteristic whereas HLPPChar columns show a variety of sizes and mineral particle shapes ranging from flat to sub-angular and longer more sinuous organic components. The scans here indicate that sampling resulted in the mixture of mineral and combusted organic materials. This makes empirical sense since HLPPChar materials were

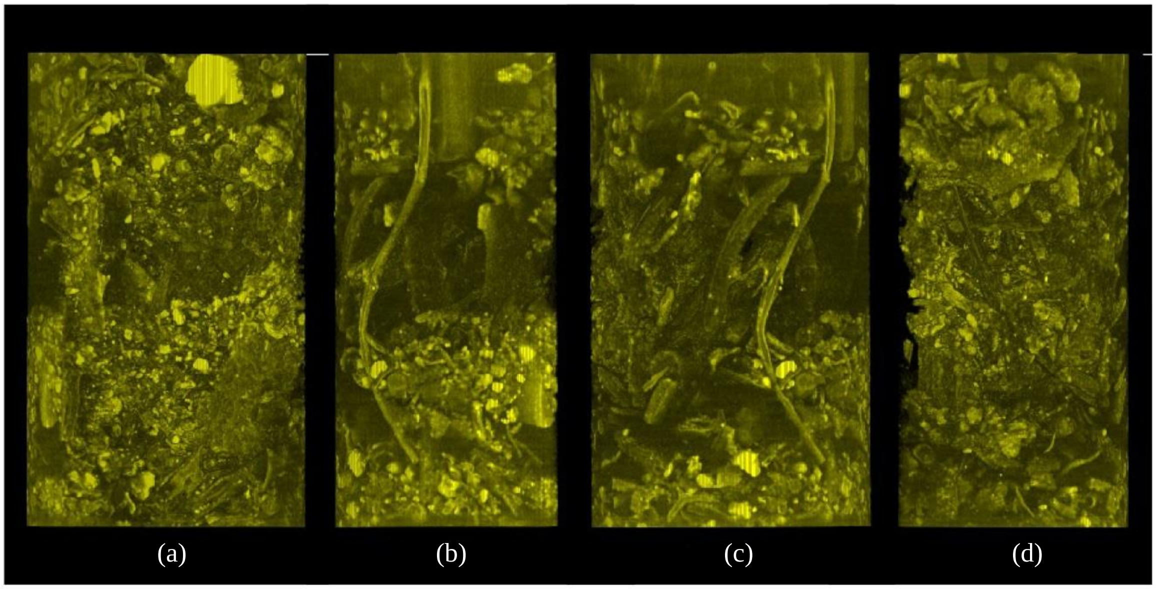

Figure 3.5 HLPPChar hydrophilic material (dry scan)

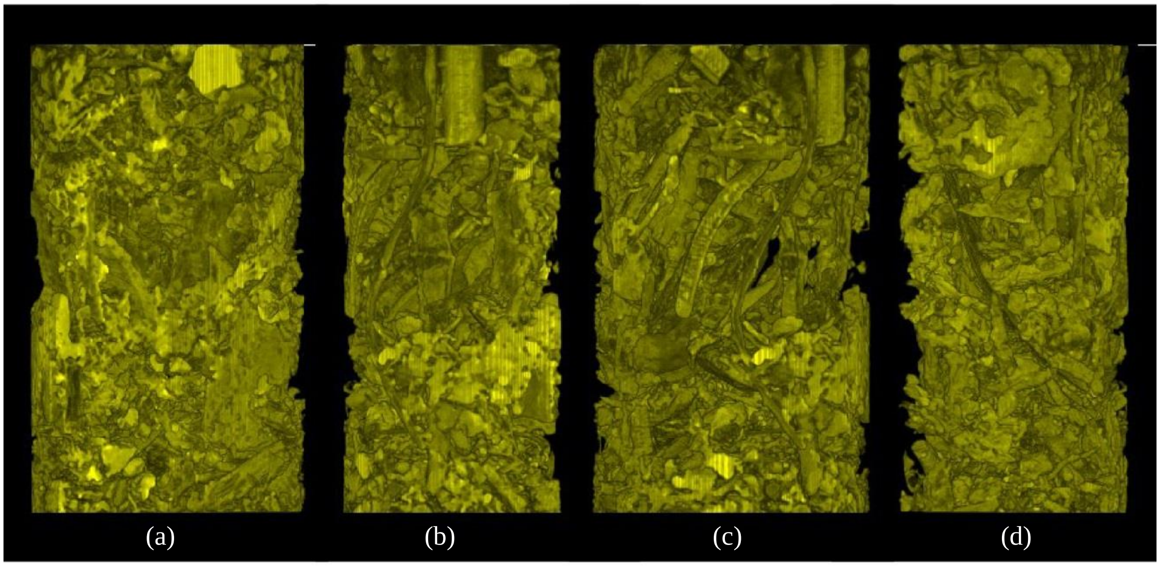

Figure 3.6 HLPPChar hydrophilic material (wet scan)

sampled much closer to subsurface mineral horizons than HLPPBrown materials. In wet scan rotations, this mineral component is not as pronounced. This likely comes as a consequence of the attenuation coefficient of the mineral particles in relation to the attenuation coefficient of the doped (KI) water and the microporosity of the interior organic materials which become more visible in the wet scan. Akin to HLPPBrown wet scan rotations, definition of overall features and contrast between void and soil particles are enhanced overall in the presence of the KI solution. It is interesting to note that fluid blobs are much less pronounced and blob zones are smaller along the length of the column than visible in the HLPPBrown material scans and likely come as a consequence of the wettable microporous structure of the charred materials. It is probable that increased wettability of these char materials facilitated the uptake of the KI solution into soil micropores preferentially, as these would be a source of the smallest pores in the column.

While entrapped air is also visible within blob zones, blob zones themselves are not as large or nearly as distinguishable by intensity value as observed in the HLPPBrown columns. This indicates that the averaged voxel value of a given wet soil particle is being affected somewhat equally by the attenuation properties of the soil particle and the doped water taken into the particle structure. One could expect that HLPPBrown materials would exhibit a similar uptake of water into microporous structures. What this suite of scans from both materials indicates is that even at ~3.5 hours of wetting time, HLPPBrown materials are not as fully wetting as HLPPChar materials.

Figures 3.7 and 3.8 show scan rotations for *hydrophilic* SUD2Philic materials. These materials can be characterized as having a mixture of both organic and mineral soil particles, with the majority of mineral materials distributed primarily in the bottom half of the column. Mineral particles are granular in texture overall, and organic particles exhibit more variability in size and shape. Large sinuous organic particles are less prevalent in these scans than in other material columns discussed previously. Similar to previous scans, vertical lines that are an artefact of column reconstruction / 3D projection generation are most visible in lighter (wet) zones with intensity values in the range of 175+.

All materials in the SUD2Philic wet scans (Figure 3.8) appear wettable, with fluid behaviours driven by wettable capillary action vs. non-wettable capillary behaviours. Scans, which include 0.3ml of distilled water show continuous, albeit cloudy water blob zones which seem to associate with the presence of organic particles, a function of their relative position at the top of the column, where mineral particles appear to be less prevalent. Wetting occurs along the entire length of the column, with the interior being more heavily wetted in the top half of the column (Figure 3.8a). Water is visible along the length of the column wall zone as well and associates with both organic and mineral materials (Figure 3.8b-d); down to an apparent capillary barrier (red line) comprised of primarily organic materials. Features are not as well resolved as observed in HLPP materials, which is likely a function of the size of resolvable features in SUD2Philic materials compared to the scanner resolution, and the higher attenuation of mineral materials compared to organics (Figure 3.8). While dopant was used in these materials, it

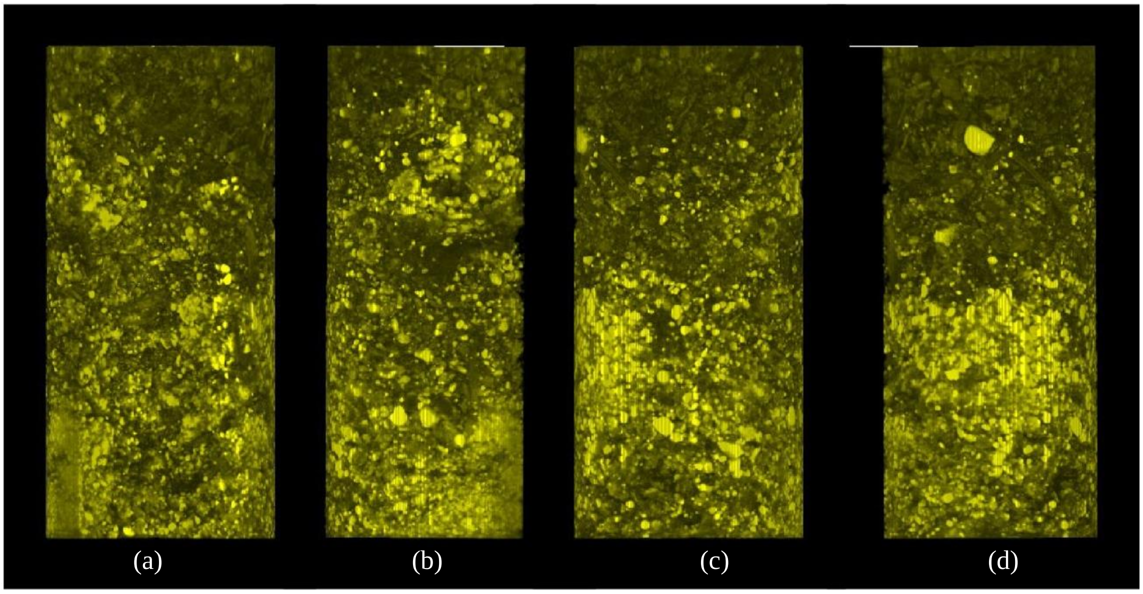

Figure 3.7 SUD2Philic hydrophilic (dry scan)

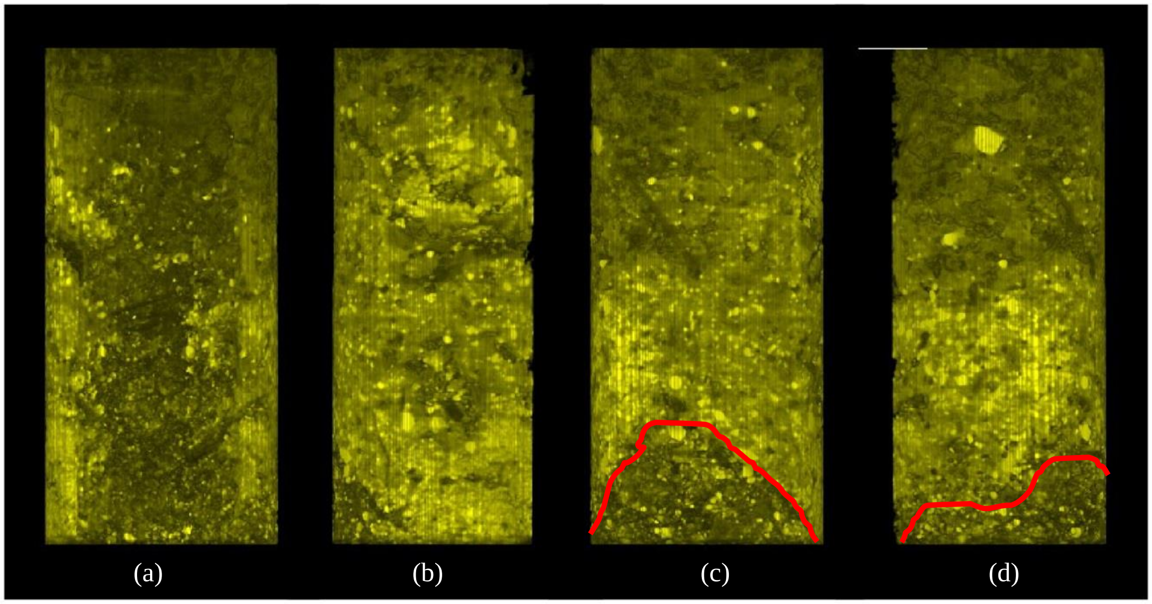

Figure 3.8 SUD2Philic hydrophilic (wet scan). Red line indicates suspected capillary barrier

appears that the mineral materials are attenuating a greater portion of incident x-rays, and assigns those materials a higher relative intensity value (than OM in relation to doped water). A higher concentration and/or scan energy may have helped to distinguish water in the column, but would have affected the visualization of the porous media. Figure 3.9 shows attenuation properties at variable scan energies for different dopants. It reveals that while the KI dopant is more attenuating than water (and OM, and air), greater phase contrast to mineral materials would require a higher scan energy (approximately 33 keV) than used here to reach its absorption edge.

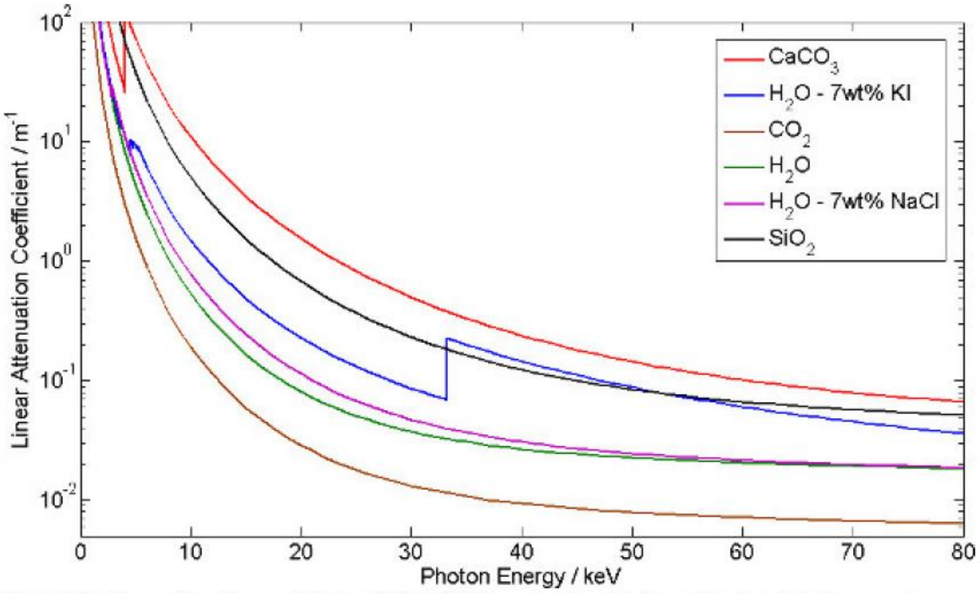

Figure 3.9 Linear attenuation coefficients of different fluids and rock materials as a function of photon energy (from Andrew et al., 2015).

Figures 3.10, 3.11, and 3.12 show scan rotations for *hydrophobic* SUD2Phobic materials collected at the SUD2 fire site. As evidenced in the form of large sinuous and flat surfaces and in contrast to the *hydrophilic* scans (Figure 3.8 and Figure 3.9), these columns contain a much larger proportion of structurally intact organic materials. While some mineral material exists, this column is primarily organic in composition. Similar to previous dry scan cases, void space, while visually transparent in the interior of the column (Figure 3.10a), is associated with higher low intensity values (~50-75) along the column wall (Figure 3.10b-d).

The wet scan (Figure 3.11) for this material showcases the effects of repellency most noticeably than all other scans. Wetting occurs primarily along the column wall (Figure 3.11b-d). This is consistent with studies in which water preferentially infiltrates along the column wall where pores are largest when positive pressures are applied via ponded water at the surface (Feng et al., 2001; Wang et al., 2000). Pore areas as seen in the interior of the column in Figure 3.11a do not show continuous water filling small pores first and then larger void zones as would be expected in a wettable media. Instead, water is residing primarily in larger void spaces adjacent to the column wall and secondarily in smaller pore spaces toward the interior of the column. This provides direct evidence of preferential wetting in larger pore spaces in water repellent media and indicates that repellency is present in these materials during ~3.5 hours of exposure to water. A fully wetting medium, as was observed in hydrophilic SUD2Philic and HLPPChar Dry/Wet comparisons exhibited much smaller amounts of interstitial water, having, presumably, been taken up into the microporous structure of the organic

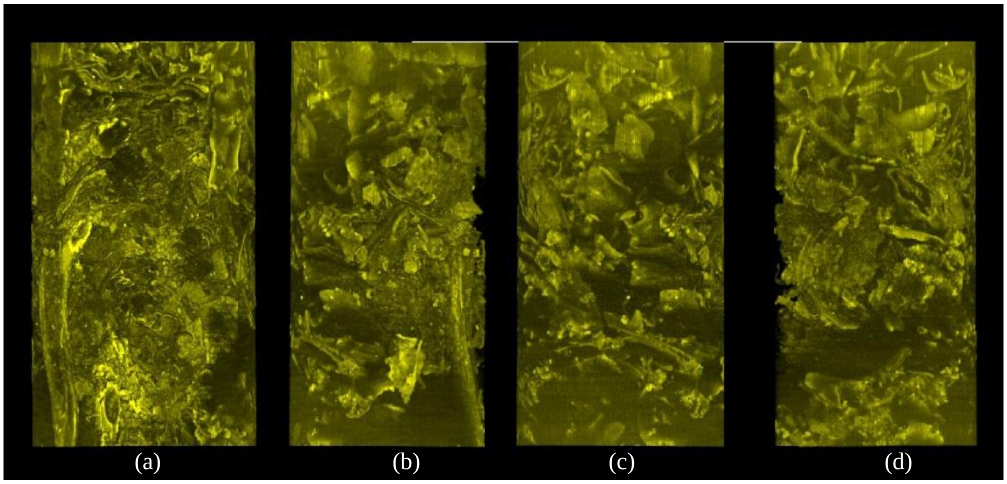

Figure 3.10 SUD2Phobic hydrophobic (dry scan)

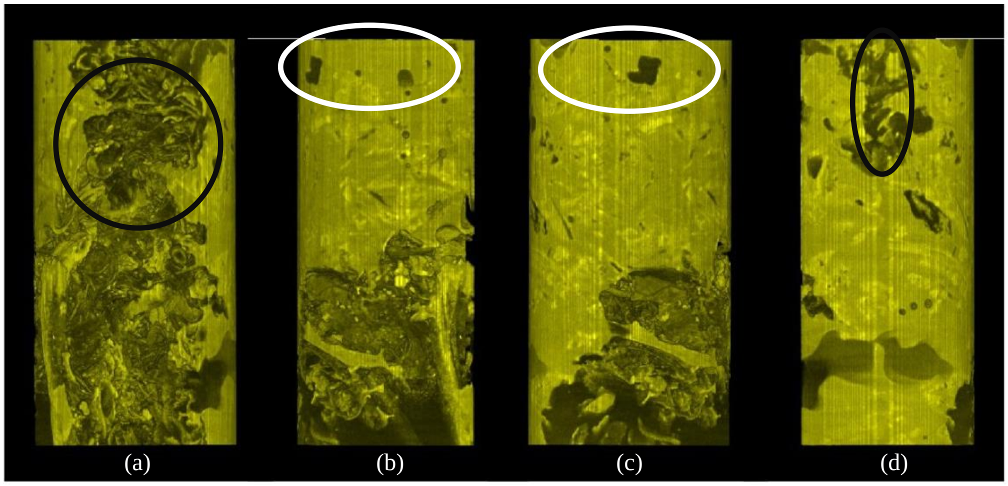

Figure 3.11 SUD2Phobic hydrophobic (wet scan)

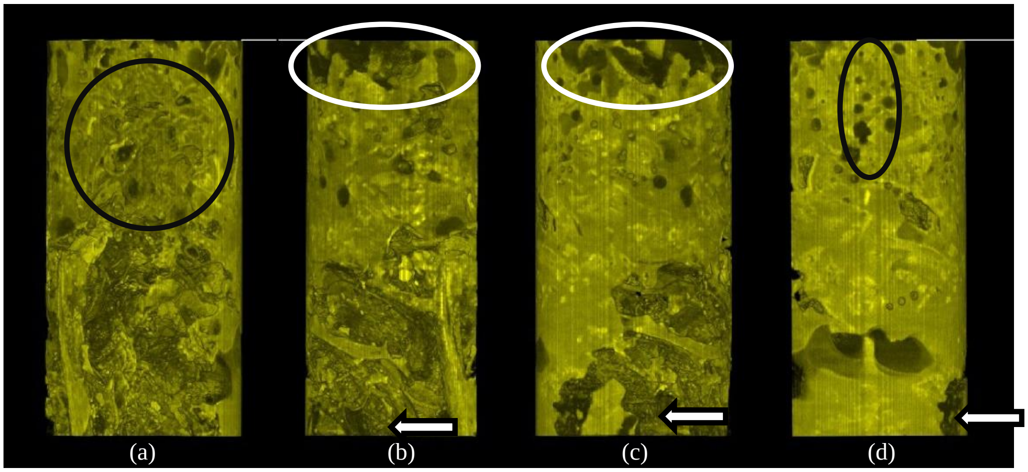

Figure 3.12 SUD2Phobic hydrophobic (water + ethanol scan)

materials. While contrast is enhanced overall in this scan (even without the KI dopant), it is likely a consequence of wetting along the surfaces of particles and not into the deeper microporous voids of the soil materials themselves.

Figure 3.12 includes the application of 0.1 ml of 95% denatured ethanol, applied after the wet scan. Three significant things occur with the application of ethanol. First, ethanol enhances wetting in the column, most notably in the interior of the column. Second, the additional volume of fluid, in addition to filling pores, also serves to drain pores and increase the number of entrapped air bubbles (most visibly at the column wall). Last, the volume of ethanol reduces overall intensity values in the column, presumably because there is a greater volume of attenuating material (i.e. fluid) in the column.

Enhanced wetting caused by the introduction of ethanol can be most readily observed in a comparison of Figures 3.10, 3.11 and 3.12. A few key things occur with the application of ethanol. First, ethanol makes visible certain structural features that are resistant to wetting using water alone, particularly in the bottom portion of the column (white arrows in Figure 3.12). The increased prevalence of entrapped air and increased contrast of features near void spaces along the column wall, which occur along the entire length of the column, indicates that ethanol is being distributed throughout the scanned column. Second, it shows how a wettable fluid preferentially fills non-water-wetting pore spaces and materials (black circles in Figures 3.11 and 3.12). It cannot be ruled out that the same volume of water could have filled the spaces now occupied by (presumably) ethanol in the interior of the column. However, Figure 3.3 and 3.4 show that over the two hour equilibration time, wetting toward the interior of the column can occur in even persistently hydrophobic materials. Since the interior of the column in Figure 3.12 is occupied by fluid only after the application of ethanol, it can be said that the centre of the column is remaining fractionally non-wettable over the duration of the scan procedure (in Figure 3.11). Lastly, pores at the top of the column drain which likely occurs as a consequence of a reduction in surface tension and related effects on capillarity (white circles in Figures 3.11 and 3.12). Surface tensions for a 33% mixture of ethanol by volume are approximately 40 dynes/cm lower than water at 25 °C. This serves as a reference for the relative difference in capillary strength of the interfaces within the column under these infiltration conditions.

The reduction in overall intensity caused by the introduction of undoped ethanol is not particularly significant for this application, but it would be relevant for work involving quantitative analysis and could serve to show how well ethanol mixes with water already in the column. For future work, another doping agent mixed with ethanol that generates attenuation coefficients above/below the peak energy threshold could develop two key insights: 1) the degree of mixing between the fluids, and 2) provide evidence for sludge effects that may be occurring as a consequence of mixing at the ‘front’. Over the course of 1.5 hours of scan time, it is expected that even mixing of both fluids would occur in hydraulically connected zones. Scanning approaches that yield quicker scan times may be required to track this reliably.

Figures 3.13 and 3.14 show scan rotations for *hydrophobic* mineral soil materials collected at the SUD1 fire site. These scans provide, most readily, visual compositional information related to particle distributions within the column. The porous matrix itself,

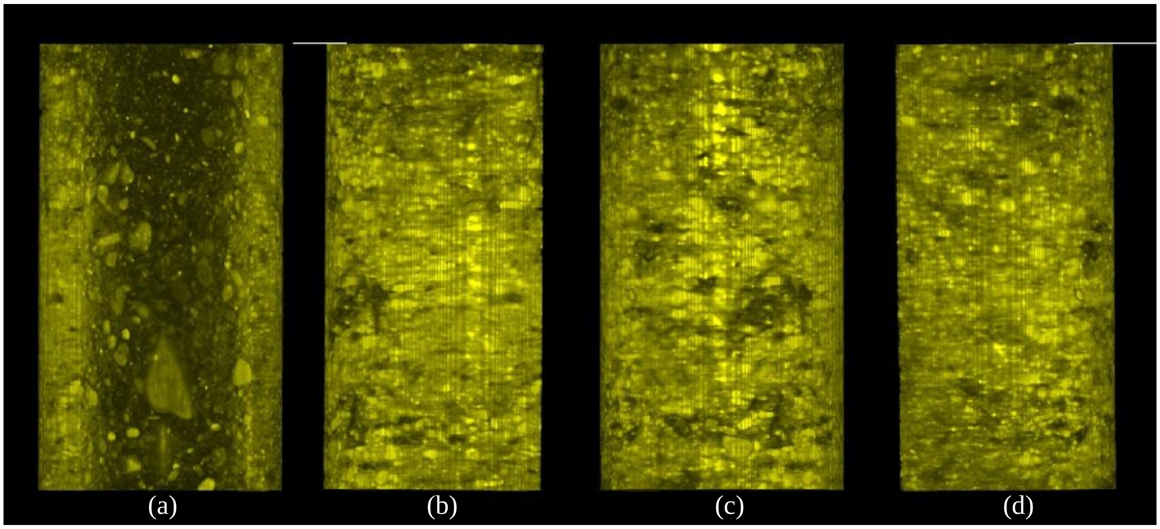

Figure 3.13 SUD1 AB Horiz hydrophobic (dry scan)

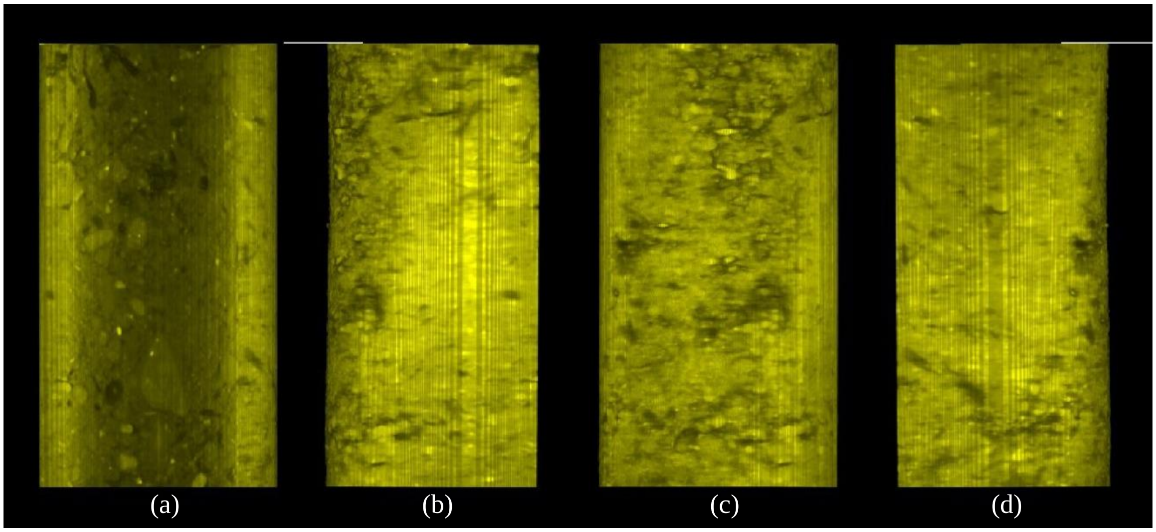

Figure 3.14 SUD1 AB Horiz hydrophobic (wet scan)

as observed in Figure 3.13 is comprised mainly of sub-resolvable mineral grains with larger sub angular and sub-rounded granular media. Darker zones can be identified as porous zones, particularly in Figure 3.13b-d, however, the interior of the column is much darker overall in relation to the scanned features at the column wall interface. This is an important limitation of the method and comes as a consequence of beam hardening, a scanning artefact in which the outermost scanned elements attenuate a higher amount of energy than interior scanned elements that are compositionally similar. This means that darker areas of resolved soil materials in the interior portion of the column should, theoretically, be brighter than they appear. Physical filters are the most effective way to address this scanning artefact, however those techniques were not employed here. Part of the lack of resolution in the interior of the column may also have come as a consequence of the scan energy used in these columns. The less dense organic materials scanned in the previous examples do not generate as much absorption of X-rays, and thus are well resolved across the diameter of the column. More dense, higher atomic weight mineral materials found in these scans may be contributing to lower intensity values in the interior. Nevertheless, larger features within the column provide stable structural references to the overall distribution of both resolvable and sub-resolvable materials in the column.

Figure 3.14 shows the mineral column after the application of 0.4 ml of water. The additional 0.1 ml of water, which represents a 25% increases in the amount of fluid applied was done because of the higher porosity expected in the fine grained materials as compared to samples with much higher OM material contributions.

The presence of water does two things. Water generates a generally cloudy appearance throughout the column, and particularly along the column wall in comparison to the scan rotations in Figure 3.13. It is not clear whether wetting is occurring homogenously throughout the column, and this makes these scans particularly difficult to interpret in terms of wetting processes. The inclusion of water also obscures some of the larger resolved features within the column by visually homogenizing intensity values in all scanned elements in the column. An indirect effect of the water is that the appearance of minor variations in packing are emphasised. These appear as large striated zones and rounded pore bodies (dark areas). These represent mechanically formed pore spaces within the column since materials were loosely packed.

Differences in intensity values between wet and dry scans exist. The same scanned features, which appear in both wet and dry scans could be expected to exhibit no change in intensity between scans. This is in contrast to the organic material scans in which significant microporosity could potentially be filled /unfilled depending on the wettability of the material over the course of scanning and in relation to the absorption properties of the infiltrated fluid. Referenced features between both scans generated a decrease in intensity of ~20 units (of 255 total) in the presence of water. This, coupled with the filling of sub-resolved pore spaces serves to visually smooth out and obscure features visible in the dry scan such that cloudy wetting appears to exist throughout the column. Lightness caused by beam hardening at the column wall may also be influenced by smaller pores and/or looser packing along the column wall. It is not wholly obvious which of these factors are most at play in these scans and are worthy of consideration and evaluation in the pursuit of quantification. This highlights one of the challenges and opportunities of generating insight at the pore scale in small pore/sub-resolvable geomaterial environments. There is significant opportunity for developing linkages between scales of heterogeneity, representative pore volumes, and resolvable pore sizes and distributions through the use of scanning technologies such as this.

3.4 Discussion

3.4.1 Scan quality

Scan quality in a μXCT environment is determined by two key variables: the scanner environment and the materials being scanned. Scanning approaches that facilitate quantitative analysis via the precise locational preservation of scanned features rely heavily on significant differences in attenuation properties (phase contrast) of scanned materials and the ability to resolve partial volume effects (Brown et al., 2014). Scanning artefacts affect the quality of resultant scans and determine the ability with which resolvable features can be analysed quantitatively and/or qualitatively.

Phase contrast, as is necessary for the numerical distinction of features by intensity values is affected by the atomic density of scanned features. Early in the scan study, it became clear that while visual distinction of different phases was feasible, histogram based segmentation techniques and image subtraction techniques to show change detection would not generate meaningful analysis. This was due to 1) lacking phase contrast between water, air, and organic matter and resulting from their comparably similar attenuation properties and 2) imperfect registration of structural soil features within the column between wet and dry scans.

To increase phase contrast in the scans, a KI dopant solution was used. Many of the materials, however, exhibited significant microporosity. The uptake of the KI solution into the microporous structure of organic particles enhanced contrast between soil and air, but was numerically indistinguishable from interpore water. In materials with a larger mineral component and lower overall microporosity partial volume effects affected the overall perceptibility of scanned features.

To enhance contrast and facilitate quantitative analysis in OM materials specifically, employing a ‘doping – drying – rewetting with a different dopant solution’ experimental sequence that serves to deposit KI into the microporous structure of organics may facilitate future quantitative studies in a μXCT scanning environment. Alternatively, applying medical science image processing techniques, which are more sensitive to low atomic density materials such as water and organics, could be useful in future organic matter scanning studies and may be the path forward in studies of this kind.

Partial volume effects develop when multiple scanned features exist within a single pixel / voxel space. The presence or absence of partial volume effects is largely determined by the scanner resolution and the size of features being scanned. This relationship was well matched in samples composed mostly of organic materials and features were well resolved as a consequence, with well-defined structural elements. Mineral materials, however, were largely sub-resolvable and generated 3D projections in which a relatively homogeneous material with larger inclusions of pebbles was observed.

This particular scanning environment was better suited to scanning the larger organic materials.

Scanning artefacts (i.e. beam hardening and visible rings) appeared in many of the 2D image stacks, though these present minimal disruption in the construction of 3D projections and/or interpretation of features since segmentation techniques were not employed. For future studies interested in registration between images and quantitative analysis, steps to remove such artefacts, using physical filters for example, may be useful.

3.4.2 Wettability and dynamic repellency

Tracking changes in wettability in an X-ray scanning environment has been investigated peripherally and only recently in multiphase flow studies (e.g. Brown et al., 2014). Moving interfaces, caused either by changes in wettability or by slow transitioning-to-equilibrium interfaces (relative to scan times) in a wettable environment result in mares tales or whisps between resolved, unmoving features. In the context of our experiments in this scanning environment, the complexity of resolvable structural features meant that the detection of mares tales features in the presence of other moving whispy-looking features in 3D would be inherently challenging. Also, the uptake of the KI solution into microporous structures within organic materials meant that fluid-particle delineations were not always visible in scans of this duration and particularly in relation to cases of more fully wetting fluid/material combinations. Long equilibration (compared to wetting behaviours observed outside the scanning environment) were employed so that wetting/non-wetting behaviours, in a semi-stable or only marginally dynamic environment could be observed and evaluated for change detection.

While visual evidence of rapid dynamic repellency (i.e. mares tales) was not found here, differences in wetting and non-wetting behaviours exist. Differences in wettability were most readily observed in the most hydrophobic materials (SUD2Phobic) which remained largely non-wettable throughout the duration of the wetting equilibration time and scanning procedure time. Water situated along the column wall and was not observed in the interior of the column until the introduction of ethanol, a fully wetting fluid. This was in contrast to more wettable materials where microporous structures absorbed water along the length and across the diameter of the column.

3.5 Conclusions

Dynamic soil water repellency was investigated through the use of a μXCT benchtop scanner system to develop insight into the nature of dynamic changes in non-wettable media at the pore scale. Eleven scans showed a variety of both wetting and non-wetting behaviours in five different materials from post wildfire sites in Northern Ontario.

Scanner resolution and its relationship to the features of interest are primary in determining the resolvability of features and interfaces. The resolution of the scanner in relation to scanned features provided excellent structural information and proof of concept images used in qualitative analysis. Low phase contrast, scanning artefacts, sub-resolvable features in some cases, and imperfect registration between dry and wet scans interfered with quantitative analysis in dry, wetted with water, and wetted with ethanol material scans. The work here shows that for qualitative analysis, robust structural information is obtainable through approaches such as this. Soils comprised of mainly sub-resolvable soil particles were less informative and are not recommended for use in this scanning environment.

Organic materials have significant microporosity. For wettable materials, this microporosity tended to fill preferentially in comparison to larger void zones within columns. In contrast, non-wettable materials showed a combination of both microporous wetting and large water blobs within the column, and indicated incomplete wetting up of organic soil particles, even after approximately 3.5 hours of wetting. The uptake of KI doped water into microporous zones enhanced contrast in these low atomic density materials (compared to air) and improved the quality of phase determination and resultant 3D projections.

Macroscopic wetting behaviours in scanned columns provided the greatest observance of changes in wettability in columns. In hydrophobic materials that remained hydrophobic throughout the scanning procedure, water preferentially wetted along column walls and secondarily moved inwards towards the centre of the column. In contrast, hydrophilic materials or hydrophobic materials that became wettable during two hour equilibration times wetted columns more thoroughly across the diameter of the column, and/or with preferential sorption into the microporosity of organic features. When ethanol was applied to the persistently hydrophobic column, wetting then occurred across the diameter of the column as a consequence of decreased interfacial tensions and caused the material to become wettable. This changed the nature of filled pores within the column by draining pores, increasing entrapped air, and enhancing absorption of fluids into persistently non-wettable microporous spaces. These observations are consistent with theoretical expectations, however, these are the first images to show that changes in fractional wettability is the primary driver for fluid movement within these soils.

Scan time is a particularly important variable when dealing with dynamic systems such as this. It is therefore useful to consider the temporal resolution of the scanner in relation to the rate of dynamic behaviours under observation. When dynamics are faster than scan durations, it is difficult to distinguish wetting dynamics caused by CA change from wettable capillary behaviours. Hydrophobic materials that had relatively fast dynamics (compared to equilibration and scan times lasting 3.5 hours) showed essentially no obvious signs of repellency in scans. More persistently repellent materials, however, exhibited increased wetting along column walls where pores were largest and likely to wet more quickly under positive pressures. Capturing dynamic interfaces due to changing CA's could provide direct rate of change information. Acquiring data on this primary process would be useful moving forward and best served by pairing rate of change behaviours (developed in infiltration based studies using drops or infiltrometers) with a scanning system capable of capturing changing interfaces at that temporal resolution. To capture moving interfaces accurately would require scanning technologies capable of sub minute or sub-second scanning, which is currently beyond existing technology.

References

Al-Raoush, R. I., & Willson, C. S. (2005). Extraction of physically realistic pore network properties from three-dimensional synchrotron X-ray microtomography images of unconsolidated porous media systems. *Journal of Hydrology*, *300*(1-4), 44–64. doi:10.1016/j.jhydrol.2004.05.005

Andrew, M., Bijeljic, B., & Blunt, M. (2015). Reservoir Condition Pore-scale Imaging of Multiple Fluid Phases Using X-ray Microtomography. Journal of Visualized Experiments, (96), 1–10. http://doi.org/10.3791/52440

Armstrong, R. T., Wildenschild, D., & Bay, B. K. (2015). The effect of pore morphology on microbial enhanced oil recovery. *Journal of Petroleum Science and Engineering*, *130*, 16–25. doi:10.1016/j.petrol.2015.03.010

Brown, K., Schlüter, S., Sheppard, a., & Wildenschild, D. (2014). On the challenges of measuring interfacial characteristics of three-phase fluid flow with x-ray microtomography. *Journal of Microscopy*, *253*(3), 171–182. doi:10.1111/jmi.12106

Duliu, O. G. (1999). Computer axial tomography in geosciences: An overview. *Earth Science Reviews*, *48*(4), 265–281. doi:10.1016/S0012-8252(99)00056-2

Feng, G. L., Letey, J., & Wu, L. (2001). Water Ponding Depths Affect Temporal Infiltration Rates in a Water-Repellent Sand. *Soil Science Society of America Journal*, *65*, 315–320. doi:10.2136/sssaj2001.652315x

Herring, A. L., Andersson, L., Schlüter, S., Sheppard, A., & Wildenschild, D. (2015). Efficiently engineering pore-scale processes: The role of force dominance and topology during nonwetting phase trapping in porous media. *Advances in Water Resources*, *79*, 91–102. doi:10.1016/j.advwatres.2015.02.005

Helliwell, J. R., Sturrock, C. J., Grayling, K. M., Tracy, S. R., Flavel, R. J., Young, I. M., … Mooney, S. J. (2013). Applications of X-ray computed tomography for examining biophysical interactions and structural development in soil systems: a review. *European Journal of Soil Science*, *64*(3), 279–297. doi:10.1111/ejss.12028

Herring, A. L., Harper, E. J., Andersson, L., Sheppard, A., Bay, B. K., & Wildenschild, D. (2013). Effect of fluid topology on residual nonwetting phase trapping: Implications for geologic CO2 sequestration. *Advances in Water Resources*, *62*, 47–58. doi:10.1016/j.advwatres.2013.09.015

Ketcham, R. A. and Carlson, W. D. (2001). Acquisition, optimization and interpretation of x-ray computed tomographic imagery: Applications to the geosciences. *Computers and Geosciences*, *27*(4), 381–400. doi:10.1016/S0098-3004(00)00116-3

Mooney, S. (2002). Three-dimensional visualization and quantification of soil macroporosity and water flow patterns using computed tomography. *Soil Use and Management*, 18(2), 142–151. doi:10.1079/SUM2002121

Taina, I. a, Heck, R. J., & Elliot, T. R. (2008). Application of X-ray computed tomography to soil science: A literature review. *Canadian Journal of Soil Science*, *88*(October 2007), 1–19. doi:10.4141/CJSS06027

Wang, W., Kravchenko, a. N., Smucker, a. J. M., & Rivers, M. L. (2011). Comparison of image segmentation methods in simulated 2D and 3D microtomographic images of soil aggregates. *Geoderma*, *162*(3-4), 231–241. doi:10.1016/j.geoderma.2011.01.006

Wang, Z., Wu, Q. J., Wu, L., Ritsema, C. J., Dekker, L. W., & Feyen, J. (2000). Effects of soil water repellency on infiltration rate and flow instability. *Journal of Hydrology*, *231,Äì232*(0), 265–276. doi:10.1016/B978-0-444-51269-7.50024-2

Wildenschild, D. and Hopmans, J. (2005). Quantitative analysis of flow processes in a sand using synchrotron-based X-ray microtomography. *Vadose Zone Journal*, 44(1), 112–126. doi:10.1029/2006WR005517

CHAPTER 4 - INFILTRATION OF WATER AND ETHANOL SOLUTIONS IN WATER REPELLENT POST WILDFIRE SOILS*

Sarah M. Beatty[a] and James E. Smith[a]

[a] School of Geography and Earth Sciences, McMaster University, 1280 Main St. West.

Hamilton, Ontario, Canada L8S 4L8

*Reproduced with permission from Beatty, S.M and Smith, J.E (2014). Infiltration of water and ethanol solutions in water repellent post wildfire soils. *Journal of Hydrology,* 514: 233-248.

Abstract

Dynamic soil water repellency is a pending challenge in water repellency research. The dynamic change or temporal dependence of repellency is commonly expressed as the persistence of repellency. Persistence, or dynamic changes in contact angle, are however, difficult to directly measure and incorporate into mechanistic conceptual and numerical models. To provide insight into the mechanistic nature of infiltration in variably repellent porous media over larger spatial and temporal scales than afforded by commonly applied characterization approaches (i.e. drop tests), this study reports upon observations made during in situ 3D tension infiltration experiments conducted at a post-wildfire site. Tension infiltration tests have proven to be uniquely sensitive to changes in repellency over time. Tension infiltration experiments using mini-disk infiltrometers were conducted. Drop tests provided initial measures of repellency. Tension infiltration experiments were used to generate insights on longer term infiltration behaviours using water, ethanol, and aqueous-ethanol solutions. Molarity of Ethanol Drop (MED) – derived aqueous ethanol solutions (of 5%, 25% and 50% ethanol concentration) were used as intermediate infiltration fluids to generate greater insight into the transitional behaviours between repellent and apparently wettable infiltration. Early time infiltration rates are not reliable indicators of longer term infiltration rates. However, relating the two measures was informative in characterising repellency across materials and at different sites, while preserving temporal differences in fluid behaviours. Comparison of the late-time infiltration rates of aqueous solutions of varying ethanol concentrations proved a useful indicator of repellency and fractional wettability effects.

Keywords: Tension disk infiltrometer, Wildfire, Contact angle, Soil water repellency, MED, Sorptivity

4.1. Introduction

Dynamic soil water repellency is a pending challenge in water repellency research. The dynamic change or temporal dependence of repellency is commonly expressed as the persistence of repellency. Persistence, or dynamic changes in contact angle, are however, difficult to directly measure and incorporate into conceptual and numerical models. Natural and anthropogenically altered soils exhibit variability in the severity and persistence of water repellency.

Fractional wettability is a term commonly used in the multiphase flow and contaminant literature that describes bulk media in which some portion are water-wettable (with contact angles less than 90°) and some portion of the surfaces are water-repellent (with contact angles greater than 90°) (Al-Futaisi and Patzek, 2004 and O'Carroll et al., 2005). In natural media, fractional wettability speaks directly to the 'severity of repellency' and heterogeneity of observed contact angles, implicitly describing a theoretical continuum over which a given porous media can exist ranging from wholly water wettable to wholly water repellent. While contact angles at the extremes (of 0° and 180°) are theoretical in nature, e.g. there is always some attraction between a liquid and solid (Doerr et al., 2000), 0° is used by convention to facilitate calculations of pore radius and/or for scaling purposes. It is questionable whether these extreme contact angles (particularly with respect to the use of 0°) generate meaningful results in hydrologic models. Additionally, in natural media, where non-zero contact angles are common, contact angle dynamics generate time dependent changes in relative proportions of wettable and non-wettable fractions (Beatty and Smith, 2013). Contact angle dynamics speak directly to the ‘persistence of repellency’, and indicate a physical mechanism. Quantitatively speaking, mechanistic challenges are presented when trying to reliably simplify fractionally wettable systems, non-uniqueness being the most significant culprit. This has made these systems difficult to track, quantify, and model accurately using traditional approaches. Not surprisingly, mechanistically oriented studies investigating fractional wettability and contact angle dynamics in natural materials are uncommon.

In spite of oft-cited limitations, Water Drop Penetration Time (WDPT) and Molarity of Ethanol Drop (MED) tests capture fundamental information about fractionally wettable and dynamically changing materials through simple and reliable methodologies (Dekker et al., 2009 and Letey et al., 2000). As two of the most frequently applied methods in water repellency research, WDPT measures the dynamic change of repellency or persistence of water repellency when exposed to water and MED (or Critical Surface Tension, Alcohol Percentage) tests approximate the surface tension required to initiate infiltration instantly (Letey et al., 2000). While more sophisticated measures of repellency are available, no particular approach has found such widespread utility and acceptance as these.

While informative at the small scale and in a variety of testing environments, the prevalent use and reporting of drop tests has emphasised the measure, analysis and reporting of rapidly measured small spatial scale/small volume data in water repellency investigations. This is particularly the case for field investigations where longer term or larger scale testing is functionally difficult (Logsdon, 1997). Infiltration investigations in water repellent media do employ larger volumes and sample larger areas (e.g. Beatty and Smith, 2013, Clothier et al., 2000, Doerr and Thomas, 2000, Ganz et al., 2013, Pierson et al., 2008 and Woods and Balfour, 2010). Systematic evaluations, however, tend to occur more often in the laboratory and remain subject to shorter duration testing experimental bias. Clothier et al. (2000) drew attention to this during an infiltration investigation in naturally repellent loams, noting the expression of wettable-like infiltration behaviour at early time with subsequent repellent behaviour being expressed at much later time, beyond time frames which would normally be observed by an operator. Beatty and Smith (2013) observed a possible transition between primarily hydrophobic and primarily wettable states occurring at later time during laboratory infiltration tests on ‘undisturbed’ post-wildfire soil materials.

It is common to capture short duration (early time) data sets in wettable media, however, non-wettable media express a wider range of behaviours and non-uniqueness over the course of infiltration (Imeson et al., 1992) which may or may not be systematically indicated by early-time infiltration behaviour. Questions still remain around time and spatial scales appropriate for capturing characteristic and meaningful responses of fluid behaviours in hydrologic systems expressing dynamic hydraulic properties (Moody et al., 2013 and O’Carroll et al., 2010). With this in mind, understanding infiltration behaviours during critical transitions and across a range of time scales is important to accurately quantify, model, and make predictions about infiltration responses and infiltration-related processes in water repellent media. In the presence of techniques capable of greater spatial and temporal sensitivity to repellency, there is an opportunity to utilize existing sophisticated methods developed for infiltration into wettable media, while incorporating repellency-oriented analytical approaches that generate greater mechanistic insights for non-wettable systems.

Through an *in situ* systematic field investigation in post-wildfire materials that (1) links existing and often-used methodological approaches, and (2) develops mechanistic insight into the nature of fractional wettability and contact angle dynamics in naturally occurring water repellent soils, we sought to answer the following questions. First, can early and late time tension infiltration rate data be directly related to enhance understanding of fractional wettability and contact angle dynamics? And second, can infiltration experiments using different aqueous ethanol solutions (between 0% and 100% ethanol concentration) provide additional insight into the nature of contact angle dynamics and fractional wettability in dynamically wettable materials during longer term testing?

4.2 Theory

Differences between simple wettable porous media, upon which many of our conceptual and theoretical models are built, and fractionally wettable and dynamically changing media are well expressed during infiltration. One of the most obvious differences between water wettable and water repellent infiltrations are the shapes of infiltration rate and cumulative infiltration plots (Clothier et al., 2000; DeBano, 1981; Pierson et al., 2008; Wallach and Graber, 2007). With or without the application of positive pressures at the surface, in layered systems, infiltration rates in wettable soils will decrease over time (Feng et al., 2001; Hillel, 1982). This can be related to the sorption of water into wholly or partially wettable materials (DeBano, 1981; Beatty and Smith, 2013). This early time behaviour is for the most part well defined, being driven primarily by capillarity, water capacity, and a steep hydraulic gradient associated with the wetting front (Hillel, 1982). In contrast, non-wettable materials can exhibit increases in infiltration rate during a single test (Beatty and Smith, 2013; Clothier et al., 2000; DeBano, 1981; Fischer et al., 2013; Wallach and Graber, 2007) and/or over the course of successive infiltrations (Leighton-Boyce et al., 2007; Quyum et al., 2002). In more complex layered systems, particularly in the field, early time infiltration rates, which may exhibit either wetting or non-wetting behaviours, can be followed by longer term highly nonlinear behaviours that include both increasing and decreasing rates (Beatty and Smith, 2013; Clothier et al., 2000; DeBano, 1981; Imeson et al., 1992; Pierson et al., 2008). In dynamically water repellent materials hydraulic gradients are initially substantially diminished, capillarity impedes water flow (Feng et al., 2001; Wang et al., 2000) and repellent fractions of the porous media are unable to participate until later time (Beatty and Smith, 2013). Consequently, it is less clear which mechanisms are acting primarily, when they are acting, in what magnitudes, and for how long. This helps to explain why sorptivity is a concept with limited meaning in water repellent media.

Tension infiltrometers have proven to be uniquely sensitive to spatial differences (Lewis et al., 2006; Hallett et al., 2004) and temporal changes (Beatty and Smith, 2013; Clothier et al., 2000) in repellency. During longer term testing, laboratory work using tension infiltrometers has shown that two distinct mechanisms can contribute to observed later time increases in infiltration rates: 1) the dynamic change of contact angles in bulk media (Beatty and Smith, 2013) and/or 2) the build-up of local pressures in the presence of internal ponding (Clothier et al., 2000; Feng et al., 2001). When observed in cumulative infiltration vs. time or square root of time plots, this behaviour manifests as a convex (Wallach and Graber, 2007) or a “hockey-stick-like” (Lichner et al., 2013) curve and is unique to that typical of wettable soils, showing concave infiltration behaviour.

One way to investigate soil water repellency is to use an infiltrating fluid other than water. Ethanol and aqueous solutions of ethanol are assumed to perfectly wet hydrophobic media and have been used as test fluids in drop penetration tests (Letey et al., 2000) and tension infiltration experiments (Hallett et al., 2004; Hardie et al., 2012; Hartmann et al., 2010; Lamparter et al., 2010; Nyman et al., 2010; Tillman et al., 1989). Repellency Index expresses a ratio of the sorptivities of ethanol to water, taking into account the difference in mobility of ethanol relative to water through a multiplier (of 1.95) (Wallis and Horne, 1992). This measure places emphasis on the acquisition and analysis of early time data.

When using ethanol solutions it is important to consider that aqueous solutions of ethanol are less mobile than water under the same fluid content (i.e. same assemblage of filled pores) in a porous medium because ethanol solutions are more viscous and less dense than water. Table 4.1 lists these properties for a range of ethanol solutions (0–100% ethanol) along with fluid mobility factors (fm) relative to water (Fetter, 1999), using

Table 4.1 Properties of aqueous ethanol solutions, modified from Lide (1993)

Ethanol concentration		Density	Viscosity	Surface tension	Fluid mobility (fm)* at 25 °C	1/fm* at 25 °C
(% mass)	(% vol)	g/ml at 20 °C	mPa s at 25 °C	mN/m at 25 °C		
0	0	1.00	0.89	72.01	1.0000	1.000
5	4.0	0.99	1.11	55.73	0.7983	1.253
10	8.1	0.98	1.32	47.53	0.6632	1.508
20	16.5	0.97	1.81	37.97	0.4771	2.096
25	20.9	0.96	2.08	35.51	0.4122	2.426
40	34.5	0.94	2.35	30.16	0.3548	2.818
50	44.2	0.91	2.3	27.96	0.355	2.817
60	54.3	0.89	2.24	26.23	0.3547	2.819
80	76.0	0.84	1.75	23.82	0.4297	2.327
100	100	0.79	1.07	21.82	0.6577	1.520

$$fm = \frac{\frac{\rho_i}{\rho_w}}{\frac{\mu_i}{\mu_w}} \qquad \text{(eq. 4.1)}$$

where subscript *w* denotes water, subscript *i* denotes ethanol solution at concentration *i,* ρ is density, μ is absolute viscosity. Eq. (4.1) only considers the effects of density and viscosity of the hydraulic conductivity term and follows from

$$K(\theta) = \frac{k(\theta)\rho g}{\mu} \qquad \text{(eq. 4.2)}$$

where *K(θ)* is the unsaturated hydraulic conductivity, *k(θ)* is the permeability at volumetric moisture content *θ,* and *g* is the acceleration due to gravity. Through equations (4.1) and (4.2) it is expressed that a less dense and/or thicker fluid has a lower conductivity than water under that same fluid content. It is a noteworthy field consideration that viscosities of ethanol solutions are also temperature sensitive with, for example, the viscosity of a 40% by weight ethanol solution at 10 °C being 87% (1.87 times) more viscous and less mobile than at 25 °C. Specifically, this means that the 1.95 multiplier used in Repellency Index measurements (Decagon Devices, 2012) is not constant under a range of common field temperature conditions.

A further consideration for infiltration of alcohol solutions into soils is that they have lower air/liquid interfacial (surface) tensions than water (Table 4.1). This lower surface tension leads to two related considerations relative to infiltration. The first consideration is the effect of concentration dependent surface tension on the capillarity component of the hydraulic gradient which follows from the Laplace equation of capillarity,

$$C_p = \sigma_i \left(\frac{1}{r_1} + \frac{1}{r_2}\right) \qquad \text{(eq. 4.3)}$$

where C_p is pressure difference across the liquid/air (l/g) interface, σ_i is surface tension at concentration i, and r_1 and r_2 are the principle radii of curvature of the interface. Smith and Gillham (1994) and Smith and Gillham (1999) and Henry and Smith (2003) present experimental data and models showing that for conditions of constant contact angles, infiltration rates of alcohol solutions change proportional to the change in surface tensions. The second consideration of ethanol having a lower surface tension than water is important for repellent soils and relates to the primary purpose of its use. Specifically, the equilibrium apparent contact angle (β_a) of aqueous ethanol solutions are lower than those of water as expressed through the modified form of Young's equation,

$$\sigma_{lg} \cos\beta_a = \sigma_{sg} - \sigma_{sl} \qquad \text{(eq. 4.4)}$$

where subscripts l, g, and s denote the liquid, gaseous (air), and solid (soil) phases respectively.

Including contact angle into the consideration of the soil water pressure is commonly expressed by replacing the radius of curvature of the interface ($1/r_1 + 1/r_2$) in Eq. (4.3) (Laplace Equation of Capillarity) with the cosine of the apparent contact angle divided by the equivalent circular radius of curvature of the soil pore (r), which expressed in head units relative to gauge pressure is

$$h = -\frac{2\sigma_i \cos\left(\beta_{a_i}\right)}{\rho g r} \quad \text{or} \quad h = -\frac{2[\sigma_i(t)] \cos\left(\beta_{a_i}(t)\right)}{\rho g r} \qquad \text{(eq. 4.5)}$$

where *h* is the soil water pressure head, and the time dependence (dynamics) of surface tension and contact angle are shown explicitly in Eq. (4.5b). Since the contact angle and/or size of pore occupied by the interface cannot be independently measured in situ in the field, and since ethanol solution concentration is known to be changing the liquid mobility factor (*fm*) and contact angles over time, it is not possible to know at any given time during an infiltration event which effect is primary or prevailing. Specifically, it is not readily apparent how much the local capillary pressure is being proportionally changed by decreasing contact angles (causing decreases in *h*), increasing soil moisture contents (causing increases in *h*), decreasing liquid/water surface tensions (causing increases in *h*), and/or decreasing liquid density and increasing liquid viscosities (causing decreased unsaturated hydraulic conductivities).

Studies and models which consider soil water repellency under conditions when the wettability of the soil is fractionally constant or relatively constant significantly advance our understanding of soil water repellency (Diamantopoulos et al., 2013), particularly as observed at low level repellency in the field (Ganz et al., 2013). However, there is a lack of and persistent need for studies and models which consider soil water behaviour under conditions when the contact angle is changing substantially over the time scale of the interest (e.g. duration of infiltration event) such that the soil hydraulic properties are time dependent. In such systems, the rate of change in the wettability and the rate of change in the relative fractions that are wettable are primary drivers of flow, i.e. the kinetics are primary. Simulation using time dependent soil hydraulic properties linked to dynamic repellency poses major numerical modelling challenges. With full consideration and awareness of the complexities and recognising the unmeasurable nature of some of these pore scale relations within the infiltration front, there is much to be learned about contact angle dynamics and fractional wettability dynamics under soil water repellency conditions using controlled measures of infiltration under applied constant tension at the soil surface.

4.3 Material and methods

4.3.1 Location

The post-wildfire study area accessed for this research is located in Northern Ontario, Canada, approximately 700 km north of Toronto, ON. The nearest climate station, 20 km away (N 48.34°, W 81.22° in Timmins, ON) reports average annual precipitation and temperature of 831 mm, and 1.3 °C, respectively (Meteorological Service of Canada, 2013). The region is part of the Boreal Shield ecozone (Statistics Canada, 2008), and is characterized by cold dry winters and relatively warm dry summers. The burn area is a historic timber harvesting and recreational site.

Forty thousand hectares of crown land burned in late May of 2012 during a high fireline intensity, moderate severity wildland fire based on visual observations. The fire started at the south western region of the burn area and spread quickly in a northerly direction. Fire suppressants were used on north eastern portions of the fire perimeter when fire balls were observed crossing the two-lane highway running north–south. Duff layers burned but remained largely intact in low and mid-elevation reaches. Upland areas showed complete consumption of the duff layer materials in some cases. Vegetation consisted primarily of mixed deciduous and coniferous trees species (Black Spruce, Trembling Aspen, White Birch, Jack Pine, White Spruce) and suckering shrubs, and ferns. Canadian Shield bedrock outcrops occur in upland elevations and erratics occur at various locations in the fire perimeter. Wisconsin period glacial tills are a dominant soil parent material for soils in the area (Gillespie et al., 1981).

Two historically logged/disturbed sites, Rocky Upland (RU) and Mid-Land (ML) were identified in the burn perimeter as possible sites exhibiting good access and favourable experimental conditions. Various potential sites were evaluated based on post-fire harvesting/logging operations, observed repellency characteristics, litter thickness, accessibility, burn condition, elevation, pre-fire vegetative cover, post-fire vegetative cover, and fire suppression related activities. The RU site (elev: 398 m) is approximately 13 km southwest as-the-crow-flies of ML (elev: 360 m). The RU site is located in an area of rockland/morainal stony and bouldered till. The ML site is located near low relief glaciofluvial (e.g. kame, esker) and morainal sediments with variable drainage (Ministry of Northern Development, 2005) and deep soil horizons (Ontario Ministry of Natural Resources, 2011). Eleven sand/gravel pits exist within a 10 km radius (east) of the ML site. The ML site is on the Mary Orthic Humo-Ferric Podzol which consists of stone free acidic outwash sands that are well drained and the RU site is on the Hanna Orthic Humo-Ferric Podzol which consists of slightly stony noncalcareous sandy loam with moderate drainage, using the Canadian System of Soil Classification (Agriculture and Agri-Food Canada, 1978, Agriculture and Agri-Food Canada, 1986 and Gillespie et al., 1981). This is consistent with observations in unburned mid-elevation areas, showing a ubiquitous LFH Horizon (duff) (approx. 4 cm to 30 cm thick), a discontinuous variable loamy sand Ae Horizon (3 cm to 15 cm thick; when present, avg bulk density 1.21 g/cm^3), over a sand Bf Horizon (18 to 25 cm thick, avg bulk density 1.34 g/cm^3), over a sand BC Horizon over a sand C Horizon (50+ cm thick, avg bulk density 1.48 g/cm^3). Soil profiles within the burn perimeter had similar horizontal sequences of soil subgroups as noted in unburned areas with minor differences in thickness; profiles showed a variably charred LFH layer (0.5–12 cm thick), underlain by a loamy sand Ae Horizon (1–8 cm thick, bulk density 1.22 g/cm^3), underlain by a relatively stone free sandy loam Bf Horizon (>25 cm thick, bulk density 1.35 g/cm^3). Post wildfire soils evaluated in this research were tested in situ approximately four months post-fire.

Black Spruce (Picea mariana) is the dominant species at the ML site with mature stands (14+ m in height/50 years old). Less mature stands (3 m in height/15 years old) of Jack Pine (Pinus banksiana) and White Spruce (Picea glauca) are present at the RU site (Ontario Ministry of Natural Resources, 2009).

4.3.2 Materials

In preliminary testing at the RU and ML sites, four soil materials/configurations were identified as materials of interest; three were duff (LFH) materials expressing variable burn and repellency condition. For duff materials: Brown materials showed minimal surface scorching/consumption by fire; Mixed materials exhibited more severe burning, and less repellency in pre-screening drop tests; Charred materials exhibited the greatest consumption by fire and expressed no apparent signs of repellency (in pre-screening drop tests). The fourth material (White) was of an Of horizon of unknown origin but apparently fibrous organic matter (vs. mineral). White materials appeared at the soil surface in isolated patches, and also at times as a discontinuous layer beneath scorched duff materials. White materials were distinguishable from A-horizon soil materials by colour and relative density. At both RU and ML sites, a mostly continuous duff layer was present, with patchy charred zones. More charring and a somewhat thinner duff layer was observed at the RU site. Across both sites, microtopography contributed to the accumulation of charred materials in local depressions, as could be expected from typical erosional/transport processes during post-fire rainfall. It was assumed that all duff materials for each site would have formed under similar conditions and vegetation, and that key differences in repellency, be they influenced by fire or not, would be expressed across those materials found at the site. Recent work has shown that the organic component of soil materials at the surface (sometimes reported as ash or scorched & charred duff) to have complex and an important effect on the overall repellency and hydrologic response during and after an infiltration event (e.g. Beatty and Smith, 2010, Beatty and Smith, 2013, Bodi et al., 2012, DeBano, 1981 and Woods and Balfour, 2010). Subsurface material characteristics are shown in soil profiles (Figure 4.1).

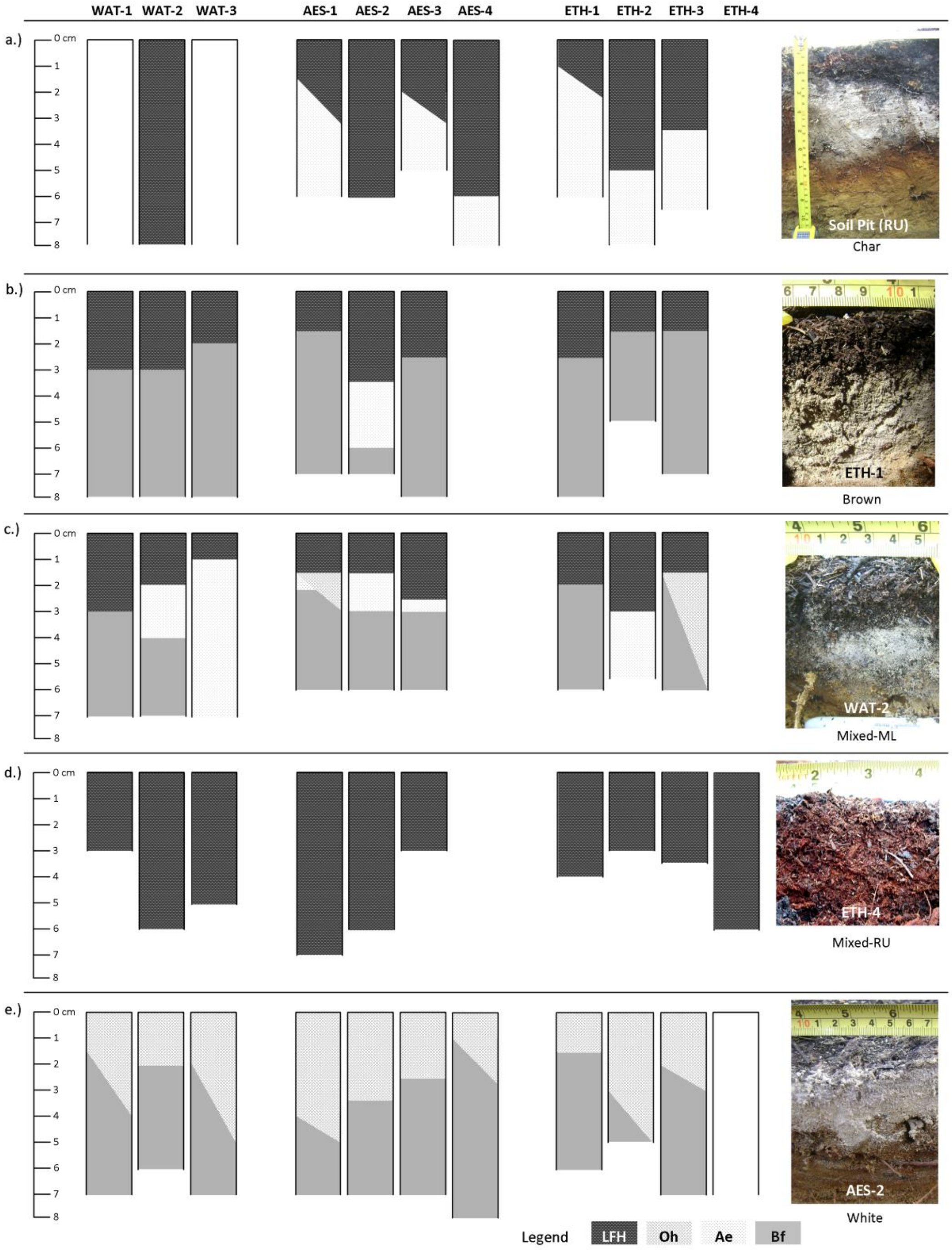

Figure 4.1 Infiltration test soil profiles constructed from post-infiltration photos showing a.) Char, b.) Brown, c.) Mixed-ML, d.) Mixed-RU, and e.) White materials. WAT, AES, and ETH column headings denote replications of water, aqueous ethanol solution, and ethanol test fluids respectively. Profiles showing outlines only denote completed tests with no soil profile available.

4.3.3 Drop tests

In the field, Water Drop Penetration Time (WDPT) tests were used only to identify materials expressing repellency. They were carried out by placing five drops on the soil surface and observing the time required for disappearance via infiltration, up to 60 s of testing. To test for repellency below surface, a subsample, approx. 10 cm × 1.5 cm rectangle × 7 cm (depth) was cut vertically into the soil profile adjacent to the surface WDPT test. This subsample was extruded from the soil profile with minimal disturbance and positioned horizontally (laid flat) on the soil surface. Drops were then placed on the sample at regular (depth) intervals, up to a few cm's from the surface/where repellency was no longer observed in drop tests.

Molarity of Ethanol Drop (MED) tests were carried out using laboratory-prepared mixtures of 95% denatured ethanol and deionized water (Letey et al., 2000). Ethanol concentrations (by volume) of 1%, 3%, 5%, 7%, 10%, 13%, 15%, 20%, 25%, 30%, 40%, 50% were used. Five drops were placed on soil materials similar to the process described for WDPT tests. The mixture required for drop disappearance of all drops in less than 5 s, for all tested depths was chosen as the designated ethanol concentration for that material type. In most cases, drop disappearance was less than 1 s, which we define as spontaneous infiltration. This concentration was subsequently used during Aqueous Ethanol Solution infiltration tests. Soil materials with longer Water Drop Penetration Times were preferentially targeted in MED tests to ensure that infiltration solutions would overcome repellency in materials expressing the strongest observed hydrophobicity.

4.3.4 Infiltration tests

A total of 49 infiltration tests were carried out. The spatial distribution of infiltration tests for ML and RU sites are shown in Figure 4.2. The maximum observed depth of infiltration was approximately 4 cm. Positions for both ambient volumetric moisture content and infiltration locations were mapped using a combination of triangulated field measured distances (within sites) and recreational GPS coordinates (between-sites) with a 1–3 m mapping accuracy. Spatial scales across material testing areas are somewhat variable, the dimensions for each of the sub-sites are as follows: Char = 1.5 m^2, Mixed-RU = 1 m^2, Mixed-ML = 6 m^2, White = 7 m^2, Brown = 11 m^2.

Tension disc infiltration tests using water (WAT), reagent grade (95%) ethanol (ETH), and MED-derived aqueous ethanol solutions (AES) were carried out at the Mid-Land (ML) site over four days (September 26–29, 2012). Rocky Upland (RU) tests were carried out two weeks prior (September 11–12). Onsite temperatures for Sept 11–12 (Rocky Upland sites) and September 26–29 (Mid Land sites) were 25±2 °C and 15±3 °C, respectively. An exception was the singular test that ran overnight (White-WAT1) during which the temperature dropped to approximately 2 °C. Decagon mini-disk infiltrometers set to a disc tension of −2 cm and filled to the specifications of the user manual were used in all cases. At the ML site, for each of three material types tested (Brown, White, Mixed), a minimum of three infiltration tests per liquid were carried out, totalling a minimum of nine infiltration tests per material. Before use in all cases, the infiltrometer was rinsed with distilled water.

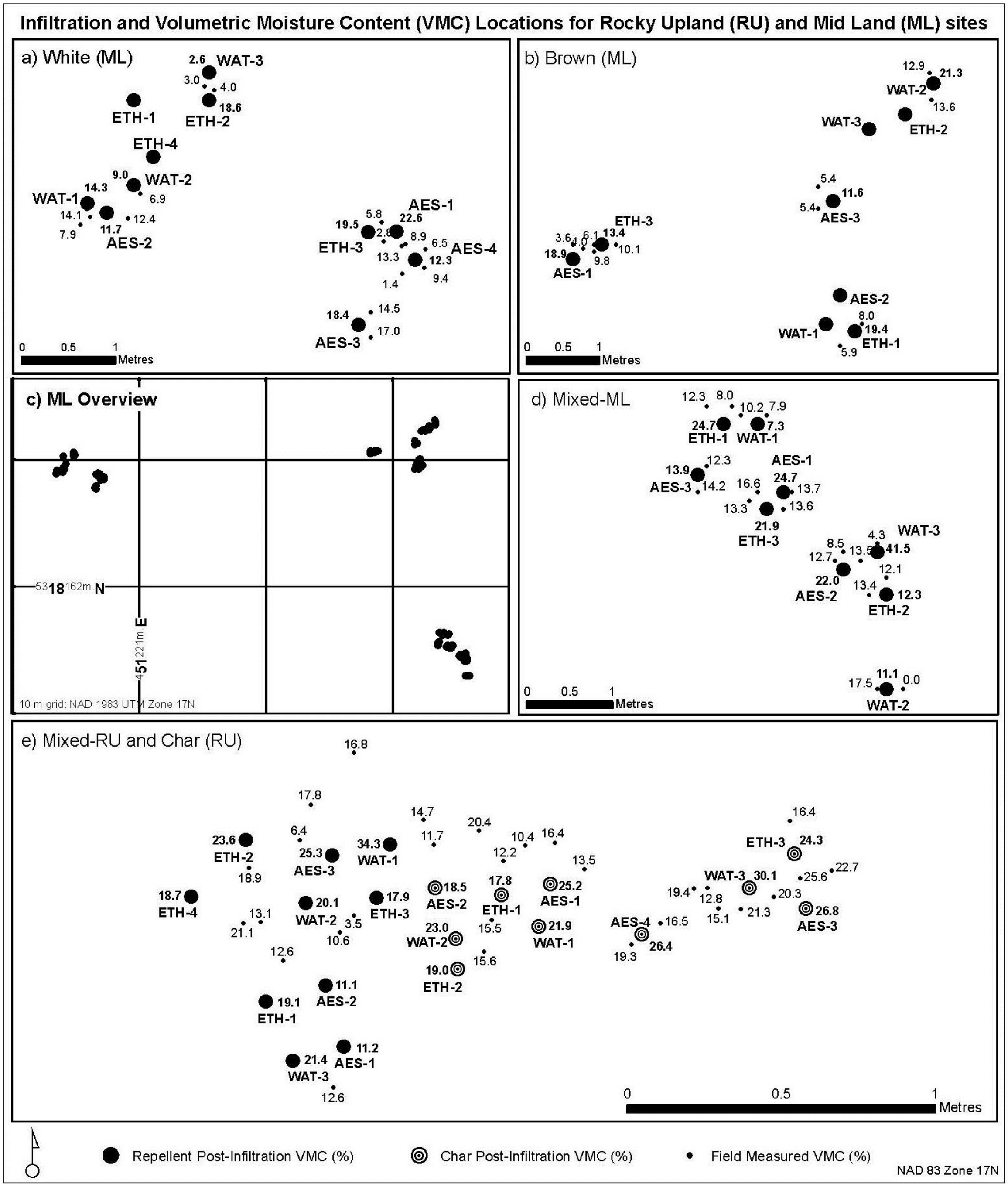

Figure 4.2 a) Locations of infiltration tests and volumetric moisture content measures showing a) ML-White, b) ML-Brown, c) ML overview, d) ML-Mixed, and e) RU-Mixed and RU-Char. Post-infiltration volumetric moisture content values are bold. Rocky Upland (RU) site is approximately 13 km south west of Mid Land (ML) as the crow flies.

For water infiltration tests only, an additional parameter, Time to First Five Bubbles (TFFB), was collected at the beginning of each infiltration test. In earlier (unpublished) field work, using a time to first bubble method similar to that described by Lewis et al. (2006), showed that observed early time infiltration behaviours and the overall repellency of surface materials as measured in WDPT and early time infiltration rates were related. For our purposes, the instrument was primed by initiating a bubble at the end of the bubble tube prior to use. After the infiltrometer was placed on the soil surface, the time to each of the first five bubbles was captured. Earlier (unpublished) work suggested that initial calibration of the instrument occurs between time zero, when the instrument is placed on the surface, and the first bubble. Consequently, times to the first bubble may reflect shorter/longer durations than representative of the actual infiltration rate into the soil. Each bubble represents approximately 0.20 ml of infiltration into the soil and tracks higher resolution early time infiltration data than available via graduated markings on the infiltrometer cylinder. Five bubbles is approximately equivalent to the first 1 ml of infiltration. TFFB data were collected for water infiltrations on primarily repellent materials only since the bubble rate was too fast to be recorded for primarily wettable materials.

Aqueous ethanol solutions for infiltration tests were prepared on site immediately prior to AES infiltration tests being conducted, using concentrations as determined via the described MED method. Testing solutions for White, Brown and Mixed-ML sites were 50% ethanol by volume. A 25% AES solution was used in Mixed-RU materials. Since Char materials showed no resistance to wetting in WDPT tests, a 5% AES solution was used. The AES solutions were used to investigate possible fluid related linkages and generate field applicable comparisons between pure water and alcohol related infiltrations in all field materials. We hypothesised that AES solutions would only infiltrate the portion of the soil sensitive to the selected concentration i.e. infiltrate into a smaller fraction than ethanol and larger fraction than water. Due to the nonlinearity of the surface tension to ethanol concentration relationship, an observable influence was expected during all AES infiltration tests.

Soil surfaces were prepared minimally before test initiation by removing very large pinecones and pieces of bark/char from the soil surface to ensure good disc contact with the surface. Infiltrometers were positioned and clamped to a retort stand to maintain a vertical orientation and secure contact with the soil surface throughout the test. Volume and time readings were recorded continually at semi-regular intervals, and multiple tests were conducted concurrently. In most cases, infiltration tests were carried out until the infiltrometer was empty. Tests lasting more than several hours were terminated at the end of the daylight period in most cases. Two tests were allowed to run over night, with readings continuing the next morning.

Moisture contents were captured for 43 of 49 infiltration tests, the exceptions being two White and four Brown tests due to problems with the data logger. In situ soil moisture contents were collected using Decagon Echo 5 cm (EC-5) moisture sensors and a battery operated Decagon EM50 data logger set to record at 1 min intervals. The EC-5 determines volumetric water content (VWC) by measuring the dielectric constant of the soil using capacitance/frequency domain technology at 70 MHz. Ambient (initial) moisture content data was collected concurrently to infiltration tests, with moisture sensors inserted vertically into the soil profile between 5 and 30 cm away from the infiltration area (average distance was approximately 20 cm for all tests). At the end of each infiltration test, another 5 cm Echo moisture sensor was inserted into the infiltration area, placed at a 45° angle across the disc diameter imprint to capture the final moisture content (θ_f) within the wetting bulb zone for a minimum of 11 min post infiltration.

4.4 Results and discussion

4.4.1 WDPT

Water Drop Penetration Time (WDPT) data are shown in Figure 4.3. At each measured depth, the proportions of (five) drops as measured up to 60 s are shown. This threshold of 60 s falls into the ‘slight repellency’ categorization established in work by Bisdom et al. (1993) and Doerr et al. (2009). Drops lasting longer than 60 s were observed in multiple instances in the most repellent materials, in some cases beyond 9 min.

Char materials showed no signs of repellency in two WDPT test locations, and thus are not shown. White materials exhibit the highest proportion of repellent materials at depth, whereas Brown and Mixed-ML show greater proportions of repellency at the surface. Surface repellency was observed for Mixed-RU materials, however, drop disappearance was difficult to assess due to the coarseness of surface materials, and are therefore not included.

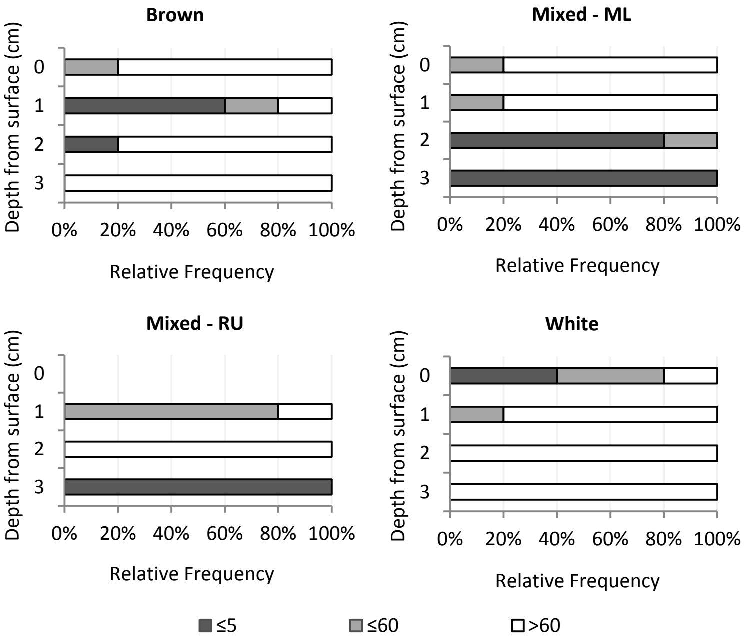

Figure 4.3 Relative frequency of three observed WDPT classes (*n*=5 at each depth) in RU and ML materials. Tests were pragmatically terminated at 60s.

4.4.2 Cumulative infiltration behaviours

In wettable soils, 'early-time' data are typically identified as having occurred within the first few minutes of infiltration. This data is regularly used in sorptivity calculations. Since infiltration into water repellent soils typically takes much longer, and it is not yet mechanistically clear which mechanisms are acting at which times, here we define 'early-time' data as the time over which the first 1 cm of fluid infiltrated (approx. 17% of infiltrometer capacity). We further refine this definition to only include the linear section as defined by a maximized correlation coefficient greater than 0.90 over several data points (most correlations were above 0.99). We define operational 'late-time' data based on the last approximately 2.5 cm of infiltration (~42% of infiltrometer capacity). Late-time linear correlation coefficients were higher than early-time values, with most being above 0.99. Discussion using early- and late-time terminology can also be accurately thought of as early- and late-volumes.

4.4.2.1 Wettable media: Char

Plots of Cumulative Infiltration vs. Time for wettable infiltration tests (Char) are presented in Figure 4.4. This figure illustrates a set of reference relationships showing differences in infiltration between water, ethanol, and an aqueous ethanol solution (of 5% ethanol by volume in this case (AES-5)) for wettable media.

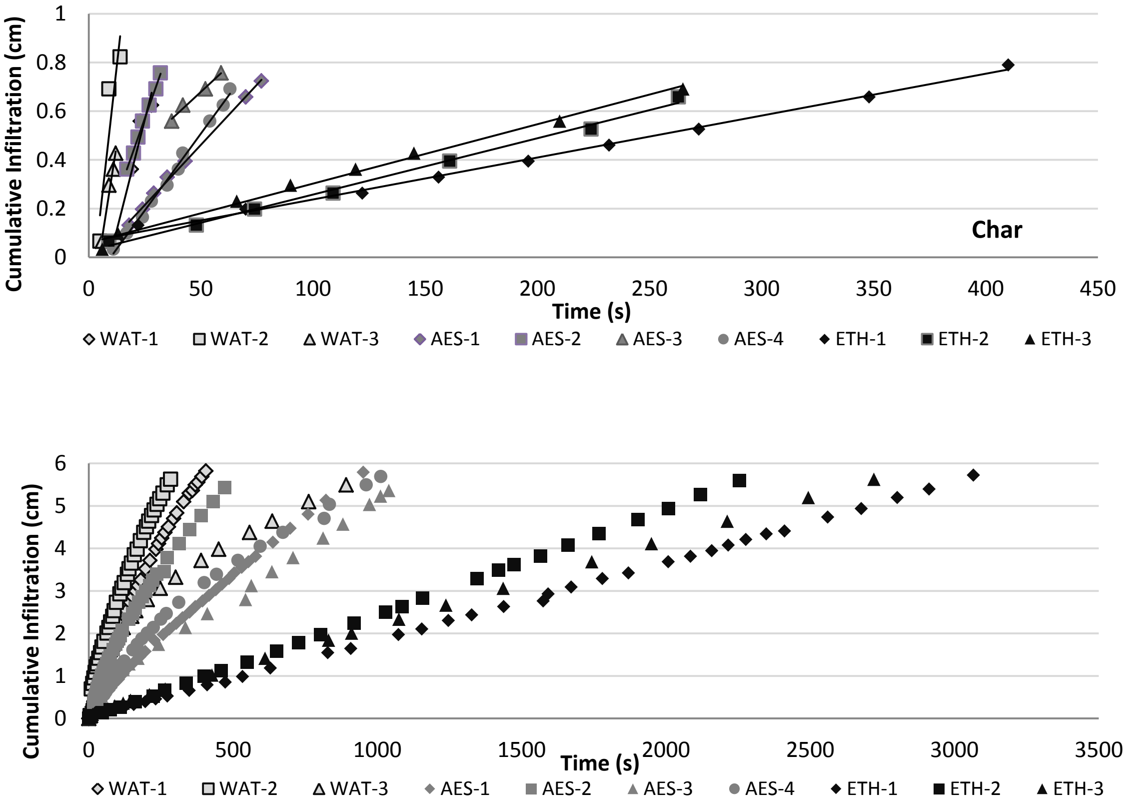

Figure 4.4 Cumulative Infiltration vs. Time for Char materials a) early time b) entire data set

This suite of *in situ* experiments showcase an easily detectible wettable infiltration response and serves an reference case to contrast against repellent soil behaviours in this study. The difference in infiltration rates for each of the fluids can be explained relatively well by established infiltration theory describing fluid flow in porous media and reduced fluid mobility caused by increased ethanol concentrations. In these wettable media, as (1) surface tension and density decrease and (2) viscosity increases, fluid mobility and associated average infiltration behaviours of early- and late-time cumulative infiltration versus time slopes flatten (slow down). Water exhibits the fastest cumulative infiltration versus time rates (10^{-2} cm/s), ethanol the slowest (10^{-3} cm/s in all cases), and AES-5 at an intermediate cumulative infiltration rate approximately half as fast as water. Water and AES-5 cumulative infiltration versus time plots exhibit some overlap, but good separation overall. Ethanol plots exhibit readily distinguishable behaviours in comparison to the other two infiltrating fluids with slower infiltration, i.e., about 5 times slower than Water. The explicit consideration of what we term here as the ‘sludge effect’ may be significantly contributing to the observed behaviours. Surface tensions for aqueous ethanol solutions exhibit a nonlinear surface tension versus concentration relation. In contrast, the viscosity versus concentration relation for ethanol and water exhibits a maxima around 50% ethanol, with both water and 100% ethanol having substantially lower viscosities. The term ‘sludge effect’ refers to condition where solute transport and dispersion within the advancing infiltration front will generate a zone (within the front) that has lower mobility than either the antecedent water or the infiltrating ethanol solution. For soils containing antecedent water, this means that the simple mobility scaling factor used in most repellency literature (i.e. 1.95) only partially accounts for the overall fluid property effects on infiltration rates during ethanol infiltration.

4.4.2.2 Non-wettable media: Brown

For direct comparison to wettable Char, plots of Cumulative Infiltration vs. Time for a non-wettable case (Brown) appear in Figure 4.5. The most striking contrast to the wettable case is that this repellent soil produces a similar set of cumulative infiltration versus time curves. However, the relationship between the three different test fluids (water, ethanol, and AES of 50%) is reversed. That is, the three test fluids generate three distinct self-similar groupings. However, in these non-wettable materials, water shows consistently slower infiltration rates (10−3 to 10−4 cm/s), ethanol the fastest (10−2 to 10−3 cm/s), and AES-50 expressing an intermediate behaviour. Specifically, at early-time, AES-50 tests behave similarly and are essentially indistinguishable from ethanol infiltrations and ranging between 10^{-2} and 10^{-3} cm/s. At late time, a similar pattern of cumulative infiltration versus time emerges but with clearer distinction between the different fluids.

The observed trend in these repellent soils must be attributable to differences in ethanol concentration and the resultant impact on contact angles, with water testing durations taking up to 5 times longer than ethanol infiltrations. Late-time infiltration rates for AES-50 are approximately twice those observed for water infiltrations and half to one-third of those observed for ethanol infiltrations. Recall from the wettable Char tests above that the difference in viscosity, density, and capillarity of these infiltrating fluids induces the ethanol solutions to be slower than water in the presence of antecedent

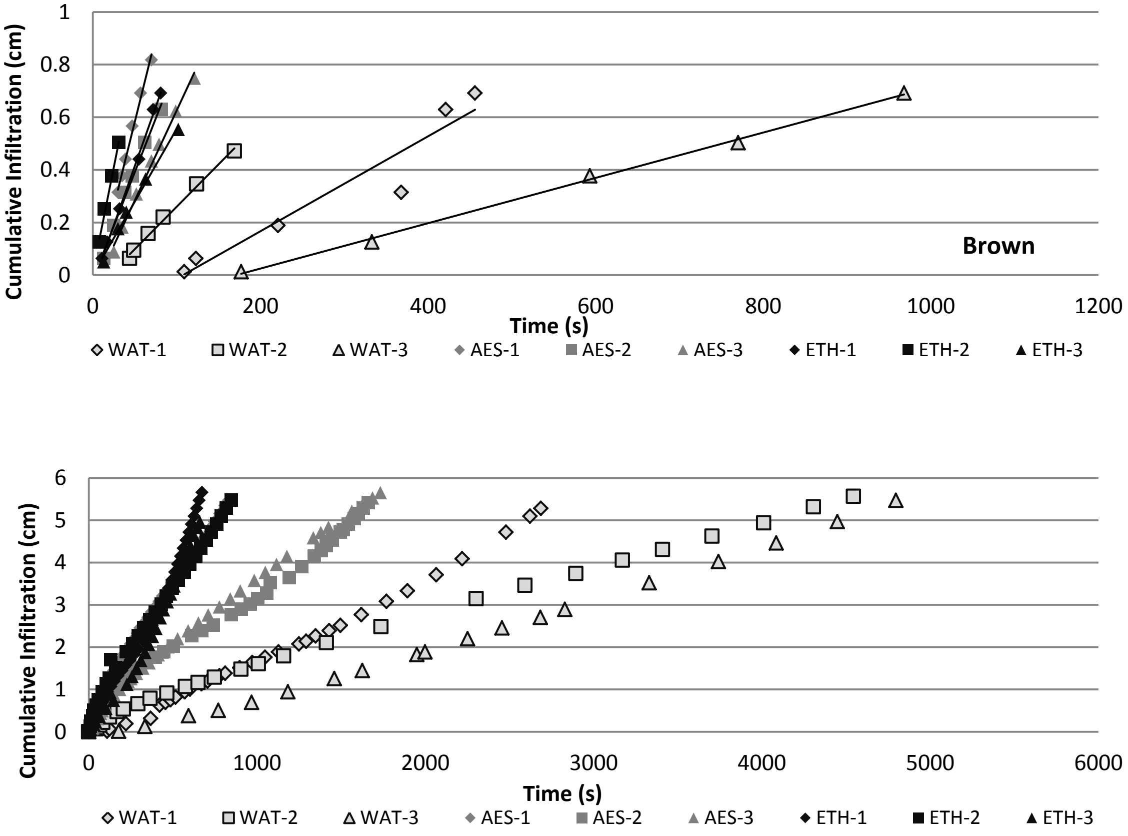

Figure 4.5 Cumulative Infiltration vs. Time for Brown materials a) early time b) entire data set

moisture. In this case the AES-50 solution is inducing time-dependent changes in the infiltration rate at later times but is not inducing observable differences in the three observed cases at early-time. It is unlikely this can be attributed to bulk soil spatial variability of saturated hydraulic conductivities given the distinct grouping of the infiltration results by fluid. In this case, within treatment variability is much smaller than between treatments.

4.4.2.3 Infiltration into more complicated media: Mixed & White

Plots of Cumulative Infiltration vs. Time for Mixed-ML tests appear in Figure 4.6. With the exception of ETH-2, previously discussed relationships between the three different fluids are echoed in these repellent, albeit, more complex media. Wider/overlapping ranges and testing durations indicate an increased variability of repellency encountered in infiltrated materials and that the fluids are sensitive to these differences, particularly with AES-50 and ethanol tests.

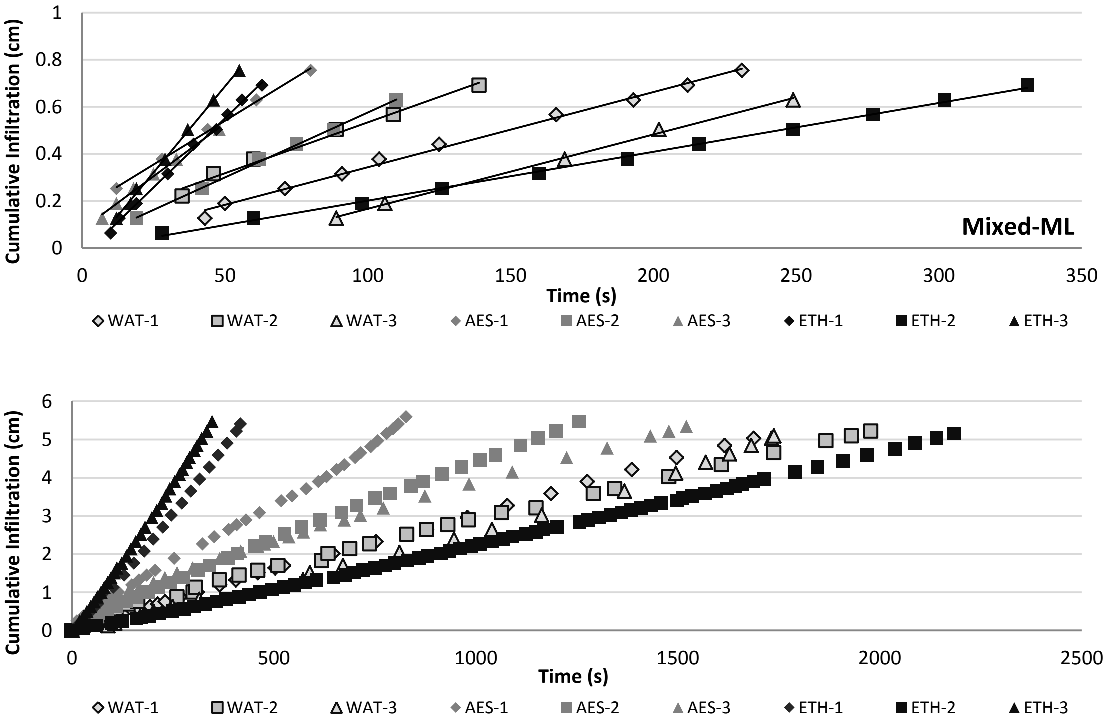

Figure 4.6 Cumulative Infiltration vs. Time for Mixed-ML materials a) early time b) entire data set

There is good separation between early-time infiltration behaviours for ethanol and water in the majority of tests. The majority of early time ethanol and AES-50 infiltrations are approximately half an order of magnitude greater than observed water (10^{-3} cm/s). AES-50 tests also express an intermediate behaviour that transitions from behaving closer to ethanol at early time to behaving more like water at later time. AES-50 tests are approximately twice as fast as water tests in the beginning, becoming only marginally faster than water tests at later time. This may indicate that this AES-50 solution causes rapid changes in contact angle initially, but that little additional change occurs over the duration of testing/deeper in the profile.

Unusually low early- and late-time infiltration rates (10^{-3} cm/s for both) are observed for ETH-2. This effectively bounds the entire data set with ethanol tests. In primarily wettable materials, as noted earlier, significantly lower infiltration rates and longer testing durations are expected for ethanol infiltrations (compared to water infiltration in the same media) since the fluid mobility factor is lower. In the presence of generally systematic relationships in the rest of this suite of tests, this outlier suggests that a ‘wettable zone’ or some other spatial heterogeneity may have been captured in this experiment. This low infiltrability is present at both early- and late-time and would be consistent with a material having significantly lower saturated hydraulic conductivity.

Plots of Cumulative Infiltration vs. Time for Mixed-RU tests appear in Figure 4.7. Fluid infiltration behaviours in Mixed-RU materials are distinguishable from each other (as was observed in the ML materials) and express an overall repellent response. Water is more mobile in these materials compared to Mixed-ML materials as suggested by relatively higher surface tension used for AES infiltrations and the shorter testing durations for water. Comparatively, the domains of ethanol and water infiltrations are not well separated by an intermediate set of AES-25 infiltration curves. Infiltrations using AES-25 and water do exhibit distinct infiltration rates, with AES-25 and water on the orders of 10−3 cm/s and 10−3 to 10−4 cm/s, respectively. Ethanol infiltrations exhibit the most variability with infiltration rates ranging between 10−2 cm/s and 10−4 cm/s and overlapping AES-25 experiments. It is not fully clear why ethanol cumulative infiltrations curves exhibit such a large spread, but may be a consequence of a more evenly distributed

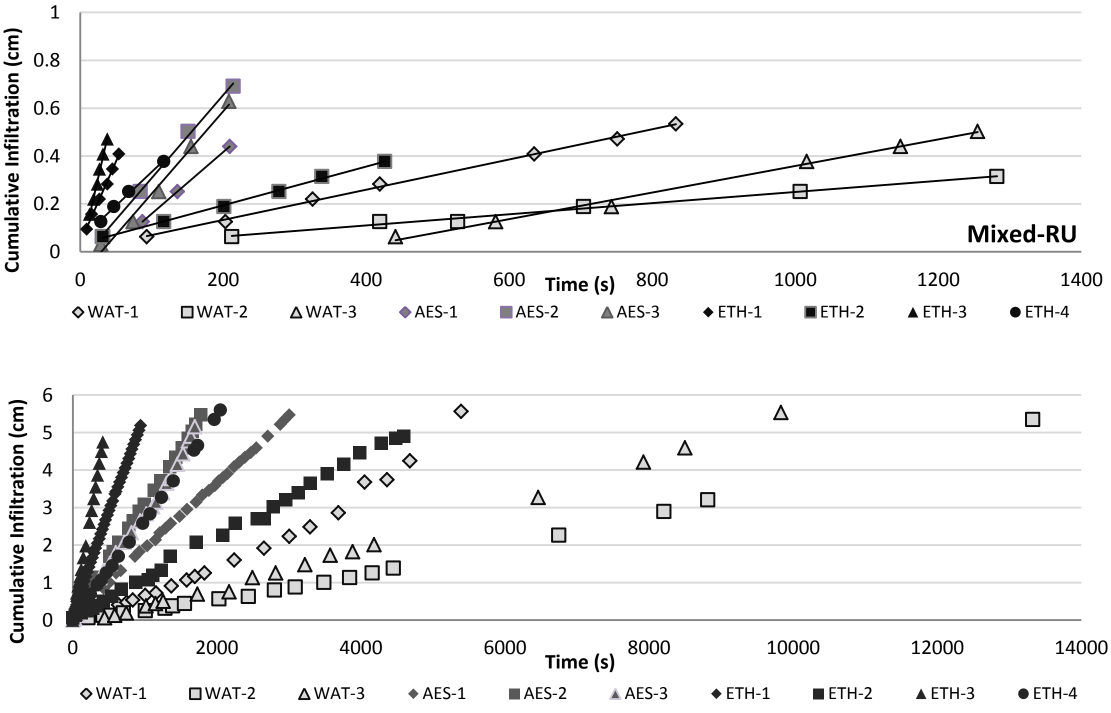

Figure 4.7 Cumulative Infiltration vs. Time for Mixed-RU materials a) early time b) entire data set

(e.g. than observed at the Mixed-ML site) wettable fraction, and/or the ‘sludge effect’. This is particularly important to consider during field investigations on materials showing intermediate wettable characteristics, with moisture contents of consequence. Notable in this data set is the infiltration curve of ETH-2, which is indistinguishable from water infiltration in these materials. The relatively higher final moisture content may help to explain the comparatively slow infiltration rate. However, it is important to note that none of these data express the type of concave infiltration curve that is more commonly observed for ethanol infiltration into repellent media. In this sense, this data is more complex and less easily explained than the cases discussed previously.

Plots of early-time Cumulative Infiltration vs. Time for White tests appear in Figure 4.8. These were the most repellent materials observed in this study. As observed in the previous cases, water and ethanol infiltrations separate neatly into two distinct groups, tests in which the infiltrometer empties before 1000s and those that do not. In contrast to the previous cases, AES-50 tests do not exist within an intermediate space between water and ethanol infiltrations. Instead, AES-50 infiltrations are distinctly associated with either ethanol or water infiltrations. It is probable that the 50% ethanol solution, while effective in related MED testing, was a solution ineffective at generating apparently ‘wettable’ bulk infiltration behaviour in the majority of White tests. Another interesting aspect is that in the majority of tests, it shows no clear signs of accelerating contact angle changes relative to water tests, in spite of MED testing indicating otherwise. This suggests that the AES-50 mixture acts like a thresholding liquid and represents the relative fractional wettability of the medium at this particular surface tension i.e. the surface tension of a

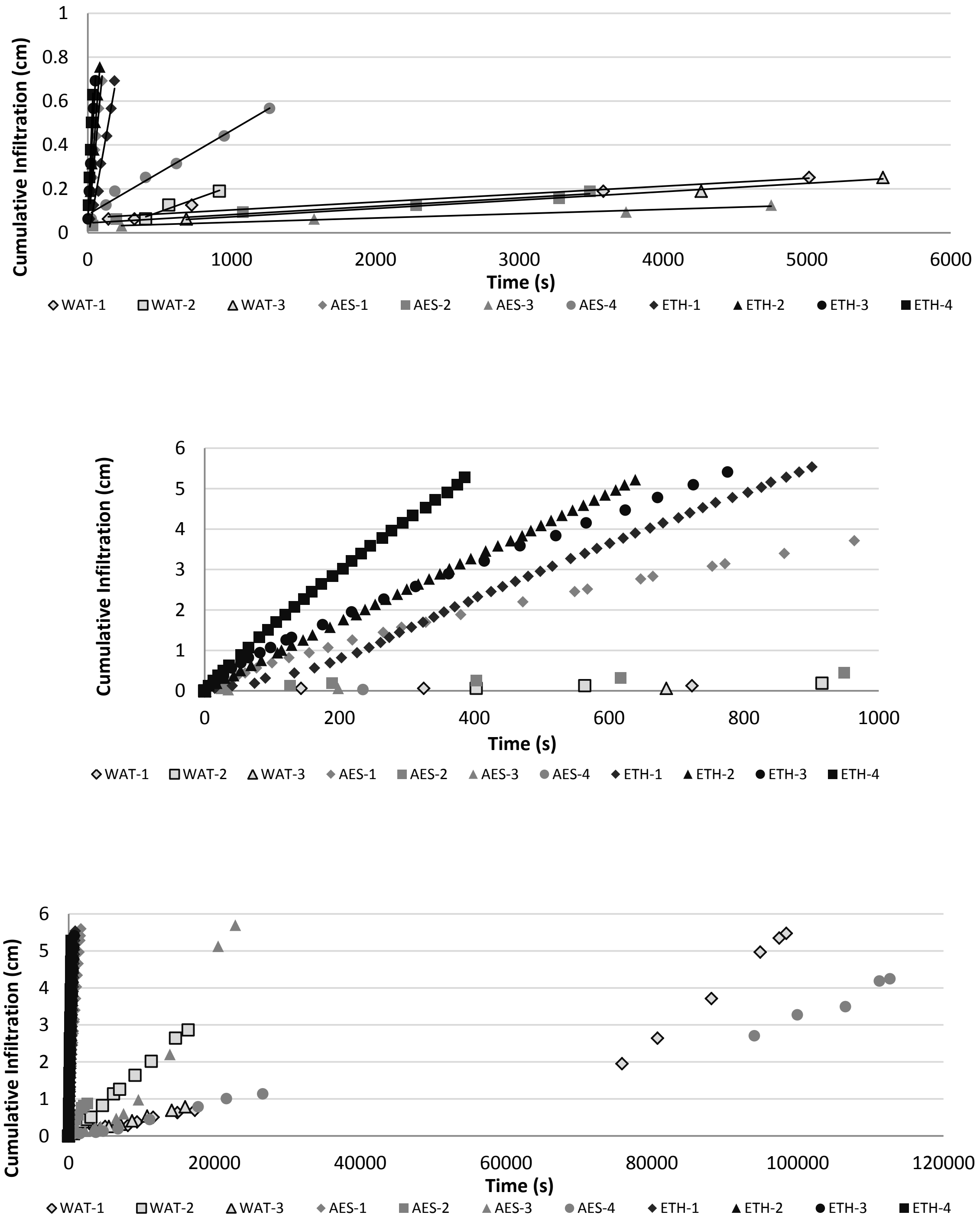

Figure 4.8 Cumulative Infiltration vs. Time for White materials. Showing a) "early time" (up to 1cm of infiltration) b) first 2500 s of data to facilitate viewing of early time ETH and AES-1infiltrations and c) entire data set

50% solution is unable to generate bulk ‘wettable infiltration’ in approximately 75% of the materials tested. Given the very slow infiltrability, two of four infiltration experiments (WAT-1 and AES-4) were left to run over night, and thus represent >24 h duration tests. In contrast, two water infiltration experiments (WAT-2 and WAT-3) had to be terminated early (at approx. 4.5 h testing duration), and thus are only used to represent ‘early-time’ infiltrated volumes (i.e. <3 cm and <1 cm of cumulative infiltration, respectively). For context, <1 cm of infiltration is typically used in sorptivity calculations in wettable soils, and is generally considered an ‘early-time’ volume.

Infiltration tests using water show small infiltration rates in the range of 10^{-4} to 10^{-5} cm/s. Three of four AES-50 tests exhibit similar behaviour with infiltration rates in the same range of values. The ethanol infiltration tests and one AES-50 test (i.e. AES-1) show consistently faster infiltration rates at early time (10^{-2} to 10^{-3} cm/s). These differences in infiltration behaviour at early time can be attributed to ethanol wetting the media (reducing repellency) within the advancing infiltration front more so than water. This apparent ‘smoothing’ effect of ethanol may be a result of compounded effects on the radius of curvature term (through the contact angle term) *and* the interfacial tension as shown in equation 5a.

Late time infiltration rates convey fundamental information about the nature of changes in these materials. Late time cumulative infiltration vs. time behaviours for water and two of three AES-50 experiments, while appearing more variable than those observed for ethanol tests, fall within a similar narrow range of values observed at early time (10^{-4} to 10^{-5} cm/s), albeit with slightly weaker correlation.

4.4.2.4 Unsaturated hydraulic conductivity (K_f) and Sorptivity (S)

We calculated Sorptivity (*S*) and hydraulic conductivity at the final (end of test) moisture content (K_f) following the methods presented by Moody et al. (2009). That is, we fit the following 2nd order polynomial to the cumulative infiltration (*I*) versus square root of time data to get *S* and the K_f related term *B*.

$$I = St^{1/2} + B\left(t^{1/2}\right)^2 \qquad \text{(eq. 4.6)}$$

Then calculated K_f using,

$$K_f = \frac{3}{2-\beta}\left[B - \frac{\gamma S^2}{r_d(\theta_f - \theta_i)}\right] \qquad \text{for } \theta_i/\theta_f < 0.5 \qquad \text{(eq. 4.7a)}$$

$$K_f = \left[B - \frac{\gamma S^2}{r_d(\theta_f - \theta_i)}\right] \qquad \text{for } \theta_i/\theta_f > 0.5 \qquad \text{(eq. 4.7b)}$$

where r_d is the radius of the infiltrometer disc (2.25 cm), θ_f is the final moisture content, and θ_i is the initial water content. Following Moody, we used γ equal to 0.7, and β equal to 0.6. The resultant data are presented in Table 4.2 and serve as a reference set for readers interested in *S* and K_f values of this investigation. However, it may not be well justified to use these *S* and K_f values for hydrologic simulations of repellent soils using standard hydrologic models. Specifically, the infiltration theory expressed by the fitted equations does not include any consideration for dynamic contact angles, i.e. changing repellency with time. The large proportion of physically impossible negative values of S

Table 4.2 Calculated Sorptivities (S), and Hydraulic Conductivities (K_f) and moisture contents by infiltration test (from Moody et al., 2009). Site averaged initial volumetric moisture contents (Char = 0.173, Brown = 0.077, Mixed-ML = 0.133, Mixed-Ru = 0.113, and White = 0.085) were used to calculate K_f (avg θ_i).

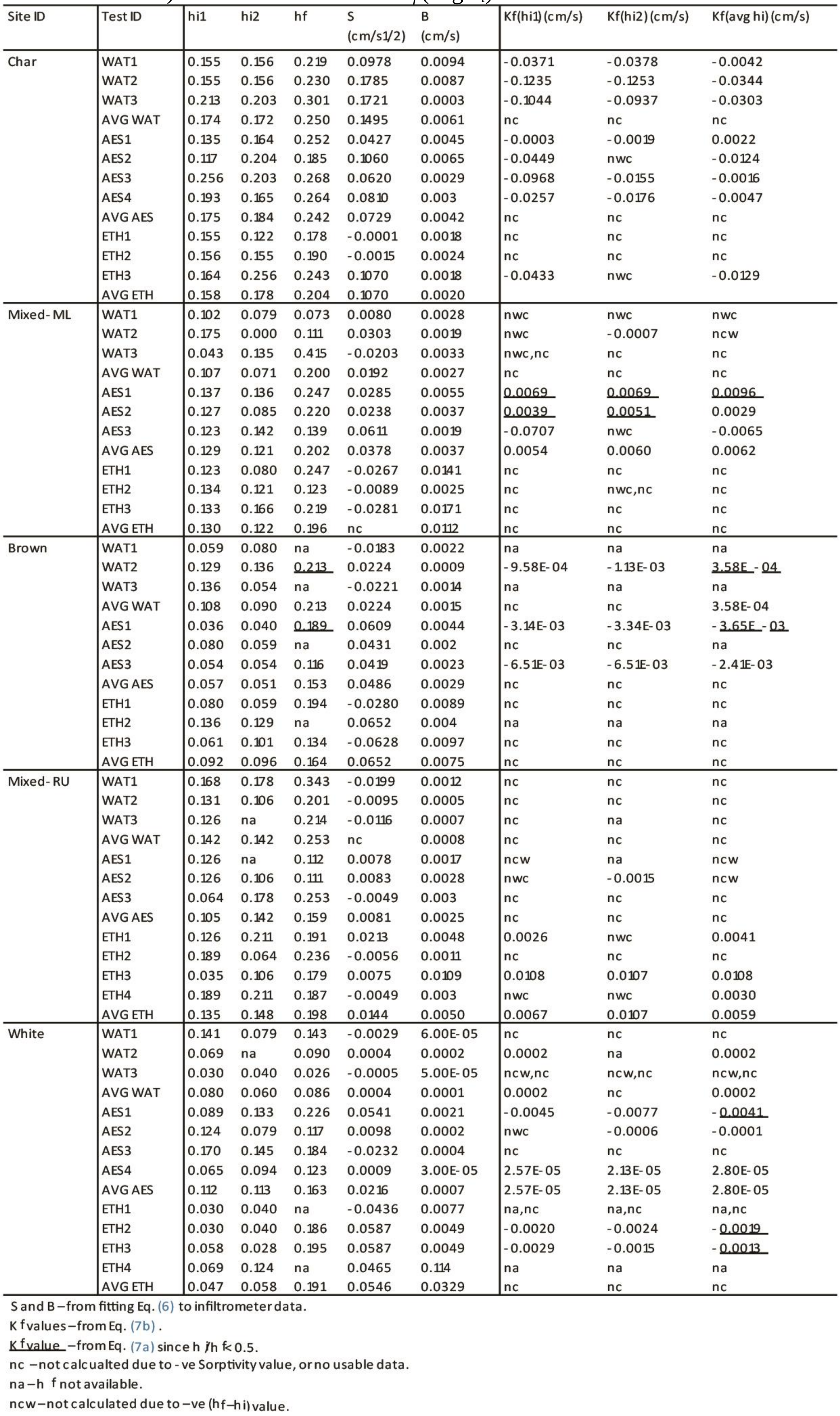

Site ID	Test ID	hi1	hi2	hf	S (cm/s1/2)	B (cm/s)	Kf(hi1) (cm/s)	Kf(hi2) (cm/s)	Kf(avg hi) (cm/s)
Char	WAT1	0.155	0.156	0.219	0.0978	0.0094	-0.0371	-0.0378	-0.0042
	WAT2	0.155	0.156	0.230	0.1785	0.0087	-0.1235	-0.1253	-0.0344
	WAT3	0.213	0.203	0.301	0.1721	0.0003	-0.1044	-0.0937	-0.0303
	AVG WAT	0.174	0.172	0.250	0.1495	0.0061	nc	nc	nc
	AES1	0.135	0.164	0.252	0.0427	0.0045	-0.0003	-0.0019	0.0022
	AES2	0.117	0.204	0.185	0.1060	0.0065	-0.0449	nwc	-0.0124
	AES3	0.256	0.203	0.268	0.0620	0.0029	-0.0968	-0.0155	-0.0016
	AES4	0.193	0.165	0.264	0.0810	0.003	-0.0257	-0.0176	-0.0047
	AVG AES	0.175	0.184	0.242	0.0729	0.0042	nc	nc	nc
	ETH1	0.155	0.122	0.178	-0.0001	0.0018	nc	nc	nc
	ETH2	0.156	0.155	0.190	-0.0015	0.0024	nc	nc	nc
	ETH3	0.164	0.256	0.243	0.1070	0.0018	-0.0433	nwc	-0.0129
	AVG ETH	0.158	0.178	0.204	0.1070	0.0020			
Mixed-ML	WAT1	0.102	0.079	0.073	0.0080	0.0028	nwc	nwc	nwc
	WAT2	0.175	0.000	0.111	0.0303	0.0019	nwc	-0.0007	ncw
	WAT3	0.043	0.135	0.415	-0.0203	0.0033	nwc,nc	nc	nc
	AVG WAT	0.107	0.071	0.200	0.0192	0.0027	nc	nc	nc
	AES1	0.137	0.136	0.247	0.0285	0.0055	0.0069	0.0069	0.0096
	AES2	0.127	0.085	0.220	0.0238	0.0037	0.0039	0.0051	0.0029
	AES3	0.123	0.142	0.139	0.0611	0.0019	-0.0707	nwc	-0.0065
	AVG AES	0.129	0.121	0.202	0.0378	0.0037	0.0054	0.0060	0.0062
	ETH1	0.123	0.080	0.247	-0.0267	0.0141	nc	nc	nc
	ETH2	0.134	0.121	0.123	-0.0089	0.0025	nc	nwc,nc	nc
	ETH3	0.133	0.166	0.219	-0.0281	0.0171	nc	nc	nc
	AVG ETH	0.130	0.122	0.196	nc	0.0112	nc	nc	nc
Brown	WAT1	0.059	0.080	na	-0.0183	0.0022	na	na	na
	WAT2	0.129	0.136	0.213	0.0224	0.0009	-9.58E-04	-1.13E-03	3.58E-04
	WAT3	0.136	0.054	na	-0.0221	0.0014	na	na	na
	AVG WAT	0.108	0.090	0.213	0.0224	0.0015	nc	nc	3.58E-04
	AES1	0.036	0.040	0.189	0.0609	0.0044	-3.14E-03	-3.34E-03	-3.65E-03
	AES2	0.080	0.059	na	0.0431	0.002	nc	nc	na
	AES3	0.054	0.054	0.116	0.0419	0.0023	-6.51E-03	-6.51E-03	-2.41E-03
	AVG AES	0.057	0.051	0.153	0.0486	0.0029	nc	nc	nc
	ETH1	0.080	0.059	0.194	-0.0280	0.0089	nc	nc	nc
	ETH2	0.136	0.129	na	0.0652	0.004	na	na	na
	ETH3	0.061	0.101	0.134	-0.0628	0.0097	nc	nc	nc
	AVG ETH	0.092	0.096	0.164	0.0652	0.0075	nc	nc	nc
Mixed-RU	WAT1	0.168	0.178	0.343	-0.0199	0.0012	nc	nc	nc
	WAT2	0.131	0.106	0.201	-0.0095	0.0005	nc	nc	nc
	WAT3	0.126	na	0.214	-0.0116	0.0007	nc	na	nc
	AVG WAT	0.142	0.142	0.253	nc	0.0008	nc	nc	nc
	AES1	0.126	na	0.112	0.0078	0.0017	ncw	na	ncw
	AES2	0.126	0.106	0.111	0.0083	0.0028	nwc	-0.0015	ncw
	AES3	0.064	0.178	0.253	-0.0049	0.003	nc	nc	nc
	AVG AES	0.105	0.142	0.159	0.0081	0.0025	nc	nc	nc
	ETH1	0.126	0.211	0.191	0.0213	0.0048	0.0026	nwc	0.0041
	ETH2	0.189	0.064	0.236	-0.0056	0.0011	nc	nc	nc
	ETH3	0.035	0.106	0.179	0.0075	0.0109	0.0108	0.0107	0.0108
	ETH4	0.189	0.211	0.187	-0.0049	0.003	nwc	nwc	0.0030
	AVG ETH	0.135	0.148	0.198	0.0144	0.0050	0.0067	0.0107	0.0059
White	WAT1	0.141	0.079	0.143	-0.0029	6.00E-05	nc	nc	nc
	WAT2	0.069	na	0.090	0.0004	0.0002	0.0002	na	0.0002
	WAT3	0.030	0.040	0.026	-0.0005	5.00E-05	ncw,nc	ncw,nc	ncw,nc
	AVG WAT	0.080	0.060	0.086	0.0004	0.0001	0.0002	nc	0.0002
	AES1	0.089	0.133	0.226	0.0541	0.0021	-0.0045	-0.0077	-0.0041
	AES2	0.124	0.079	0.117	0.0098	0.0002	nwc	-0.0006	-0.0001
	AES3	0.170	0.145	0.184	-0.0232	0.0004	nc	nc	nc
	AES4	0.065	0.094	0.123	0.0009	3.00E-05	2.57E-05	2.13E-05	2.80E-05
	AVG AES	0.112	0.113	0.163	0.0216	0.0007	2.57E-05	2.13E-05	2.80E-05
	ETH1	0.030	0.040	na	-0.0436	0.0077	na,nc	na,nc	na,nc
	ETH2	0.030	0.040	0.186	0.0587	0.0049	-0.0020	-0.0024	-0.0019
	ETH3	0.058	0.028	0.195	0.0587	0.0049	-0.0029	-0.0015	-0.0013
	ETH4	0.069	0.124	na	0.0465	0.114	na	na	na
	AVG ETH	0.047	0.058	0.191	0.0546	0.0329	nc	nc	nc

S and B – from fitting Eq. (6) to infiltrometer data.

K_f values – from Eq. (7b).

K_f value – from Eq. (7a) since $h_i/h_f < 0.5$.

nc – not calcualted due to -ve Sorptivity value, or no usable data.

na – h_f not available.

ncw – not calculated due to –ve ($h_f - h_i$) value.

(46.7% for water; 38.8% for all fluids) and K_f (33.3% for water; 34.7% for all fluids) demonstrates the limited utility. Also, the positive values of S (53.3% for water; 61.2% for all fluids) and K_f (6.7% for water; 22.4% for all fluids) calculated and reported in Table 4.2 may be subject to errors caused by the primary role changing repellency plays over time. That is, the sensitivity of this method of calculating S and K_f values to dynamic repellency is not known. Moody et al. (2009) reported greater success for laboratory infiltration test data and for soils expressing lesser repellency. Relative to Moody et al. (2009) we measured similar S values for water infiltration into Char materials (avg S 0.15 cm/s$^{1/2}$) with all other materials' S values (avg S 0.02 to 0.0004 cm/s$^{1/2}$) being approximately 2–100 times lower. It is noteworthy that our lowest S value coincided with a very low θ_f value of only 0.09 which was similar to the local initial value (θ_i). The only successfully calculated K_f value for water was 1.9×10^{-4} cm/s is one to two orders of magnitude lower than the materials reported by Moody et al. (2009).

4.4.3 Time to first five bubbles

Cumulative Infiltration vs. Time plots for Time to First Five Bubbles (TFFB) appear in Figure 4.9. No delays in infiltration (time to first bubble = 0 s) were observed for Char materials, and for that reason are not shown. Cumulative infiltration was calculated based on the total volume infiltrated over the duration of five bubbles. Bubble sizes averaged 0.20 ml or 0.0126 cm of infiltration, with the exception of the faster rates at the Mixed-ML site which averaged 0.5 ml.

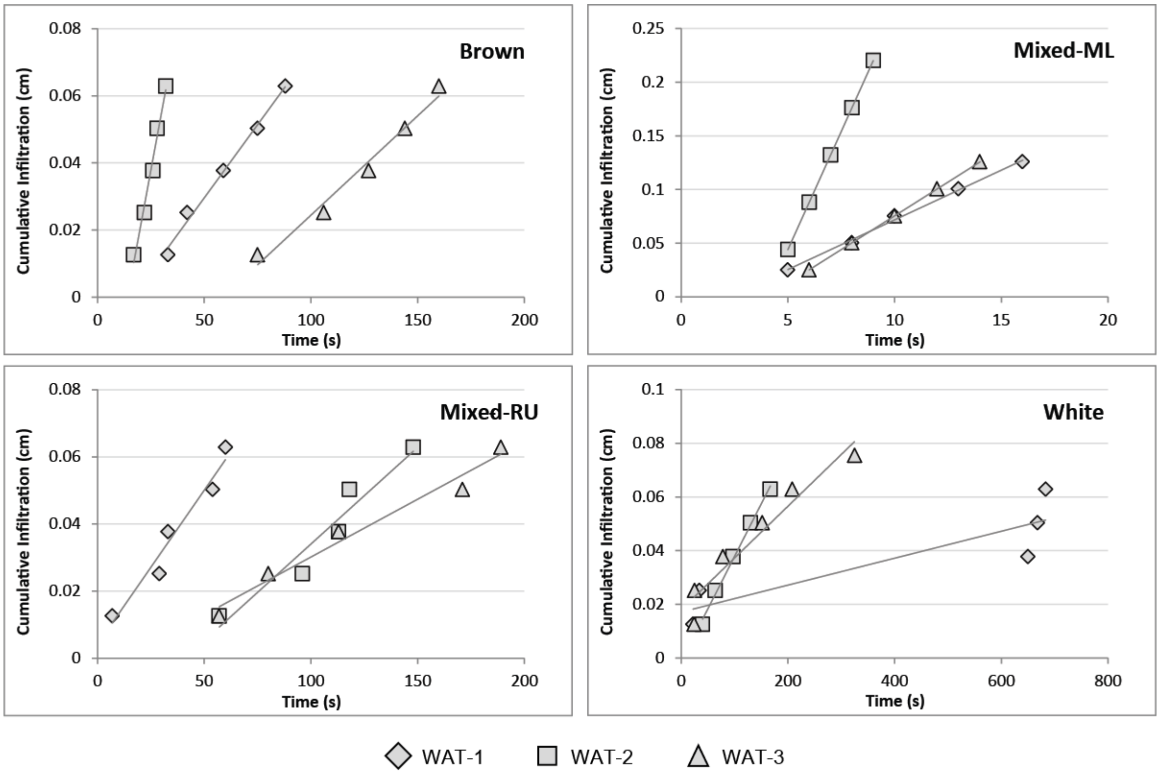

Figure 4.9 Cumulative Infiltration vs. Time to First Five Bubbles (TFFB) of water for materials exhibiting water repellency.

The vast majority of tests initiated the first bubble within the first minute of testing and similar trends as observed in previous figures exist in these materials. Mixed-ML materials exhibit the quickest time to first bubble (5, 5, and 6 s) and infiltration rates (10^{-3} cm/s to 10^{-2} cm/s). White materials exhibit consistently long delays to initiation, with more observed variability (22, 24, and 40 s) and the slowest rates (10^{-5} cm/s to 10^{-4} cm/s). Brown and Mixed-RU materials exhibit similarly variable first bubble times with (17, 33, and 75 s) and (7, 57, and 57 s), respectively and TFFB infiltration rates in the range of 10^{-4} cm/s to 10^{-3} cm/s (for both).

4.4.4 Infiltration rate relationships

4.4.4.1 Early-time vs. time to first five bubbles

Early time vs. TFFB for water (only) infiltration rates appear in a log–log plot in Figure 4.10. With the exception of Brown tests, the majority of tests fall below the 1:1 line, representing faster TFFB infiltration rates compared to early time infiltration rates. It is noteworthy that the TFFB data represents the infiltration of <1 mm of water. Consequently, this data represents infiltration into only the nearest surface materials. We are in agreement with Lewis et al. (2006) that the minidisk has a clear advantage over WDPT since infiltration initiation measurements can be directly related to early time infiltration rate data. TFFB numbers falling below the 1:1 line indicate that the nearest surface materials are generally more wettable than materials accessed during ‘early-time’ infiltration, i.e. the first approximately 1 cm of infiltration. Mixed material cases for both RU and ML sites combined are interesting in that while the TFFB range is nearly two orders of magnitude wide, the early-time infiltration range for these materials is much smaller. In circumstances such as this, time to first bubble and TFFB times would not be a suitable representation for slightly larger scale (early-time) infiltration rates. It is promising that early time infiltration behaviours are so well described by the TFFB data, however, using such results to predict or inform on larger scale infiltration processes should be done with some caution.

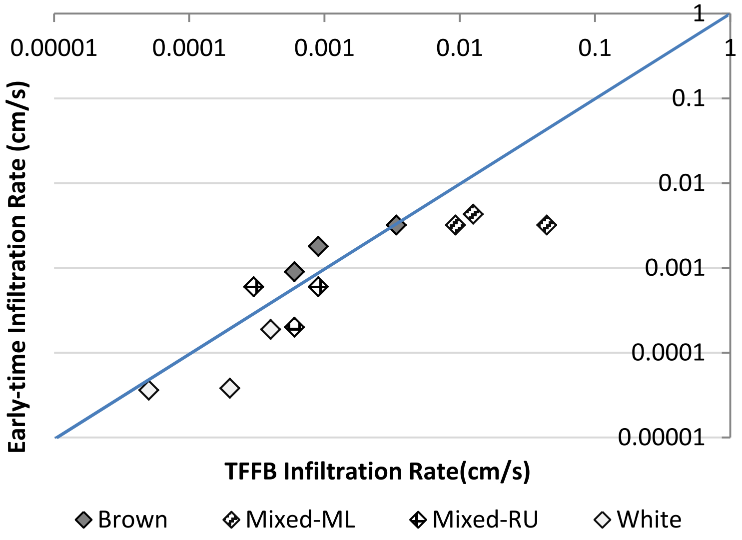

Figure 4.10 Early-time infiltration rates (slope of CI vs. Time plots for <1cm of infiltration) vs. Time to First Five Bubbles (TFFB) for water infiltrations on repellent materials only. Line drawn at 1:1.

4.4.4.2 Early-time vs. late-time infiltration rates

During wettable infiltration, slopes of cumulative infiltration vs. time are expected to decrease between early and late time as functions of changes in the physical mechanisms (namely, hydraulic gradients, capillarity, water capacity, and gravity) driving infiltration in porous media. These relationships are well described by soil physics theory. Figure 4.11 is a log–log plot of Early vs. Late-time Infiltration Rates showing individual data for 46 tests completed. Tests that were terminated early do not have late-time rates and are thus excluded (White: AES-2, WAT-2, and WAT-3). Using Figure 4.11, we coarsely categorize between infiltration behaviours reflecting ‘predictable’ infiltration and ‘dynamic’ infiltration. We cannot fully account for the role that field heterogeneity may be contributing to ‘dynamic’ behaviours, and consequently, only suggest that contact angle dynamics are consistent with and may be taking part in the observed ‘dynamic’ behaviours.

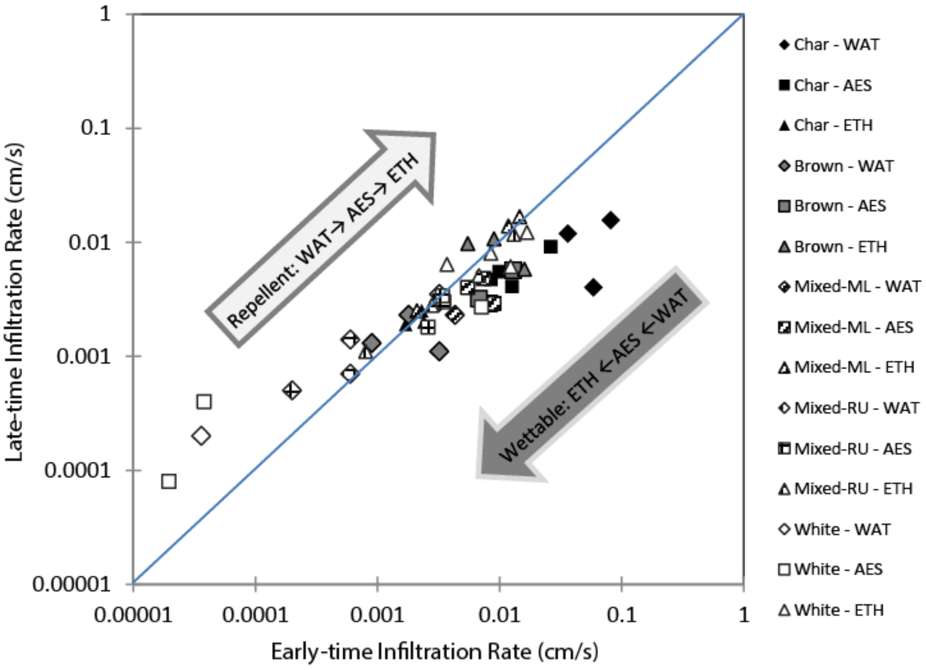

Figure 4.11 Early-time Infiltration Rates (slope of CI vs. Time plots for <1cm of infiltration) vs. Late-time Infiltration Rates. Line drawn at 1:1. Arrows depict overall trend differences between wettable and water repellent infiltrations for different ethanol concentrations (between 0% and 100% by volume). Each point represents one infiltration test. Individual symbols may appear up to four times, e.g. the ◆ Char-WAT symbol appears three times, to represent three infiltration tests.

This figure shows the complexity of field heterogeneity and repellency differences (i.e. within sites and between fluids), while at the same time capturing within and across site systematic trends in behaviour. In these complex layered materials, the majority of tests fall below the 1:1 line. In a single layer system, wettable-type infiltration would fall below the 1:1 line, with faster infiltration rates initially and slower infiltration rates at later time. Material/fluid combinations with early-time infiltration rates less than late-time infiltration rates plot above the 1:1 line indicating dynamic infiltration behaviours (hockey stick infiltration). Points falling directly on the 1:1 line depict no difference between late- and early-time infiltration rates.

Wettable materials (in this case Char) exhibit a trend from higher early and late time infiltration rates below the 1:1 line to lower early and late time infiltration rates that converge on the 1:1 line as ethanol concentration increases from 0% to 100%. In contrast, water repellent materials (i.e. all other cases) trend in the opposite direction, exhibiting a trend from lower to higher (early- and late-) infiltration rates somewhat scattered about the (1:1) line as ethanol concentration increases from 0% to 100%. Note that two Mixed-ML-WAT data points are obscured by two Mixed-RU-AES data points situated approximately on the 1:1 line at 0.003). We suspect that the specific values/ranges of values within a given material convey important information on differences in fractional wettability and contact angle dynamics between different materials and are complimentary to the contrasting trend directions.

Across all materials, water and AES infiltrations exhibit the largest amount of spread both within and between materials. ETH infiltrations cluster less and appear more evenly distributed along, and straddling the 1:1 line. This is somewhat unexpected since ethanol is typically regarded as a perfectly wetting fluid in both water wettable and water repellent media, and consequently theoretically would not exhibit increasing rates over time (i.e. appear above the 1:1 line). Ethanol tests that increase in magnitude (0.003 cm/s) suggests the detection of an additional process, mechanism, or variable not present in the other experiments (e.g. sludge effect) and/or materials that retain dynamic hydraulic properties in the presence of ethanol.

With the exception of the Char and the majority of White materials, AES tests (regardless of concentration) generally exhibit similar early-time infiltration rates as ETH tests, but distinctly lower late-time infiltration rates, a decidedly more ‘wettable’ (vs. dynamic) infiltration response. In controlled 1D laboratory experiments, increases in the infiltration rate over time can more directly be attributed to, as noted earlier, the dynamic change of contact angles in repellent materials and/or the build-up of local pore water pressures (Beatty and Smith, 2013; Clothier et al., 2000; Feng et al., 2001). In the field, three dimensional spatial heterogeneity may be contributing to the observed relationship and as in most field studies poses a persistent challenge to data interpretation.

4.4.5 Fluid effects on average late-time infiltration rates for water, AES, and ethanol

Figure 4.12 shows the average late time infiltration rates for water, AES, and ethanol for each material, i.e. Char, Brown, Mixed-ML, Mixed-RU, and White. Each bar represents the average of three or four tests with the exception of AVG WAT bar for the White site which had only one late-time infiltration rate value. As described earlier, Char materials are wettable. In response to varying concentrations of ethanol in solution, these

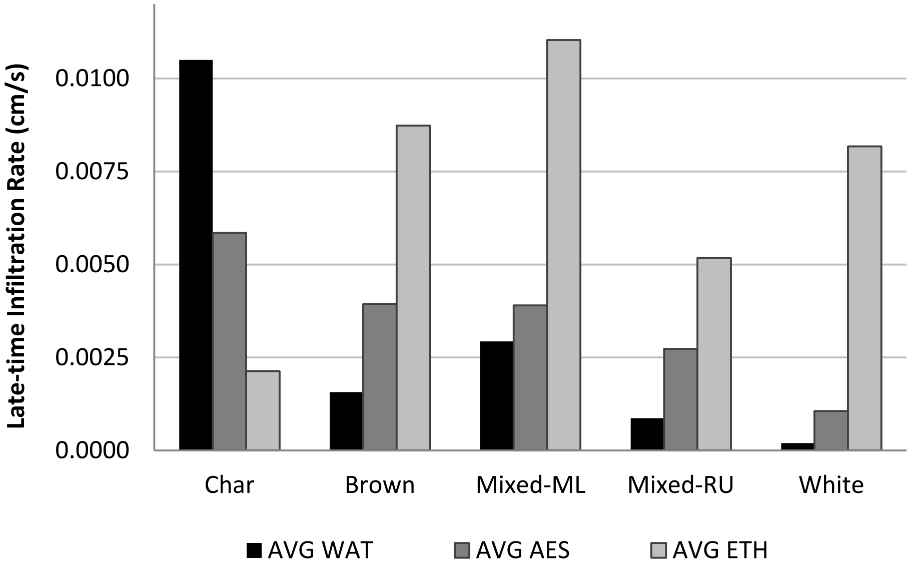

Figure 4.12 Fluid effects: average late-time infiltration rates for water, AES, and ethanol by material type

tests exhibits a fundamentally different response compared to repellent materials. Specifically, water has the highest infiltration rate (1.05×10^{-2} cm/s), AES (5%) is about 56% as fast (water 1.8 times faster) and ethanol is 20% as fast as (water 5 times faster) water. These slower rates for the ethanol solutions are relatively consistent with the mobility factors listed in Table 4.1, the initial average soil water content of 17.3% and "sludge effect" in the solute front, as well as the lower soil water pressure heads ((eq. 4.3), (eq. 4.4) and (eq. 4.5a and b)). That is, diminishing infiltration rates in the order water > AES > ethanol is characteristic of water-wet soils.

In response to varying concentrations of ethanol, infiltration rates for repellent materials increase in the order of water < AES < ethanol. Water has the slowest late-time infiltration rates, AES faster and ethanol the fastest. This is opposite to the effect caused by mobility factors (eq. (4.1); Table 4.1) meaning that the increase in infiltration induced by contact angle dynamics, changes in fractional wettability, and related changes in continuously fluid filled pore structures have a primary and larger affect. As shown in Figure 4.12, the repellent soils have the following late-time infiltration rates: Brown water 1.6×10^{-3} cm/s, with AES 2.5 times faster and ethanol 5.6 times faster than water; Mixed-ML water 2.9×10^{-3} cm/s, with AES 1.3 times faster and ethanol 3.8 times faster than water; Mixed-RU water 8.7×10^{-4} cm/s, with AES is 3.2 times faster and ethanol 6.0 times faster than water; White water 2.0×10^{-4} cm/s, with AES 5.3 times faster and ethanol 41.9 times faster than water. White materials were the only ones for which the 5 cm long moisture sensors captured substantially higher final moisture contents (θ_f) for ethanol solution tests compared to water tests, i.e. 2.2 times higher at 0.19 versus initial water content (θ_i) of 0.086. While this moisture content difference is consistent with observed infiltration rates, caution is warranted since 5 cm long moisture probes are limited in their ability to resolve smaller scale moisture contents.

Figure 4.12 expresses well that the AES solutions cause intermediate changes in infiltration rates, i.e. falls between water and ethanol. The results of these infiltration experiments suggest that the AES solutions are only wetting up a fraction (proportion) of the soil which is less than that for ethanol infiltration. These differences in infiltration rates for varied ethanol concentrations express hydraulic information about fractional wettability. While beyond the present work (herein), we expect this information yields valuable quantitative measures for the development of empirical hydraulic functions for repellent soils expressing contact angle dynamics and fractional wettability.

4.5 Summary and conclusions

This work explored the relationships between different repellency measures to help provide insight into fractional wettability and contact angle dynamics in field materials using water, ethanol and Molarity of Ethanol Drop (MED)-derived aqueous solutions. Four key post-wildfire materials exhibiting repellent and/or wettable characteristics were targeted during the field investigation to evaluate differences in fluid behaviours as indicators of differences in fractional wettability and contact angle dynamics.

Infiltration of water, ethanol, and MED-derived aqueous ethanol solutions generated meaningful graphical representations of differences in fractional wettability and contact angle dynamic differences between sites and materials. When combined in cumulative infiltration vs. time plots, within site/material trends became pronounced and differences attributable to fractional wettability and contact angle dynamics were observable. In the most persistently repellent (and lower fractional wettability) materials, water generated long delays to infiltration and testing durations. AES infiltrations exhibited behaviour consistent with wetting up of different fractions (proportions) of the soil through intermediate (between water and ethanol) and threshold infiltration responses. Only one aqueous ethanol solution was used per material. Systematic work using more mixtures could prove useful for isolating and quantifying different (key) non-wettable and wettable fractions within fractionally wettable soils and their relative influence on unsaturated hydraulic conductivities.

Ethanol is typically used for Repellency Index (RI) calculations that focus on pairing early time data. Here we evaluated replicate tests over longer durations and larger volumes to observe within-material response/variability for each of the infiltrating fluids vs. pairing locations, materials, etc. as would be beneficial for a more reliable RI calculation. Infiltrations using ethanol were faster in non-wettable media and slower in wettable media when compared to water. In all materials, ethanol elicited less variable early-time infiltration rates than observed for water. However, one factor not considered in these behaviours initially was the role of antecedent moisture content. In field materials, ambient moisture can cause the wetting front to slow down as a consequence of mixing of the soil solution and infiltrating ethanol within the solute front. In field investigations, this is likely to be more problematic for wettable soils with higher relative moisture contents, and contributing to slower rates. Fractionally wettable media are also likely to be influenced according to the size of the wettable fraction and its connectedness with initial soil moisture content. Any investigation using alcohols in the field/on field moist samples should take this into consideration.

We modified a newer approach (Time to First Bubble (TFB)) to capture high resolution early time/small spatial infiltration data. The initialization of the mini disk infiltrometer (MDI) can generate uncertainty in the TFB as it travels down the reservoir tube in slow-to-initiate materials. This is resolved through a new approach, which we termed Time to First Five bubbles (TFFB). This approach effectively calibrates the instrument after the first bubble is released. TFFB data were directly relatable to early-time infiltration rate data and were useful for characterizing repellency. Some later/larger scale information is captured in these small scale measures, however, these data best inform on the wettability of near surface materials. When differences in fractional wettability occur spatially and into the soil profile, they serve as a complement to longer duration / larger volume testing.

A comparison of early- vs. late-time infiltration rates for each of the materials generated systematic trends within each of the liquid groupings whereby wettable materials could be directly compared to repellent materials. Relative position anchoring and ranges between fluid clusters (within a given material) informs on the nature of fractional wettability spatially and can be used as a fractional wettability indicator as highlighted by the water, ethanol, and AES infiltration tests. Further work using these graphical representations may be informative.

One topic worth discussing is around the definition of appropriate temporal and spatial scales of investigation in repellent soils. This work shows that while early-volume/time measures capture some longer term/larger scale information, meaningful differences in materials are best expressed over the longer term larger scale response, which is unique to each site / material / environmental condition. The value of shorter duration testing (and ‘quicker’ fluids) is enhanced when coupled with longer duration testing, which can sometimes be greater than 24 h. Generating robust long-duration data sets such as these are of great value and can likely assist in addressing some of the knowledge gaps that exist, even when pragmatically difficult to generate.

In the absence of datasets such as these, it may be desirable and tempting to seek a set of type curves and parameters that can be used with existing hydrological models formulated for wettable soils. We think this should be approached with caution. The accuracies and validity of such parameters and models which lack any mechanistic expression or kinetic relations of the primary role of dynamic repellency (i.e. contact angle dynamics and fractional wettability) need to be more fully investigated. More data sets from dynamically repellent soils will be useful in extracting empirical kinetic parameters and/or dynamic scaling relations for hydraulic properties suitable for emerging numerical models of repellent soils.

Acknowledgements

This work was funded in part by the R. Edward Munn Ontario Graduate Scholarship and the Natural Sciences and Engineering Research Council (NSERC) of Canada Discovery Grant Program. We would like to acknowledge the assistance of the Ontario Ministry of Natural Resources Timmins, ON Fire Office in this work. Special thanks to Nicole Galambos, Tony Rachwalski, Joel Legasy and Fred Welch (all with OMNR) for knowledge sharing, assistance in accessing sites, and reference materials used in this work. Thanks also to Chad St. Amand of Tembec Inc. for data sharing and insights on forest resources inventory information. Thanks to Andrew Trapp for providing assistance in the field.

References

Agriculture and Agri-Food Canada. 1978. [online] Soils of Timmins-Noranda-Rouyn area Ontario. Soil Survey Report no. 46. 1:250,000. Ottawa, Department of Energy, Mines and Resources. http://sis.agr.gc.ca/cansis/publications/surveys/on/on46/index.html. Accessed July 15, 2013.

Agriculture and Agri-Food Canada. 1986. [online] Soils of Gogama area Ontario. 1:250,000. Land Resource Research Institute, Agriculture Canada, Ottawa, Ontario. http://sis.agr.gc.ca/cansis/publications/surveys/on/on59/index.html. Accessed January 18, 2014.

Al-Futaisi, A., Patzek, T.W. 2004. Secondary imbibition in NAPL-invaded mixed-wet sediments. J. Contam. Hydrol. 74: 61-81.

Beatty, S.M., Smith, J.E. 2010. Fractional wettability and contact angle dynamics in burned water repellent soils. J. Hydrol. 391:99-110.

Beatty, S.M., Smith, J.E. 2013. Dynamic soil water repellency and infiltration in post-wildfire soils. Geoderma 192: 160-172.

Bisdom, E.B.A., Dekker, L.W., Schoute, J.F.T. 1993. Water repellency of sieve fractions from sandy soils and relationships with organic material and soil structure. Geoderma 56:105-118.

Bodi, M.B., Doerr, S.H., Cerda, A., Mataix-Solera, J. 2012. Hydrological effect of a layer of vegetation ash on underlying wettable and water repellent soil. Geoderma 191:14-23.Clothier, B.E., Vogeler, I., Magesan, G.N. 2000. The breakdown of water repellency and solute transport through a hydrophobic soil. J. Hydrol. 231-232:255-264.

DeBano, L.F. 1981. Water Repellent Soils: A State-of-the-Art. USDA, Forest Service General Technical Report: PSW-46. 21 pp.

Decagon Devices. 2012. Mini Disk Infiltrometer User’s Manual, version 10. Pullman, WA. 26 pp.

Dekker, L.W., Ritsema, C.J., Oostindie, K., Moore, D., Wesseling, J.G. 2009. Methods for determining soil water repellency on field moist samples. Water Resour. Res. 45: W00D33, doi:10.1029/2008WR007070.

Diamantopoulos, E., Durner, W., Reskowska, A., Bachmann, J. 2013. Effect of soil water repellency on soil hydraulic properties estimated under dynamic conditions. J. Hydrol. 486:175-186.

Doerr, S.H., Thomas, A.D., 2000. The role of soil moisture in controlling water repellency: new evidence from forest soils in Portugal. J. Hydrol. 231–232:134-147.

Doerr, S.H., Shakesby, R.A., Walsh, R.P.D. 2000. Soil water repellency: Its causes, characteristics and hydro-geomorphological significance. Earth Sci. Rev. 51:33-65.

Doerr, S.H., Woods, S.W., Martin, D.A, Casimiro, M. 2009. Natural background soil water repellency in conifer forests of the north-western USA: Its prediction and relationship to wildfire occurrence. J. Hydrol. 371:12-21.Feng, G.L., Letey, J., Wu, L. 2001. Water ponding depths affect temporal infiltration rates in a water-repellent sand. Soil Sci. Soc. Am. J. 65:315-320.

Fetter, C.W. 1999. Contaminant Hydrogeology 2nd Ed. Macmillan Publishing Co., 458 p.

Fischer, T., Yair, A., Veste, M., Geppert, H. 2013. Hydraulic properties of biological soil crusts on sand dunes studied by 13C-CP/MAS-NMR: A comparison between an arid and a temperate site. Catena 110:155-160.

Ganz, C., Bachmann, J., Lamparter, A., Woche, S.K., Duijnisvel, W.H.M., Gobel, M-O. 2013. Specific processes during in situ infiltration into a sandy soil with low-level water repellency. J. Hydrol. 484:45-54.

Gillespie, J.E., Acton, C.J., Hoffman, D.W. 1981. Soils of the Gogama map sheet, (41P) Ontario, Report No. 59. [online] Available: http://sis.agr.gc.ca/cansis/publications/surveys/on/on59/index.html. Ontario Institute of Pedology, Guelph, Ontario. Accessed January 18, 2014.

Hallett, P.D., Nunam, N., Douglas, J.T., Young, I.M. 2004. Millimeter-scale spatial variability in soil water sorptivity: Scale, surface elevation, and subcritical repellency effects. Soil Sci. Soc. Am. J. 68:352-358.

Hardie, M., Deurer, M., Doyle, R.B, Lisson, S., Cotching, W.E, Mattern, K. 2012. Development of unstable flow and reduced hydraulic conductivity due to water repellence and restricted drainage. Vadose Zone J. 11(4), 11 pp.

Hartmann, P., Fleige, H., Horn, R. 2010. Water repellency of fly ash-enriched forest soils from eastern Germany. Eur. J. Soil. Sci. 61:1070-1078.

Henry, E.J., Smith, J.E. 2003. Surfactant-induced flow phenomena in the vadose zone: A review of data and numerical modeling. Vadose Zone J. 2:154–167.

Hillel, D. 1982. Introduction to Soil Physics. Academic Press. Toronto, ON. 364p.

Imeson, A.C., Verstaten, J.M., van Mulligen, E.J., Sevink, J. 1992. The effects of fire and water repellency on infiltration and runoff under Mediterranean type forest. Catena 19:345-361.

Lamparter, A., Bachmann, J., Deurer, M., Woche, S.K. 2010. Applicability of ethanol for measuring intrinsic hydraulic properties of sand with various water repellency levels. Vadose Zone J. 9:445-450.

Leighton-Boyce, G., Doerr, S.H., Shakesby, R.A., Walsh, R.P.D. 2007. Quanitfying the impact of soil water repellency on overland flow generation and erosion: a new approach using rainfall simulation and wetting agent on in situ soil. Hydrol. Process. 21:2337-2345.

Letey, J., Carrillo, M.L.K., Pang, X.P. 2000. Approaches to characterize the degree of water repellency. J. Hydrol. 231-232:61-65.

Lewis, S.A., Wu, J.Q., Robichaud, P.R. 2006. Assessing burn severity and comparing soil water repellency, Hayman Fire, Colorado. Hydrol. Process. 20:1-16.

Lichner, L., Hallett, P.D., Drongova, Z., Czachor, H., Kovacik, L., Mataix-Solera, J., Homolak, M. 2013. Algae influence the hydrophysical parameters of a sandy soil. Catena 108:58-68.

Lide, D.R. (ed.) 1993. Handbook of Chemistry and Physics, 74th Edition. Viscosity of Aqueous Solutions (6-198). Taylor & Francis. Ann Arbor. 2624 pp.

Logsdon, S. 1997. Transient variation in the infiltration rate during measurement with tension infiltrometers. Soil Sci. 162:233-241.

Meteorological Service of Canada. 2013. [online] Timmins Victor Power A. Canadian Climate Normals 1971-2000 Station Data. http://climate.weather.gc.ca/climate_normals. Accessed August 19, 2013.

Ministry of Northern Development. 2005. Northern Ontario Engineering Geology Terrain Study (NOEGTS) – Polygons. [Shapefile geospatial data]. Scholars GeoPortal. Last updated, 2005.

Moody, J.A., Kinner, D.A., Ubeda, X. 2009. Linking hydraulic properties of fire-affected soils to infiltration and water repellency. J. Hydrol. 379:291-303.

Moody, J.A., Shakesby, R.A, Robichaud, P.R., Cannon, S. H., Martin, D.A. 2013. Current research issues related to post-wildfire runoff and erosion processes. Earth-Sci. Rev. 122:10-37.

Nyman, P., Sheridan, G., Lane, P.N.J. 2010. Synergistic effects of water repellency and macropore flow on the hydraulic conductivity of a burned forest soil, south-east Australia. Hydrol. Process. 24:2871-2887.

O’Carroll, D.M., Abriola, L.M., Polityka, C.A., Bradford, S.A., Demond, A.H. 2005. Prediction of two-phase capillary pressure-saturation relationships in fractional wettability systems. J. Contam. Hydrol. 77:247-270.

O’Carroll, D., Mumford, K., Abriola, L., Gerhard, J. 2010. Influence of wettability variations on dynamic effects in capillary pressure. Water Resour. Res. 46, W08505, doi:10.1029/2009WR008712.

Ontario Ministry of Natural Resources. 2009. Forest Resources Inventory – Status [Shapefile geospatial data]. Scholars GeoPortal, Ontario Council of University Libraries. Toronto, Canada. Last updated, 2009.

Ontario Ministry of Natural Resources. 2011. Forest Resources Inventory – Planning Composite [Shapefile geospatial data]. Scholars GeoPortal, Ontario Council of University Libraries. Toronto, Canada. Last updated, 2011.

Pierson, F.B., Robichaud, P.R., Moffet, C.A., Spaeth, K.E., Williams, C.J., Hardegree, S.P., Clark, P.E. 2008. Soil water repellency and infiltration in coarse-textured soils of burned and unburned sagebrush ecosystems. Catena 74:98-108.

Quyum, A., Achari, G., Goodman, R.H. 2002. Effect of wetting and drying and dilution on moisture migration through oil contaminated hydrophobic soils. Sci. Total Environ. 296:77-87.

Smith, J.E., Gillham, R.W. 1994. The effect of concentration-dependent surface tension of the flow of water and transport of dissolved organic compounds: A pressure head-based formulation and numerical model. Water Resour. Res. 30:343–354.

Smith, J.E., Gillham, R.W. 1999. Effects of solute-concentration-dependent surface tension on unsaturated flow: Laboratory sand column experiments. Water Resour. Res. 35:973–982.

Statistics Canada. 2008. [online] Map 1 Terrestrial Ecozones. Accessed Oct. 1, 2013. http://www.statcan.gc.ca/pub/16-002-x/2008002/map-carte/5212684-eng.htm

Tillman, R.W., Scotter, D.R., Wallis, M.G., Clothier, B.E. 1989. Water-repellency and its measurement by using intrinsic sorptivity. Aust. J. Soil Res. 27:637-644.

Wallach, R., Graber, E.R. 2007. Infiltration into effluent irrigation-induced repellent soils and the dependence of repellency on ambient relative humidity. Hydrol. Process. 21:2346-2355.

Wallis, M.G., Horne, D.J. 1992. Soil water repellency. Adv. Soil S. 20:91-146.Wang, A., Wu, Q.J., Wu, L., Ritsema, C.J., Dekker, L.W., Feyen, J. 2000. Effects of soil water repellency on infiltration rate and flow instability. J. Hydrol. 231-232:265-276.

Woods, S.W, Balfour, V.N. 2010. The effects of soil texture and ash thickness on the post-fire hydrological response from ash-covered soils. J. Hydrol. 393:274-286.

CHAPTER 5 - DYNAMIC SOIL WATER REPELLENCY: A PRIMARY DRIVER DURING INFILTRATION UNDER TENSION*

Abstract

Dynamic soil water repellency is a poorly understood phenomenon in the vadose zone. This study investigates dynamic soil water repellency through the use of tension infiltrometry. Twenty infiltration columns, instrumented with moisture sensors were dry packed with a combination of hydrophilic and/or hydrophobic air-dried field materials collected from a post-wildfire site. Three different wetting fluids (water, ethanol, and an aqueous ethanol solution of 25% ethanol) were used on three separate material configurations (Mineral, Organic Matter+Mineral, Organic Matter+Impermeable Boundary). Tension infiltrometers customized for use with ethanol maintained a constant negative pressure head throughout repellent layers in 9.5 cm ID infiltration columns which prevented positive pressure heads in repellent materials. Applying a tension of -4 cm at the surface defined a different operational pore space as elicited by different effective tensions according to the surface tension of the applied fluid. This applied tension resulted in effective tensions of -4 cm, -8.5 cm, -13.2 cm for water, aqueous ethanol solution, and ethanol, respectively. In hydrophilic soils, differences in infiltration could be explained via differences in fluid properties alone and behaved as expected with water being fastest, ethanol slowest, and the aqueous ethanol solution with an intermediate response. While increasing ethanol concentration can generate faster infiltration responses through increases in wettability in repellent soils, changes in fluid mobilities and effective tensions generated more complex infiltration relationships than are typically reported. In repellent configurations, the aqueous ethanol solution was fastest, ethanol slowest overall, and water had an intermediate response. This is significant since ethanol is typically considered a ‘quicker’ fluid in water repellent media through changes in contact angle caused by reduced interfacial tensions. The results of our work indicate that effective tensions and layering in water repellent systems interact in a complex fashion with changes in wettability, fluid properties, and the operational pore space in a given medium even under relatively weak tensions. This generated insight into the nature of unsaturated hydraulic conductivity in materials where contact angle dynamics and changing fractional wettability are primary drivers of infiltration.

Keywords: fractional wettability, dynamic soil water repellency, soil water repellency, contact angle, MED, ethanol, sorptivity, tension infiltrometer

5.1 Introduction

Dynamic contact angles and changes in fractional wettability are foundational concepts in the investigation of dynamic soil water repellency. While much work has been done in characterizing the persistence and severity of repellency, small scale measures of repellency reveal less about dynamic changes in repellency in larger spatial and temporal scales and mechanistic linkages. Consequently, our mechanistic understanding of the combined roles of fractional wettability and contact angle dynamics on fluxes and storage in repellent materials is somewhat limited. Being able to better define the contribution of soil water repellency in terms of their combined influence on fluxes, storage, and fundamental hydraulic parameters is therefore an important knowledge gap to resolve in the hydrologic and soil sciences.

Fractional wettability is a term that describes porous media in which some portion of the matrix is (water) wettable, some portion is water repellent, and some portion may exhibit intermediate wettability (Chapter 1, Figure 1.2). With the exception of homogeneous porous media, which is unlikely to occur in natural settings, soils exhibiting water repellency can express a range of wettabilities, with contact angles (CA's) extending over a potential continuum between 0^{o} (by convention) and 180^{o} (theoretically), and which are apt to change in greater or lesser amounts based upon environmental conditions and time (Diehl, 2013; Beatty and Smith, 2010). This has, in part, made the investigation of soils expressing fractional wettability and contact angle dynamics in both natural and laboratory settings challenging.

One pragmatic challenge in generating greater mechanistic understanding has been the temporal scales over which contact angles change and infiltration occurs in water repellent media. Infiltration rates and/or hydraulic conductivities, as determined through traditional approaches and calculations, are often significantly reduced in water repellent media compared to wettable media, with singular wetting events sometimes requiring extended periods of continued measure lasting beyond one month (Doerr and Thomas, 2000; Reszkowska et al., 2014; Moody et al.,2013; Lichner et al., 2013; Nyman et al., 2014). Further, a number of studies have shown complex and mechanistically difficult-to-describe infiltration behaviours for a range of applications and porous media (Beatty and Smith, 2013; Clothier et al., 2000; Imeson et al. 1992; Vogelmann, et al., 2013; Aelamanesh et al., 2014; Hardie et al., 2013; Buczko et al., 2006; Moody et al., 2009; Jarvis et al., 2008; Letey et al., 2000). Few models attempt to conceptually or numerically model time- or dynamic contact angle-dependent changes in hydraulic properties in water repellent soils (e.g. Beatty and Smith, 2013; Diamantopoulos and Durner, 2013; O'Carroll et al., 2005). Additionally, the theoretical framework upon which calculations of hydraulic conductivity and sorptivity are based do not account for non-uniqueness caused by initially positive pore water pressures generated by hydrophobic contact angles and/or changes in contact angle with time (Beatty and Smith, 2014). Consequently, it is uncertain what calculations of sorptivity or hydraulic conductivity actually reveal about the porous media in question at any given time (Moody et al., 2009) and the accuracy of results generated through such approaches. Nevertheless, important insights in characterizing hydraulic properties and processes in dynamically repellent media have been exposed via alternative applications and through the pursuit of accurately describing system behaviours and parameters. Two approaches regularly employed to generate such insights include 1) introducing reduced-surface tension fluids that effectively lower CA's (Diamantopolous et al., 2013; Graber et al., 2007; Lamparter et al., 2010; Leighten-Boyce et al., 2007; Jeyakumar et al., 2014; Jarvis et al., 2008; Feng et al., 2002; Hardie et al., 2012), and 2) overcoming repellent displacement pressures by forcing water into pores via ponding (Wang et al., 2000; Feng et al., 2001; Bauters et al., 2000). In both instances, the introduction of an additional mechanism (changing fluid properties, increased hydraulic gradients and positive applied pressures) contribute to non-uniqueness. When multiple mechanisms can generate a similar measured or modelled response, uncertainty prevails. Needless to say, comprehensively describing these systems presents unique and complex challenges and there is much to be learned through systematic experimental work in dynamically repellent soils.

Recent work using tension infiltrometers has shown that by removing the competing mechanism of positive pore water pressure heads, which often develops during ponded infiltration and can lead to macropore flow, greater sensitivity to changes in repellency can be observed over the duration of an infiltration event (Beatty and Smith, 2013). Because soil materials must be or become wettable before infiltration occurs, tension infiltrometers and the data they provide can therefore generate greater insight into fractional wettability and changes in contact angles with time (Beatty and Smith, 2013; 2014). There is great opportunity to develop our understanding of fluid flow processes in dynamically water repellent media through the use of tension infiltrometry.

Chapter 4 evaluated the effectiveness of using variable surface tension fluids, namely water, ethanol, and Molarity of Ethanol Drop (MED)–derived aqueous ethanol solutions to isolate, observe, and characterize fractional wettability and contact angle dynamics in materials expressing differing levels of repellency in the field. Over the course of 49 long duration *in situ* infiltration tests, there were systematic infiltration rate relationship trends in response to the different fluids and regardless of differences in aqueous ethanol solution concentrations between materials and sites. Differences in the distribution of those relationship behaviours provided insight into the nature of fractional wettability and contact angle dynamics for each of the materials and provided a robust comparison of site specific wettability characteristics.

This Chapter builds upon ideas explored during that field investigation via a series of laboratory column experiments using larger diameter tension infiltrometers, homogenized soil materials, *in situ* moisture sensors, and variable fluids. This work seeks to better understand the mechanistic nature of infiltration in two sampled field materials and dynamically repellent systems in general by removing some of the complexity caused by material heterogeneity and varying moisture contents in the field. Moisture contents and long term infiltration rates of water, ethanol, and aqueous ethanol solutions were measured and compared to determine if competing mechanisms contributing to non-uniqueness in infiltration data (e.g. fundamental hydraulic properties, changing contact angles, fractional wettability) may be more readily identifiable in naturally repellent materials, and thusly, more easily targeted and parameterised in future investigations. This included determining whether infiltration relationships observed in the field are maintained under controlled laboratory conditions after materials have been air dried and a solute induced slow-down at the front caused by the mixing of water and ethanol (a.k.a "sludge effects") is removed as a possible competing mechanism during ethanol infiltrations. We also sought to determine if aqueous ethanol solutions, which were found to be particularly informative on the nature of fractional wettability differences in the field, would generate intermediate and notable differences in infiltration behaviours, in accordance with fluid properties and differences in dynamic soil water repellency as observed in field experiments. Lastly, we sought to determine if fluid scaling techniques could provide insight into wetting behaviours when used on wettable fluid analogues in repellent materials (e.g. ethanol and aqueous ethanol solutions) and were compared to wettable materials found at the fire site.

5.2 Materials and Methods

This study utilizes materials collected from a post-wildfire site located in Northern Ontario, Canada, approximately 700 km North of Toronto, ON. In Spring, 2012, 40,000 ha of crown land burned during a high fireline intensity, moderate severity fire. The site was accessed for field work in Fall, 2012 and was sampled at that time. All samples used in this study were collected at the Mid-Land (ML) site as described in Chapter 4 / Beatty and Smith (2014). This site was a low-relief galciofluvial/morainal sediment area with variable drainage and deep (mineral) soil horizons that are part of the Mary Orthic Humo-Ferric Podzol and consisting of stone free acidic outwash sands (Ministry of Northern Development, 2005; Agriculture and Agri-Food Canada, 1978, 1986). Part of the Boreal Shield ecozone, local weather stations report average annual precipitation of 831 mm and temperature of 1.3 ^{0}C (Meteorological Service of Canada, 2013). Vegetation at the site consists mostly of mixed deciduous and coniferous tree species and suckering shrubs. Bedrock outcrops occur throughout the site. Wisconsin period glacial tills are a dominant soil parent material for soils in the area (Gillespie et al., 1981).

Field samples were collected to represent components of the forest soil: organic duff and mineral soil. The organic duff was sampled from a distinct and ubiquitous layer (LFH horizon: 1-8 cm thick) of brown coloured material which was consistently water repellent in Water Drop Penetration Time (WDPT) and Molarity of Ethanol Drop (MED) tests, and minimally charred. They were sampled in undisturbed blocks approximately 20 cm x 20 cm x 4 cm. It overlaid a mineral Bf Horizon, which was sampled and collected separately as composite samples in plastic containers.

All samples were air dried for a minimum of one month prior to use in laboratory columns. Large roots, pine cones, and visible leaf debris were removed from the organic duff surface by hand. Undisturbed blocks were then lightly crushed by hand, homogenized and passed through a 4 mm mesh to remove large twigs and roots, which accounted for roughly 18% of the total sample weight. Homogenized duff materials were split using a Versa Splitter (Humboldt Manufacturing, Model No. SP-2.5) prior to use in infiltration columns. The mineral Bf Horizon materials were sieved by hand using a 2 mm and then 1 mm mesh. The >1 mm fraction was discarded, and the <1 mm fraction was homogenized and split using the Versa Splitter.

5.2.1 Drop tests & testing fluids

In the laboratory, Water Drop Penetration Time (WDPT) and Molarity of Ethanol Drop (MED) tests on the air-dry and homogenized organic materials were performed by placing drops on the surface of packed columns that had similar bulk density and pore size/particle spacing characteristics as would be tested during infiltration tests. WDPT tests measured the amount of time required for 30 drops to disappear via infiltration (Hallin et al., 2013). Water drops (approximately 50 μl) were larger than pore spaces and multiple soil particles were touching each drop. MED tests measured the ethanol concentration required to generate infiltration for five drops in less than five seconds (Roy and McGill, 2002). This (successful) MED solution concentration was used in infiltration tests as a partial (intermediate) wetting fluid which happened to be the same aqueous ethanol solution concentration used by Beatty and Smith (2014) during *in situ* field experiments on the same materials. MED identifies (theoretically) the 90^0 CA on flat surfaces (Roy and McGill, 2002). There is some uncertainty on what particular angle (wetting or non-wetting) is accessed in porous media since particle and pore geometries also play a role in lowering the required (apparent) contact angle for infiltration (Czachor et al., 2010).

Deionised water was used for all water (WAT) experiments, 95% denatured ethanol was used for all ethanol (ETH) experiments, and a 25% (by volume) solution of ethanol and deionised water was used in all aqueous-ethanol solution (AES) experiments, which corresponded to the (successful) MED test results. AES solutions were mixed immediately prior to use in infiltration column experiments.

5.2.2 Infiltration tests

Twenty infiltration tests instrumented with soil moisture sensors were carried out in this study. Three different material configurations were used: Mineral, OM+Mineral, and OM+Impermeable Boundary. Two replicate tests were done on each material configuration, for each of three different test fluid treatments, WAT, ETH, and AES (equalling six total infiltration tests per material configuration). Two additional OM+Impermeable Boundary tests were carried out using water to determine pore water – pressure head relationships for different applied tension intervals when apparent steady state conditions were reached.

For Mineral and OM+Mineral column experiments, a 9.5 cm diameter x 20 cm long column constructed of polycarbonate tubing was used and fitted with coarse metal mesh and fine nylon mesh screening at the bottom to allow air flow down the column. A second column was designed to isolate the OM material behaviours using an impermeable lower boundary at the same depth as the OM-mineral boundary in the OM+Mineral experiments (approximately 3 cm from the top of the column). This short column with an impermeable lower boundary included fitting a polycarbonate plug permanently fixed and sealed with silicone sealant around the circumference/at the column wall to prevent fluid flow down the sides of the plug / column wall. Eight small air ventilation holes were drilled into the side wall and three 2 mm tall x 1.5 cm length ventilation slots were cut at the top of the plug into the column sidewall (at approx. 3 cm from top of the column) to allow free air flow out of the OM+Impermeable Boundary column.

Mineral column soil materials were poured into columns using a dry continuous pour and vibration technique. Over pour and near-surface materials were leveled and tamped before and again after insertion of moisture sensors. For OM+Mineral columns, which included an organic surface layer, a short column extension was placed on top and used as a guide to ‘drop’ pre-poured organic materials onto the prepared mineral sublayer inside the column. A nylon plug, slightly smaller than the inside diameter of the column was used to push the organic materials consistently into the (20 cm) column and generate a level surface at 2mm above the top of the column for good contact with the infiltrometer. This same technique was used in OM+Impermeable Boundary (short) columns (i.e. without the inclusion of the mineral sub-layer).

In both column designs, two access ports were cut 1.5 cm from the top of the column, in parallel and on a 45^0 angle to allow insertion of moisture sensors for higher resolution moisture content data in organic materials, while maintaining contact with only organic materials and avoiding possible ponding and runoff from the sensor blades. Three additional sensor access ports were cut vertically into the column used for Mineral and OM+Mineral experiments and centered at 4 cm, 8 cm, and 12 cm, from the top of the column. The sensor ports were cut into the side wall of the column in a winding pattern to allow insertion of moisture sensors along the length of the column and avoid moisture content shadows potentially generated below shallower sensors. These are slight modifications of the design as presented in Beatty and Smith (2013). All ports were sealed with tape and a small incision made into the tape to facilitate no material leakage during pouring of the columns and minimal disturbance during subsequent insertion of moisture sensors.

Moisture sensors (Decagon Echo EC-5, 5 cm length) were inserted shortly before each experiment. Moisture sensor housings were double wrapped in cellophane to prevent deterioration caused by exposure to ethanol. Throughout the experiments moisture content data were collected continually at one minute intervals and logged automatically on a battery operated Decagon EM50 data logger. At the end of each infiltration experiment, column materials were collected and dried in a 45 ^{0}C oven to constant weight and used to calibrate the moisture sensors.

Soil Measurement Systems (SMS) (8 cm diameter) tension disc infiltrometers were customized for use in these experiments. All acrylic components in the original design were replaced with polycarbonate plastic tubing, fittings, and non-acrylic based adhesives. Acrylic is reactive to ethanol, and so not appropriate for use in experiments using ethanol. Infiltrometers were calibrated according to the method as described in the SMS user manual and calibrations were applied in all cases (SMS, 2006).

The bubble tube of the infiltrometer was filled with deionised water for all tests. This removed the need to employ density corrections at each applied tension for the different testing fluids such that the same applied pressure head of -4 cm (i.e. -392 Pascals) could be used in all cases. Tests were randomized according to material configuration and fluid type to avoid bias. An initial target applied pressure head of -4 cm of water was used at the start of all tests; additional tensions were used in 10 experiments and are shown in Table 5.1. Shifts in the applied tension during experiments facilitated calculations of hydraulic conductivity (in Mineral material columns) and were used to generate equivalent effective pressures within the column to facilitate more direct moisture content comparisons at later times. Small variations (1-3mm) in the applied pressure (vs. the target applied pressures of -10 cm, -4 cm, -1.2 cm, and -1.9 cm, depending on experimental conditions) resulted from a combination of human error and the level of precision with which tensions were set in the bubble tower and slight movement of the water level in response to fluid displacement caused by the bubble tube itself. For experiments that induced positive pressures in the impermeable column, the air ventilation slots were sealed with tape to prevent leakage and ensure mass balance.

Time zero was set as the time the infiltrometer was placed on the soil surface. Volume data from the tension infiltrometer water reservoir were manually recorded. A loose fitting evaporative barrier was placed around the infiltrometer / at the top of the

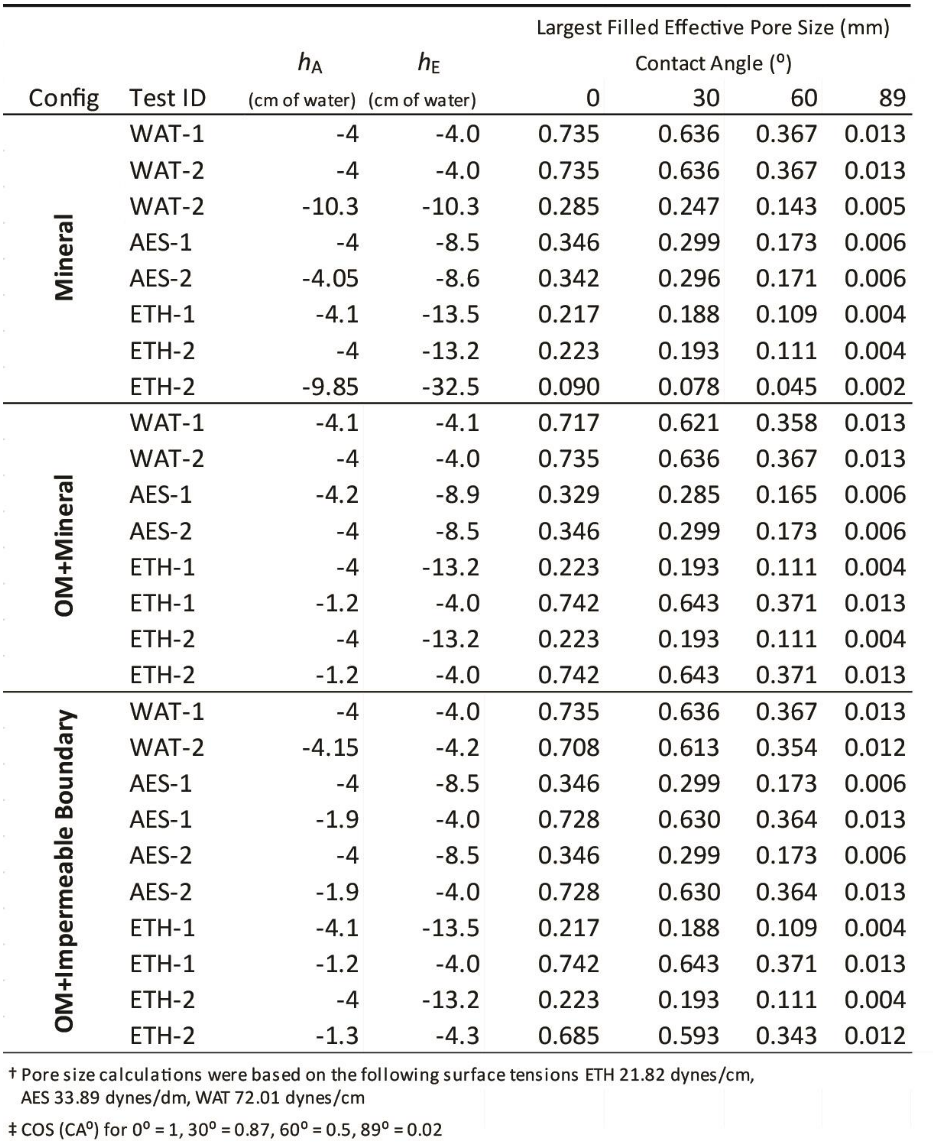

				Largest Filled Effective Pore Size (mm)			
		h_A	h_E	Contact Angle (°)			
Config	Test ID	(cm of water)	(cm of water)	0	30	60	89
Mineral	WAT-1	-4	-4.0	0.735	0.636	0.367	0.013
	WAT-2	-4	-4.0	0.735	0.636	0.367	0.013
	WAT-2	-10.3	-10.3	0.285	0.247	0.143	0.005
	AES-1	-4	-8.5	0.346	0.299	0.173	0.006
	AES-2	-4.05	-8.6	0.342	0.296	0.171	0.006
	ETH-1	-4.1	-13.5	0.217	0.188	0.109	0.004
	ETH-2	-4	-13.2	0.223	0.193	0.111	0.004
	ETH-2	-9.85	-32.5	0.090	0.078	0.045	0.002
OM+Mineral	WAT-1	-4.1	-4.1	0.717	0.621	0.358	0.013
	WAT-2	-4	-4.0	0.735	0.636	0.367	0.013
	AES-1	-4.2	-8.9	0.329	0.285	0.165	0.006
	AES-2	-4	-8.5	0.346	0.299	0.173	0.006
	ETH-1	-4	-13.2	0.223	0.193	0.111	0.004
	ETH-1	-1.2	-4.0	0.742	0.643	0.371	0.013
	ETH-2	-4	-13.2	0.223	0.193	0.111	0.004
	ETH-2	-1.2	-4.0	0.742	0.643	0.371	0.013
OM+Impermeable Boundary	WAT-1	-4	-4.0	0.735	0.636	0.367	0.013
	WAT-2	-4.15	-4.2	0.708	0.613	0.354	0.012
	AES-1	-4	-8.5	0.346	0.299	0.173	0.006
	AES-1	-1.9	-4.0	0.728	0.630	0.364	0.013
	AES-2	-4	-8.5	0.346	0.299	0.173	0.006
	AES-2	-1.9	-4.0	0.728	0.630	0.364	0.013
	ETH-1	-4.1	-13.5	0.217	0.188	0.109	0.004
	ETH-1	-1.2	-4.0	0.742	0.643	0.371	0.013
	ETH-2	-4	-13.2	0.223	0.193	0.111	0.004
	ETH-2	-1.3	-4.3	0.685	0.593	0.343	0.012

† Pore size calculations were based on the following surface tensions ETH 21.82 dynes/cm, AES 33.89 dynes/dm, WAT 72.01 dynes/cm

‡ COS (CA°) for 0° = 1, 30° = 0.87, 60° = 0.5, 89° = 0.02

Table 5.1 Target applied (h_A) and calculated effective (h_E) pressure heads for all experiments. Experiment numbers for each replicate pair are assigned arbitrarily and relate to all figures shown throughout the rest of the document. Calculated (idealized) pore sizes based on applied and effective pressures and fluids used in experimental replicates.

column for longer duration experiments, which were typically experienced with organic materials using water as the infiltrating fluid. The infiltrometer was held securely in place with a retort clamp and checked periodically to ensure continuous good hydraulic contact with the soil surface.

5.2.3 Scaling and calibrations

The Laplace equation of capillarity expresses the pressure difference between two immiscible fluids (e.g. air and water) as the capillary pressure (C_p) which is dependent upon the interfacial tension (σ) (commonly termed surface tension in air-water systems) and the curvature of the interface, specifically.

$$C_p = \sigma\left(\frac{1}{r_1}+\frac{1}{r_2}\right) = \sigma\frac{2}{r_I} \quad \text{(eq. 5.1)}$$

where, C_p is pressure difference due to capillarity across the liquid-air interface, r_1 and r_2 are the principle radii of curvature of the interface, and r_I is the radius of an equivalent spherical interface (i.e. $r_1 = r_2$). Within a given pore of apparent circular radius r_c and apparent contact angle β the relation between the size of the pore and the curvature of the interface can be written as:

$$\frac{1}{r_I} = \frac{\cos\beta}{r_c} \quad \text{(eq. 5.2)}$$

Substituting Equation (5.2) in to Equation (5.1) gives:

$$C_p = \frac{2\sigma \cos\beta}{r_c} \qquad \text{(eq. 5.3)}$$

Expressing the capillary pressure in terms of pressure head of water (h) and noting the convention that capillary pressure is positive for wetting fluid, it follows that

$$h = -\frac{C_p}{\rho g} \qquad \text{(eq. 5.4)}$$

It follows from Equations (5.1), (5.2), (5.3), and (5.4) that the pressure head for two static interfaces of the same curvature, i.e., within a pore of the same apparent radius and with the same apparent contact angle (i.e. at the same volumetric fluid content) the capillary pressures will only differ by the relative interfacial tensions of the specific fluids pairs. Therefore, for direct comparison between fluids, applied pressure heads set with the water filled infiltrometer bubble reservoir were scaled according to the ratio of interfacial tensions for fluids other than water based on Leverett (1941) and Bear (1972) using:

$$h_E = \frac{\sigma_w}{\sigma_i} h_A = \alpha_i h_A \qquad \text{(eq. 5.5)}$$

Where h_E denotes the effective pressure head, h_A is the applied pressure in the water filled bubble tower of the infiltrometer, σ is the interfacial tension, subscript *w* denotes water, subscript *i* denotes the ethanol solution at concentration *i*, and *α* is the scaling factor. Consequently, an applied pressure head of -4 cm yields an effective pressure head of -4 cm pressure head in WAT experiments, and effective pressure heads (applied at the surface) of -8.5 cm and -13.2 cm for AES and ETH tests, respectively. That is, if ethanol applied at the infiltrometer disc at -4 cm pressure head (i.e. pressure units of cm of water) hypothetically had the same wetting characteristic as water (i.e. contact angles) it would fill the same assemblage of pores as water applied at -13.2 cm at the infiltrometer disc (see Table 5.1).

Volumetric moisture contents collected using moisture sensors were calibrated using density corrected sensor specific moisture content of samples collected pre- and post-infiltration. Density corrections were used to convert mass fluid contents of samples collected at the end of each column experiment to volumetric moisture contents; for ETH and AES moisture contents, the densities used were 0.79 and 0.95, respectively.

5.3 Results and Discussion

5.3.1 Mineral infiltration columns

Infiltration into the Mineral columns establishes a baseline behaviour for fluid flow in the Mineral Bf Horizon wettable materials. In these columns, Cumulative Infiltration vs. Time plots exhibit concave infiltration behaviour, which manifest as linear in plots of Cumulative Infiltration vs. Sqrt Time for all three fluids (Figure 5.1). Replicate numbers for all material/fluid combinations in all figures were assigned arbitrarily, with the faster of the replicate pair (i.e. ones closest overall to the y-axis in the replicate pair), being assigned “-1” and the slower (farther away) of the two being assigned “-2”. If infiltration data cross for a given material/fluid pair, as is the case in WAT experiments, replicate number assignment is based on late time infiltration.

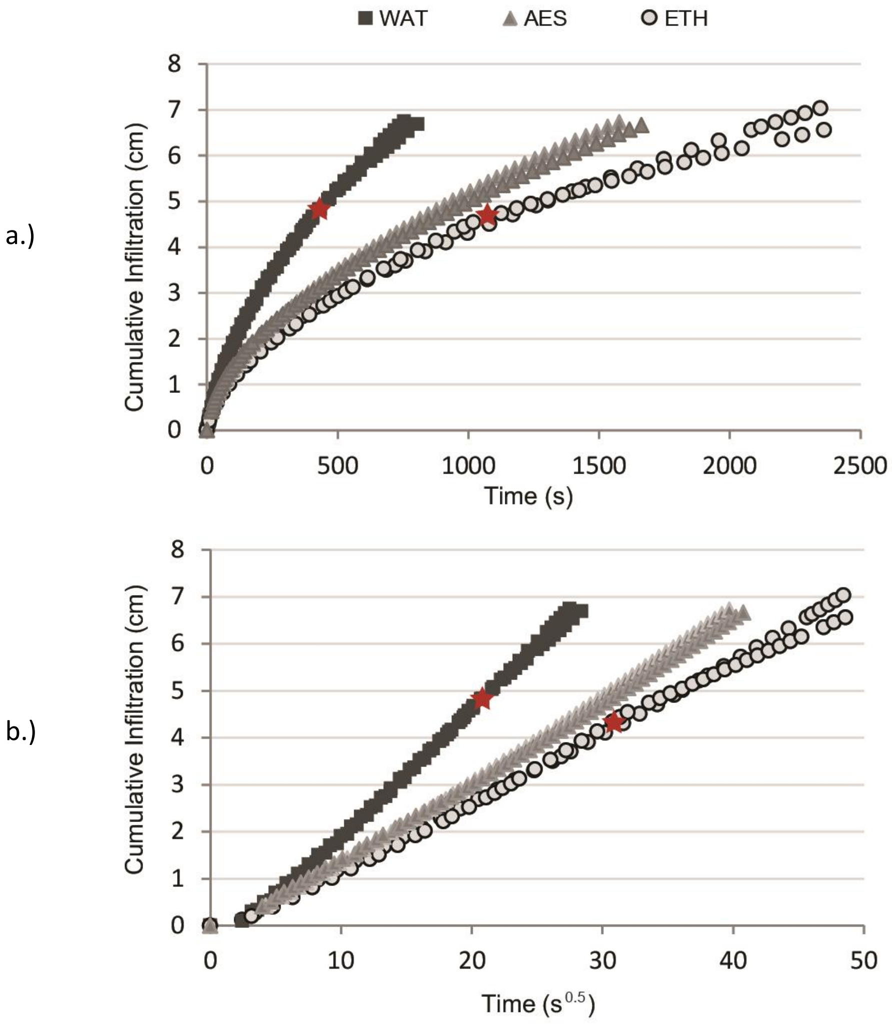

Figure 5.1 Infiltration of WAT, AES, and ETH into Mineral (B Horizon) materials. a.) Cumulative Infiltration vs. Time in seconds and b.) Square Root of Time in $s^{0.5}$. Red stars indicate a pressure shift.

All fluids show a typical wettable response and are well described by traditional infiltration theory for fluid flow in porous media. This corresponds well to WDPT results that showed no repellency (0 s) for Mineral soils. The orientation of WAT > AES > ETH was observed during *in situ* field experiments carried out in earlier work (Beatty and Smith, 2014) in which antecedent moisture content may have played a role in observed behaviours. The “sludge effect,” or a slow down within the the front caused by solute transport and dispersion of ethanol with water (as described in Beatty and Smith, 2014) is not a contributing factor to the observed relationships discussed here since all materials were air dried prior to use in laboratory columns. It can therefore be assumed that this orientation of WAT > AES > ETH is likely to appear in field or laboratory investigations of hydrophilic materials / fluid combinations.

Overall differences in the cumulative infiltration between fluids in these wettable mineral soils can be readily explained by differences in fluid properties (surface tension, density, and viscosity) and resulting mobility factors. These contribute to shallower slopes and an overall weakening of the capillary component of the hydraulic gradient as surface tension decreases and fluids become less dense at higher ethanol concentrations. Viscosity acts variably, with AES being approximately twice that of WAT and ETH. As a result of these effects, early time infiltration for WAT is approximately one order of magnitude (10^{-3} cm/s$^{0.5}$) larger than for AES and ETH infiltrations (10^{-4} cm/s$^{0.5}$). Early time rates are defined here as the time required to reach approximately 1 cm of cumulative infiltration. WAT infiltrations required 31 s (average) and elicited responses 250% faster than ETH (77 s average) and 52% faster than AES infiltrations (60 s average). These relationships are approximate as slight variation exists in the volumes used to determine ‘early-time’ rates near the 1 cm delineation (i.e., cumulative infiltration up to 0.90 and 0.94 cm were used in WAT cases and up to 0.98, 1.01, 1.02, 1.03 cm were used in AES and ETH cases). Over the long term, WAT experiments run on average 781s (12m54s), which are 304% faster than ETH (2355s or 39m15s average) and 45% faster than AES (1620s or 26m59s average). There is good replication (overlap) in fluid-specific experiments. Note that WAT-2 and ETH-2 tests express some variability between replicates at later times. This is caused by the step change in the applied pressure at the infiltrometer disc from -4 cm to an applied pressure of h_A= -9.85 cm at 405 s (20.12 $s^{0.5}$) for WAT-2, and to h_A= -10 cm at 1020 s (30.94 $s^{0.5}$) for ETH-2.

5.3.2 OM + Mineral infiltration columns

Differences in repellency between air dried (laboratory) and *in situ* conditions are commonly observed (Dekker and Ritsema, 1994; Taumer et al., 2005; Oostindie et al., 2013; Dekker et al., 2009). While key mechanistic behaviours were expected to appear in lab experiments, exact replication of field experiments was not expected. Differences in initial moisture content conditions, sample disturbance, and higher laboratory temperatures (~10-15 ^{0}C higher than in the field and which generate differences in fluid properties: lower viscosity, surface tension, and density) contributed to this expectation.

Plots of Cumulative Infiltration generated for OM+Mineral (i.e. 3 cm layer of Organic Material over 17 cm of mineral B) columns (Figure 5.2) exhibit more complex differences relative to each other and to Mineral columns (Figure 5.1). Some notable differences in the shapes and relationships between curves occur as a result of the

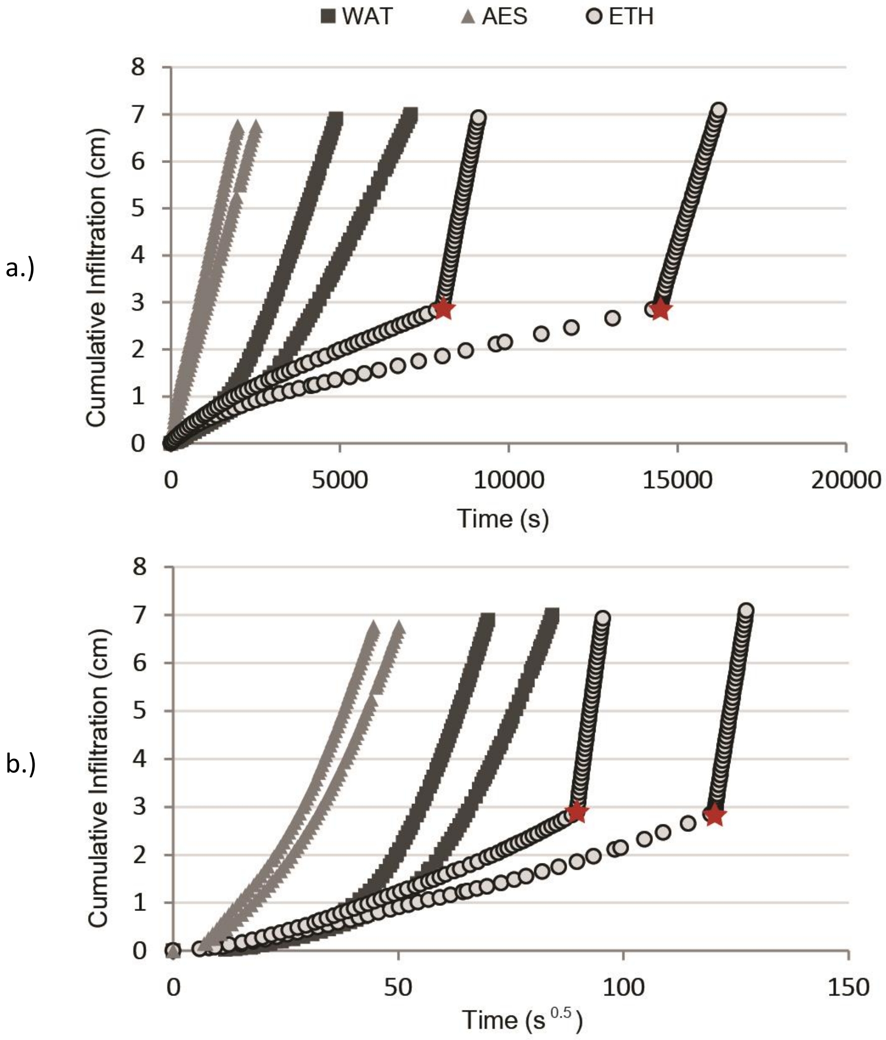

Figure 5.2 OM+Mineral infiltration replicates shown in Cumulative Infiltration vs. a.) Time in seconds and b.) Square root of Time in $s^{0.5}$. Red stars represent mechanical pressure shifts identified in Table 5.1. Replicate number assignment is same as in Figure 5.1, with the faster of each replicate pair being assigned “-1,” and the slower “-2”.

Table 5.2 Water Drop Penetration Time statistics (of 30 x 50ul drops)

WDPT	Average	Median	Maximum	Minimum	Std Dev.
(s)	300	261	695	71	148

introduction of a 3 cm thick dynamically water repellent layer at the surface. WDPT for the laboratory material tested homogenized OM materials are shown in Table 5.2. These materials can be classified as “strongly repellent” according to Bisdom et al. (1993) and Doerr et al. (2009) classification schemes noted in Hallin et al. (2013). Key observations for infiltration tests include the following. First, tests run much longer with the inclusion of a repellent layer. Second, the shapes of the plots are more variable, exhibiting concave (WAT), convex (ETH), and near-linear (slightly concave, AES) infiltration behaviour in Cumulative Infiltration vs. Time plots. Third, the order from faster to slower of AES > WAT > ETH generated in this material configuration is different than the Mineral columns and infiltrations observed during *in situ* field experiments on the source materials (Beatty and Smith, 2014). Fourth, there is greater variability (i.e. less overlap) between (within fluid) replicate tests.

It is well understood that water repellency slows infiltration, often by orders of magnitude (Beatty and Smith, 2010; Clothier et al., 2000). The results here support this, as early time rates in AES (10^{-3} cm/s) are an order of magnitude larger than both ETH and WAT infiltration rates (10^{-4} cm/s). With the inclusion of the repellent layer, experiments using WAT and ETH run considerably longer (approximately 44 and 30 times, respectively) over the first 1 cm of infiltration when compared to Mineral columns. Over the entire test, WAT is on average five times longer and ETH is eight times longer (than Mineral only). In contrast, AES experiments are comparatively less affected by the repellent layer, with tests running approximately 4.5 times longer than Mineral columns over the first 1 cm of infiltration and only 1.4 times longer over the entire duration.

Up to 1 cm of cumulative infiltration, visual observations in the lab and moisture contents in the mineral sublayer indicate that infiltration is only occurring in the repellent OM surface layer. It is interesting that while ethanol is a completely wetting fluid in the repellent layer and water is not, as was observed in WDPT tests, the similarity in cumulative infiltration in ETH and WAT tests is striking. Given the substantial differences in wettability, interfacial tensions, and mobility factors, it was unexpected that this similarity would exist. It is often assumed that an increase in wettability, caused by the reduction in interfacial tension and related decreases in contact angles, drives a much accelerated infiltration response when ethanol is used as an infiltrating fluid (compared to water) in repellent media. While these factors are at play in these experiments, these results convey that an additional mechanism is contributing to the observed behaviour. Recall that applied and effective pressures are surface tension dependent. Consequently, the initial applied pressure of -4 cm in both experiments generates an effective pressure head of -4 cm in the WAT experiments, -8.5 cm in AES experiments, and -13.2 cm in the ETH experiments. The grain (particle) sizes found in organic materials are larger than those found in mineral columns and the fibrous shape of OM packs together with larger pores sizes than the mineral (sandy loam) grains (Beatty and Smith, 2014). Table 5.1 shows the applied pressures in each of the replicate experiments and associated effective pore sizes based on the fluids used here and a range of effective contact angles from zero to 89^0. The applied pressure of -4 cm in ETH experiments fills effective pore sizes equal to or smaller than 0.224 mm. In contrast, water with a surface tension of 72 dynes/cm, an effective contact angle of 0^0, and applied pressure head of -4 cm is able to fill a larger range of effective pore sizes up to 0.739 mm. Assuming a log-normal distribution of pore sizes, the smaller the pore size, the smaller the operational assemblage of pores in any given fluid-material combination. This would have an effect on the relative rate of infiltration into the overlying organic materials if the OM has a portion of pores effectively larger than 0.224 mm and partly explains why ETH tests were slower in OM+Mineral columns compared to WAT tests. While a greater proportion of the repellent layer is activated as a consequence of ethanol being a wetting fluid, a smaller proportion of the overall medium is able to participate in infiltration as a consequence of higher (more negative) effective pressure heads throughout the repellent layer (Jarvis et al., 2008). That is, under a -4 cm applied pressure head, the largest assemblage of pores (greater than 0.224 mm) did not fill in ETH experiments. This appears to be offsetting increases in infiltration rate generated through the 'knocking down' of contact angles in the repellent layer, i.e. wettable with respect to ethanol. The only significant difference between ETH and WAT tests is the shape of the CI vs. Time plot. That this wettable/non-wettable ETH/WAT relationship is not so straightforward when only slightly stronger tensions than those commonly used in calculations of Repellency Index (i.e. which use applied pressure heads of -2 cm) are used. This has implications for testing involving the comparison of water and ethanol infiltrations elsewhere and consideration should be paid to the sensitivity of a given porous media to different effective pressures and related effects on unsaturated hydraulic conductivities.

The hydrophilic sublayer is also affecting infiltration differently between ETH and WAT experiments. In WAT experiments, this layer acts as an accelerating layer in the presence of a non-wettable surface layer (that limits supply). In contrast, in ETH experiments, this hydrophilic sublayer generates the effect of a two layer wettable system that is effectively being supplied with a near constant head boundary condition with a head value equal to the *effective* pressure plus the value of the thickness of the OM layer (e.g. approximately -13.2 cm + 3.2 cm = -10 cm) with lower overall unsaturated hydraulic conductivities. In experiments using AES, an intermediate response was generated in Mineral columns. This is not the case here and comes as a result of more significant decreases in infiltration rates in WAT and ETH experiments in the presence of the repellent layer. Consequently, the ETH > AES > WAT relationship observed in the field under -2 cm applied pressure heads does not hold in this context with -4 cm applied pressure heads. Instead, the relationship is AES > WAT > ETH.

The AES exhibits a more nuanced sensitivity to the inclusion of a repellent layer (compared to WAT or ETH) even though it is two times more viscous than WAT and ETH, has half the surface tension as WAT, accesses a smaller theoretical portion of the overall pore space (with effective tensions of -8.5 cm), and has a slower mobility factor than WAT or ETH replicates. The interaction of the effects of the activated pore space and fluid properties are less varied overall in both the Mineral and OM+Mineral columns in AES experiments, yet they still show near-linear non-wetting curve behaviours in cumulative infiltration plots. It is not clear in these experiments exactly what proportion of differences in overall rates of AES columns are being driven by differences in pore structure (of OM vs. B Horizon) and the presence of dynamic repellency in the overlying layer. While MED measures approximate a 90^0 contact angle, it would appear that materials more repellent than not (with angles closer to 90^{0} than 0^{o}), for the most part, are being overcome in AES experiments. This means that employing multiple AES solutions in a given media has real potential to be a powerful tool for isolating soil water repellency effects in natural dynamically repellent and fractionally wettable materials.

Differences in shapes of cumulative infiltration in the first ~1.5 cm of infiltration provide insight into the materials closest to the infiltrometer. In contrast to the Mineral columns, only ETH tests exhibit concave slopes in Cumulative Infiltration vs. Time plots which indicates a wettable infiltration response. WAT exhibit a convex infiltration response as is often observed in water repellent media (Wallach and Graber, 2007; Lichner et al., 2013). AES infiltrations exhibit only slightly concave, near-linear slopes. The near-linearity of AES infiltrations is particularly interesting since convexity vs. concavity is often used, as is the case here, as a coarse distinguishing characteristic between wettable and non-wettable infiltration behaviours. It would appear that the AES solution acts as a truly intermediate wetting fluid in this respect by generating only a slightly curved cumulative infiltration (vs. time) response. Feng et al. (2001) observed a similar ‘flip’ in infiltration response according to the magnitude of applied pressures in water infiltrations. Their system, however, used variable ponding depths to induce flow in water repellent media via overcoming pore water displacement pressures through mechanically induced positive pressures and increased hydraulic gradients applied externally. In contrast, our infiltration under tension system relies upon changes in contact angle and/or surface tension through the application of different fluids over variable time, such that internal pore water pressure heads need to change (i.e. become negative) to induce flow. Mechanistically, this shows that for these experiments, flow may be happening across the entire medium in variably sized pores up to and including those defined by eq. 5.3 (and shown in Table 5.1) as contact angles change with increased exposure to the infiltrating fluid. This excludes pores that remain persistently repellent, but that can be overcome in experimental situations where positive pressures instantaneously displace the wetting fluid (air). By not forcing water into pores, infiltration under tension remains sensitive to dynamic changes in repellency and makes it a powerful investigative tool in dynamic systems. Future work involving complimentary data sets of ponded infiltration and tension infiltration data may prove useful in characterizing repellent and/or fractionally wettable pore size distributions that generate these kinds of flips infiltration responses.

There is more spread between fluid-specific replicates in OM+Mineral columns than observed in Mineral columns. Increased spread between all replicates indicates that the overlying repellent layer is generating greater variability in flow which exerts an influence over the entire duration of these experiments. This is likely to be expressed at the field scale and likely contributes to the complexity commonly observed within and across sites, making direct data comparisons difficult based on fundamental hydraulic properties alone (Martin and Moody, 2009). In the field, at weaker tensions (-2 cm), larger variability between tests tended to be fluid specific, with the greatest variability occurring in WAT experiments (Beatty and Smith, 2014). Less variability was observed in AES and ETH experiments. It would be expected that the most repellent fluid-material combination (e.g. WAT) would generate the greatest spread between replicates when persistent fractional wettability is acting as a primary and variable determinant of flow. In the case of WAT experiments, relative to AES tests, these expectations are well met. The behaviour of the ETH experiments, however, point to the sensitivity of the fractionally wettable layer to the additional combined influence of fluid properties and applied pressures and a reduction in K_{unsat} due to lower fluid contents (i.e. an unfilled assemblage of the largest pores). Some of this variability seemed to be mechanistically observable in the form of perturbations in the wetting front through the transparent column wall. Even in these homogenized small diameter laboratory columns, certain areas become more wettable in WAT experiments with increased exposure to water over time and other zones remain less fully activated (wetted) and less participatory in flow. In the presence of variably dynamic contact angles in the bulk medium over time, slightly wettable perturbations can contribute to a feedback mechanism that encourages focused zones of preferential (increased) wetting within the repellent layer. In contrast, fewer perturbations and a more stable wetting front were observed through the column side wall during ETH experiments.

Linearity and agreement between late time and/or late volume slopes (near end of test rates) between different fluids are an indication that contact angles are no longer actively changing significantly. While both AES and ETH accelerate contact angle changes in the bulk medium, because of lower fluid mobilities, both fluids act slower than water would in a texturally comparable (air-dry) wettable medium. Assuming rapid contact angle change occurs in ETH and AES experiments, and taking fluid properties into account, the relative distance between those curves and WAT curves provide an indication of the proportion of the medium that is not yet fully wettable (under similar cumulative infiltration). For example, a comparison between WAT and AES experiments indicates that WAT experiments should theoretically move at least as quickly as AES were it a fully wetting medium, and especially since a larger theoretical portion of the overall medium would be activated at -4 cm applied pressure. Alternatively, the same assemblage of pores is activated between ETH and WAT experiments after the introduction of the second tension in ETH experiments near 3 cm of cumulative infiltration. In ETH experiments, the introduction of a second tension (h_A= -1.2cm) (at 8055 s and 14492 s) elicits a linear and notably steeper slope than observed in Mineral columns. This is a consequence of the magnitude of the increase in tension which generate end of test rates (10^{-3} cm/s) an order of magnitude faster than those that precede it (10^{-4} cm/s). These ETH rates are comparable to late time rates for both AES (10^{-3} cm/s) and WAT (10^{-3} cm/s), though AES experiments have viscosities twice that of ethanol, which serve to slow rates. This suggests that most of the difference in ETH experiments is mostly due to the activated assemblage of pores between -8.5 cm (0.348 mm) and -13.2 cm (0.224 mm) calculated by assuming 0^0 effective contact angles at these late times and less so by differences in mobility factors. The slightly lower late time rates observed for WAT experiments (compared to both ETH and AES) are likely caused by an imperfectly wettable fraction (portion) of the OM layer that is still undergoing dynamic changes in contact angle over time.

Water repellency cessation times (WRCT) were calculated based on the noted "hockey stick" like relationship of the cumulative infiltration of water (I) against the square root of time t (SQRT t) described by Lichner et al. (2012) and shown in Figure 5.3. Calculated WRCT values from data found in Figure 5.2 are shown in Table 5.3 and are estimated as the time at the intersection point of two straight lines fit to 1) early time date representing hydrophobic conditions and 2) later time nearly wettable states. The pressure shift that occurs in ETH tests at 3 cm required an extrapolation of data at the initial applied -4cm pressure to facilitate calculations. For ETH experiments, it was expected that no significant changes in infiltration behaviours would occur as a consequence of contact angle change past 3 cm of infiltration given its wettable properties. In tandem, the slope of the infiltration plot could be expected to not change significantly beyond 3 cm. Consequently, slope data near 3 cm of cumulative infiltration was used for ‘late time slope data’ in the calculation of ETH WRCT values. All other WRCT values were calculated based on data beyond 6 cm.

The water has the longest WRCT, ethanol the shortest, and AES has an intermediate value closer to ETH than WAT. There is no other WRCT data comparing these fluids in the literature. A working hypothesis that AES would behave as a fully wetting fluid and only differ from ethanol by the fluid mobility index (based upon viscosity and density) is not supported by these observations. AES substantially reduced the WRCT, yet it still expresses more persistent repellency than ethanol. This can be expressed within the framework of the working conceptual model of fractional

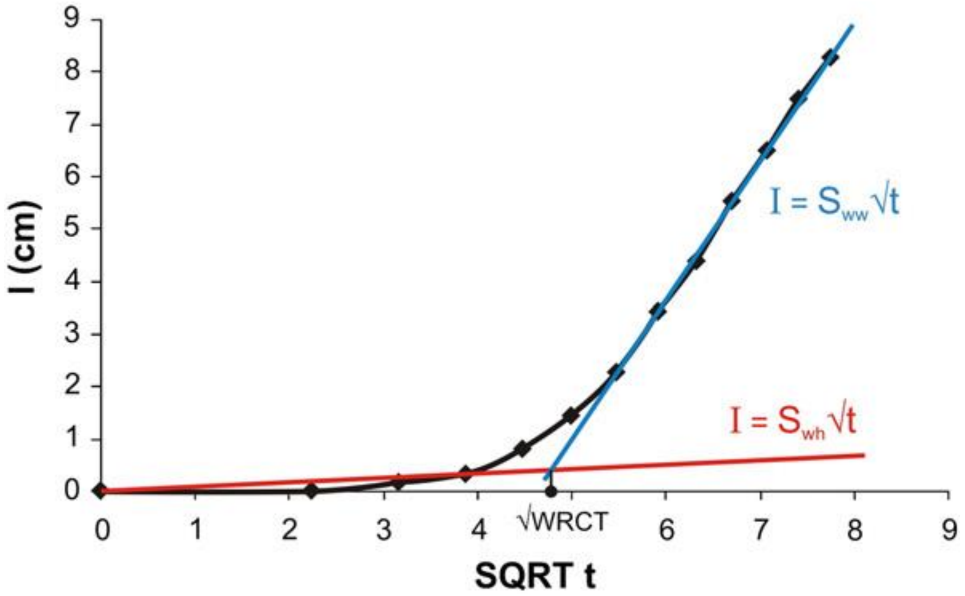

Figure 5.3 Water Repellency Cessation Time (WRCT) using Lichner et al. (2013).

Fluid		Column-1	Column-2	Difference	Average
WAT		39	56.1	16.2	45.3
AES		12.4	4.5	7.9	8.5
ETH		4.3	2.4	1.9	3.4

Table 5.3 Calculated Water Repellency Cessation Times in minutes from data shown in Figure 5.2. ETH values are for the cumulative infiltration data up to 3cm (corresponding to the star in Figure 5.2).

wettability and contact angle dynamics as the AES solution concentration (25%), while instantaneously infiltrating, was only expressing a fraction of the bulk OM. That is, an observable fraction of the OM was not instantaneously wetted by AES and expressed its persistent contact angle dynamic effects through the WRCT index. This hold promise for further studies to better quantify and model dynamic repellency.

5.3.3 OM + Impermeable boundary infiltration columns

Cumulative Infiltration vs. Time and Square Root of Time for the OM+Impermeable boundary (short) columns are shown in Figure 5.4 and have been plotted using a logarithmic scale to facilitate viewing over the duration of all experiments. There is notable apparent overlap between WAT and ETH experiments. ETH experiments are slightly faster to start, yet differences between these two infiltrating fluids are relatively small over the first day of infiltration. This is somewhat different than OM+Mineral experiments where large differences were generated between WAT and ETH tests. While complex, these data serve to compliment OM+Mineral column behaviours by helping highlight the relative effect of a wettable sublayer in the presence of different testing fluids. ETH and AES experiments ran for approximately one day. This facilitated apparent equilibration before pressures were mechanically changed between 2 and 3 cm of cumulative infiltration. One exception to this was the AES-1 replicate test. A small leak in the infiltrometer was observed at approximately 45 minutes (2.45 cm of infiltration) when rates slowed down when the wetting front reached the impermeable boundary; this experiment was then expedited and terminated ‘early’ by shifting the pressure sooner than planned to supersede the small leak rate, which manifested during low flow. This small leak did not significantly affect overall behaviours or the nature of infiltration in this experiment and we do not expect outcomes to be different than shown. The infiltrometer was retired after this test; this highlights one of the challenges encountered in using reactive solutes such as ethanol. WAT experiments ran for six days, however, much of the infiltration occurred within the first day.

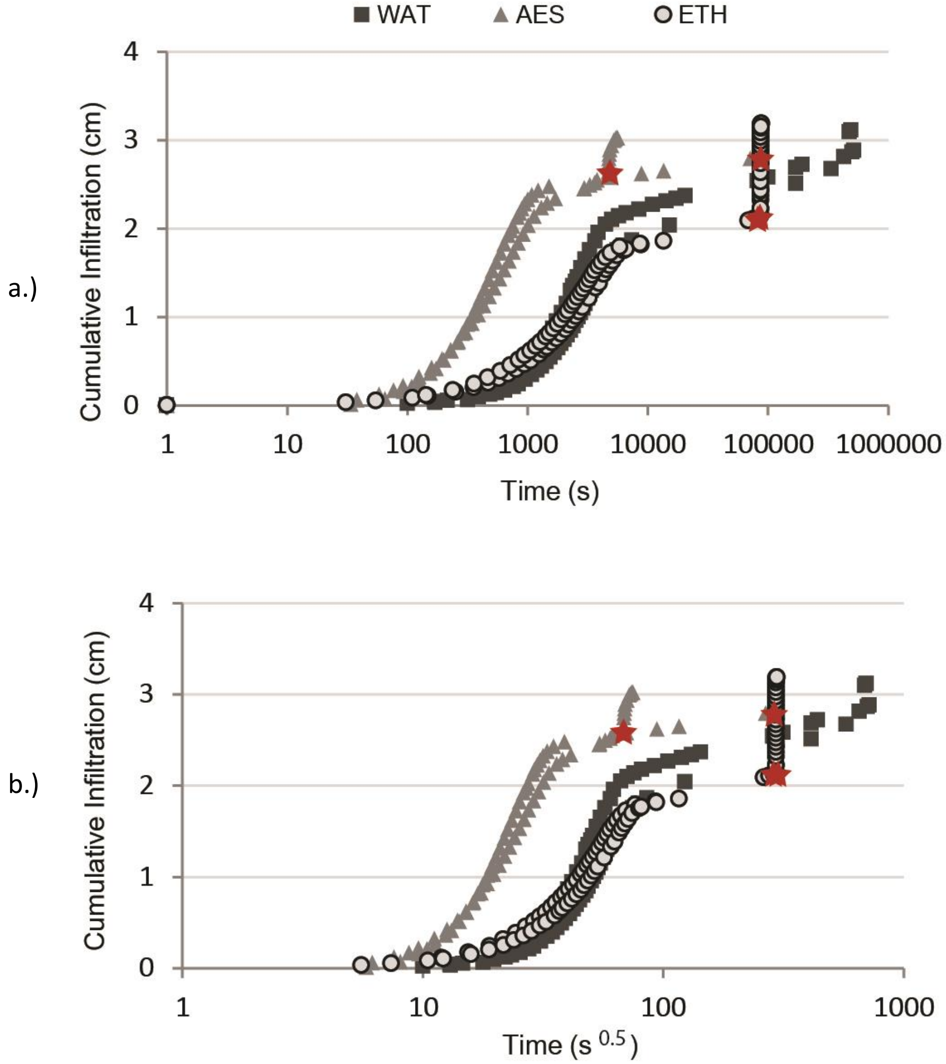

Figure 5.4 OM+Impermeable Boundary infiltration replicates shown in Cumulative Infiltration vs. a.) Time in seconds and b.) Square root of Time in $s^{0.5.}$ Red stars mechanical pressure shift identified in Table 5.1. Replicate number assignment is arbitrary, with the faster of each replicate pair being assigned "-1," and the slower "-2". The pressure shift of AES-2 is obscured by ETH infiltration data.

5.3.4 Infiltration Rates and Moisture Contents

Infiltration Rate versus Cumulative Infiltration for all columns are shown in Figure 5.5. Infiltration rates provide additional information that is not always readily visible in Cumulative Infiltration vs. Time/Square Root of Time plots and contributes to a meaningful discussion of mechanistic process as it occurs within experiments, particularly within the context of moisture content behaviours.

In Mineral experiments, infiltration rates exhibit high consistency in all replicate tests with slight variation in initial and end of test rates according to fluid type. Rates start relatively high, as capillarity is the primary driver of infiltration and decrease quickly as hydraulic gradients drop off monotonically. Moisture content behaviours are characterized by relatively steep slopes as the wetting front passes each successive moisture sensor in the column. Maximum moisture contents for WAT are 42% (avg), AES are 40% (avg), and ETH are 33%. Increased ethanol concentration increases the rate at which maximum moisture contents are reached with successively deeper sensors. The deepest sensor in all experimental configurations does not reach maximum moisture contents observed in shallower sensors at the applied tensions. The top three (shallower) sensors reach maximum levels between 3 and 4 cm cumulative infiltration, with ethanol occurring closer to 3 cm and water closer to 4 cm. Major differences in end of test moisture contents are most heavily influenced by differences in applied tension and correspond according to fluid property differences in these wettable media. One thing of note is the overshoot in apparent maximum moisture contents in the sensor centred at 8 cm. This overshoot is likely the result of a transitional wetting front that is generating

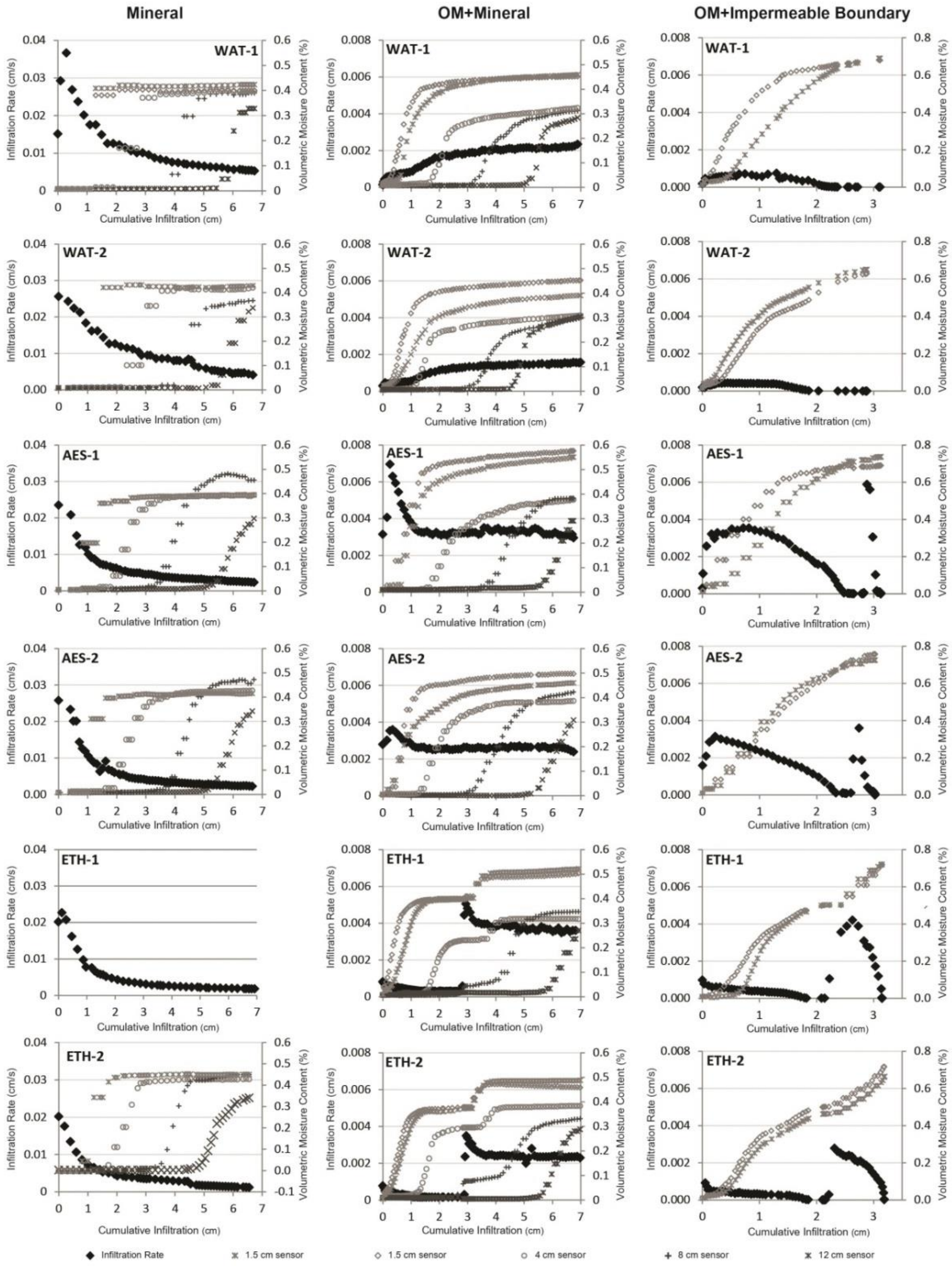

Figure 5.5 Infiltration Rates and Volumetric Moisture Contents vs. Cumulative Infiltration for all column replicates. These plots facilitate more direct comparison between variable duration tests. Moisture contents measured with the moisture probes are also plotted on these graphs. Problems with the data logger during the second ETH replicate experiment resulted in no moisture content data for that test.

negative pressures above the sensor and positive pressures through the sensor. That this is happening for AES experiments is due to the effective pressures (-8.5 cm) generated in these experiments.

In OM+Mineral replicates, infiltration rates are an order of magnitude lower than in Mineral columns across all fluids. The OM is coarser with larger pores, and it would be anticipated that K_{sat} of a perfectly saturated OM would be higher than the Mineral B loamy sand. This generates a near constant head boundary at the organic-mineral interface that supplies water at a flux rate lower than the infiltration capacity of the mineral sublayer. In comparison to Mineral columns, this affects moisture contents over the duration of the experiment in the shallowest mineral materials, which are expected to reach maximum levels earliest (WAT: 31% (avg), AES: 38% (avg), ETH: 36% (avg).

Infiltration rates in WAT experiments exhibit increases throughout experiments. This behaviour is indicative of dynamic fractional wettability, with rates increasing according to dynamic changes in contact angles across the bulk medium with increased exposure time to water. This contributes to the spatial development of wettable pore networks in the organic layer with time. This can be detected during times when moisture contents are increasing substantially, and yet increases in infiltration rate are only marginal. Low diffusivities in repellent materials have been noted elsewhere as well (Wallis and Horne, 1992). Increasing rates observed here are also influenced by breakthrough into the wettable sublayer, with rates increasing as the number of access points into the Bf Horizon material increases with time as the overlying repellent layer becomes more wettable and more conductive. Breakthrough was visually observed through the column sidewall at approximately 2.0 cm (WAT-1) and 1.4 cm (WAT-2) of cumulative infiltration and was a more accurate indication of breakthrough than the shallowest mineral moisture sensor located 0.5 cm below the organic-mineral interface.

Initial rates for AES experiments are approximately five times faster than WAT experiments and increase initially. This is caused by an imperfectly wetting fluid that accelerates changes in contact angle as observable in WAT infiltration behaviours, but at a much faster rate and with a smaller portion of the overall medium remaining resistant to contact angle change. These increases are followed by decreasing rates, starting at approximately 0.5 cm of cumulative infiltration, when the medium appears to reach a 'primarily wettable' state as evidenced in decreasing rates with time. Only ETH experiments exhibit similar behaviour as observed in Mineral columns and indicate wetting behaviours as would be expected given its wettable fluid characteristics. However, as a consequence of the smaller operational pore space defined by a stronger effective tension (-13.2 cm) ETH rates are only marginally faster than WAT experiments to start. Upon the introduction of a second tension (h_A = -1.2 cm) at approximately 3 cm of infiltration, ETH infiltration rates increase and reach levels comparable to AES experiments. While slight variations in packing may be influencing this, ETH infiltration rates are, on average, twice that of end of test WAT infiltration rates under similar tensions and slightly higher moisture contents.

Comparison between WAT tests and AES and ETH cases inform on the nature of partially filled pore spaces in both repellent and wettable test configurations. End of WAT test infiltration rates and moisture contents (in repellent material configurations) do not reach levels comparable to AES or ETH at comparable *effective* pressure heads (of -4 cm). The OM layer in these experiments is remaining unsaturated, as all values are below 0.77 and/or 0.75% (maximum observed VMC% in end of test OM+Impermeable Boundary AES and/or ETH experiments that generated partially saturated conditions via applied tensions weaker than -2 cm applied pressure heads under wetting-up conditions). In (Mineral) wettable configurations, AES are only 2% less filled. This is due to the combination of fluid properties and resultant effects on wettability expressed in earlier sections. ETH exhibit higher moisture contents comparatively, but this is partly due to the lower end-of-test (-1.2 cm) pressure heads applied at that point. WAT is most affected by the inclusion of a repellent layer at the surface, which generates an 11% difference between the Mineral and OM+Mineral replicates. This is attributable to a persistently repellent fraction within the OM that remains resistant to wetting over the durations (6 days) employed in WAT experiments.

The inclusion of a repellent layer in the OM+Mineral columns also elicits more variability in both OM and mineral material moisture contents and also dampens an overshoot effect that occurs in AES experiments (#2 mineral sensor), and possibly one of the ETH replicates. The overshoot that occurs in the ETH replicate comes after the mechanical shift in applied pressure at the surface to -1.2 cm. It is not clear why the second sensor (and not the first) is exhibiting this behaviour, but the overshoot detected by the second mineral sensor appears to be a consequence of the timing of the pressure shift in relation to the depth of the wetting front in the column and its proximity to the second mineral sensor.

The OM+Impermeable Boundary echo the OM+Mineral infiltration rate data and show increasing during the first 1 cm of infiltration in WAT and AES experiments, and decreasing rates in ETH experiments. The similarity of ETH and WAT infiltration rates in the presence of wettable and non-wettable infiltration behaviours, respectively, speak to the non-uniqueness one encounters in water repellent soils. This may, however, provide a route through which a proportional representation or surrogate measure of fractional wettability can be achieved through the use of different fluids in water repellent media, particularly when placed in context with moisture characteristic curves. End of test moisture contents in the organic layer are highest in OM+Impermeable Boundary experiments, WAT: 65% (avg), AES: 67% (avg at -4 cm) and 73% (avg at -1.9 cm, effective -4 cm), ETH: 46% (avg at -4 cm) and 69% (avg at -1.2 cm, effective -4 cm) compared to OM+Mineral WAT: 44% (avg), AES: 52% (avg), ETH: 39% (avg at -4 cm) and 48% (avg at -1.2 cm). This is a consequence of the lack of a mineral sublayer that can preferentially conduct and store water (and other fluids) in wettable pore spaces while contact angles are becoming more wettable in the overlying OM materials (of OM+Mineral columns). This means that, comparatively, the infiltrating fluid in OM+Mineral columns is not being stored in the organic layer as readily and is being transmitted to the underlying wettable material through wettable pore networks, which in turn, develop less fully than in OM+Impermeable Boundary columns. In organic material replicates, ETH shows the least amount of preferential wetting (variability between sensors #1 and #2) in the organic layer and WAT and AES exhibit similar variability between sensors. This provides direct evidence of the dynamic development of wettable pore networks and feedbacks that can cause certain zones to wet up more easily and transmit or store fluid while others remain less wettable (Beatty and Smith, 2013) until later time, even in homogenized materials. While much of the discussion on changes in contact angle and fractional wettability have been centred around movement in infiltration behaviours, moisture content slopes also provide a record of these dynamic processes and further work is warranted.

Approximately 1.3 cm of infiltration corresponds to the first observations of a wetting front perturbation touching the impermeable boundary in both WAT experiments. In one WAT replicate, rates increase over the first ~1.3 cm of infiltration, at which point rates begin to decrease. The other WAT replicate shows more complex behaviour with increasing rates occurring initially and reaching a relative maxima at ~0.7cm of cumulative infiltration, which are then followed by a gradual decrease in rate with time to ~1.35 cm of infiltration. Non-visible wetting front perturbations within the interior of the column may be contributing to this rate behaviour. In contrast, ETH infiltration rates decrease over the entire duration of the experiments with the steepest decreases observed in the first 0.2 cm of infiltration.

The AES experiments reflect earlier observations in OM+Mineral columns, showing the quickest response overall, with increasing rates over the first 0.8 cm and 0.2 cm of cumulative infiltration, which are then followed by decreases in rate over the remainder of the test. Given the agreement between tests, this 0.2-0.8 cm interval over which variable behaviours are observed in non-wetting fluid test scenarios may be expressing inherent variability or heterogeneity caused by slight differences in packing and the arrangement of water repellent particles between columns. Most notable, however, in the AES column are the amplification of behaviours observed in the less wettable (WAT) experiments. Increasing rates with time are indicators of contact angle change in all experiments since negative pressures were maintained throughout the repellent organic layer (and in the absence of mechanical shifts in pressure). That rates increase initially in the AES material indicate that the MED solution used in AES experiments does not act as a fully wetting liquid and is able to immediately wet up only a portion of the overall medium. The quicker AES experiments, while approaching values more likely found in an analogous fully wettable scenario still do not elicit a truly wetting behaviour since it exhibited increasing rates initially and therefore is exhibiting (dynamic) fractional wettability.

One would be justified in assuming a lower K_{unsat} as a consequence of smaller accessible assemblage of pores in AES replicates compared to WAT replicates as defined by the fluid-dependent effective pressures. The moisture content data, however, indicate that the operational pore space in WAT and AES experiments is similar. Only a ~5% increase in moisture content was observed in AES experiments after the pressure shift from -4 cm applied to -1.9 cm applied, which would generate positive pressures and saturated conditions in the bottom 1 cm of material. Therefore, it can be said that only a small portion of the organic pore space ‘comes online’ over the -8.5 cm (effective) to -4 cm (effective) pressure interval. In contrast, the mechanical shift in pressure applied in ETH experiments generates a much larger (23%) difference in operational pore space as observed through moisture contents at the end of tests vs. at the pre-shift applied (-4 cm) pressure.

Fluid properties are acting in AES tests to slow things down (compared to water in a wettable medium with the same physical properties), yet actually accelerate rates compared to water infiltration This generates much faster and primarily wettable response (after the 0.2-0.8 interval) in the AES impermeable columns by knocking down much of the repellency (though not all) while filling up a larger portion of pores compared to WAT that contribute to larger unsaturated hydraulic conductivities across the bulk medium. This reveals a couple things. First, fully wettable, unsaturated flow using water in physically similar materials would be at least as fast as shown in AES experiments. While still not a static reference point for unsaturated flow in these systems, approaches such as this do inform on the relative influence of repellency during unsaturated infiltration. Second, it also facilitates the observation of key fractions of the medium that are resistant to wetting. Infiltration in AES experiments beyond the 2 cm cumulative infiltration mark (i.e. the point at which only negligible infiltration is observed in WAT experiments which has a -4 cm applied tension) also indicates that entrapped air in the bulk medium would not significantly interfere with the filling of pores at -8.5 cm tension. As a comparison, even after 6 days of infiltration in WAT experiments, there is still a volume of pore space in the homogenized material that does not wet up with prolonged exposure to water.

The volumetric moisture content versus applied pressure (cm) at the infiltrometer disc data shown in Figure 5.6 is from the end of test data for the short organic material only (OM + impermeable boundary) columns experiments shown in Figure 5.5 plus the two additional WAT experiments that employed additional tensions than the -4 cm applied tension used throughout WAT-1 and WAT-2 experiments. It is apparent in the -4 cm data that WAT and AES wet the OM to similar moisture contents of about 64% while ETH only reaches 50% moisture content. Recall that it is hypothesised herein that ETH and AES both wet OM more quickly and more completely than WAT. However, Figure 5.6 indicates WAT and AES wet OM to the same moisture content and ETH has a lower value. These relationships are further evaluated by applying the scaling relation given by interface exerting the applied pressure for fluids of differing interfacial tension as listed in Table 5.1. The resultant scaled plot of volumetric moisture content versus effective pressure (cm) is shown in Figure 5.7.

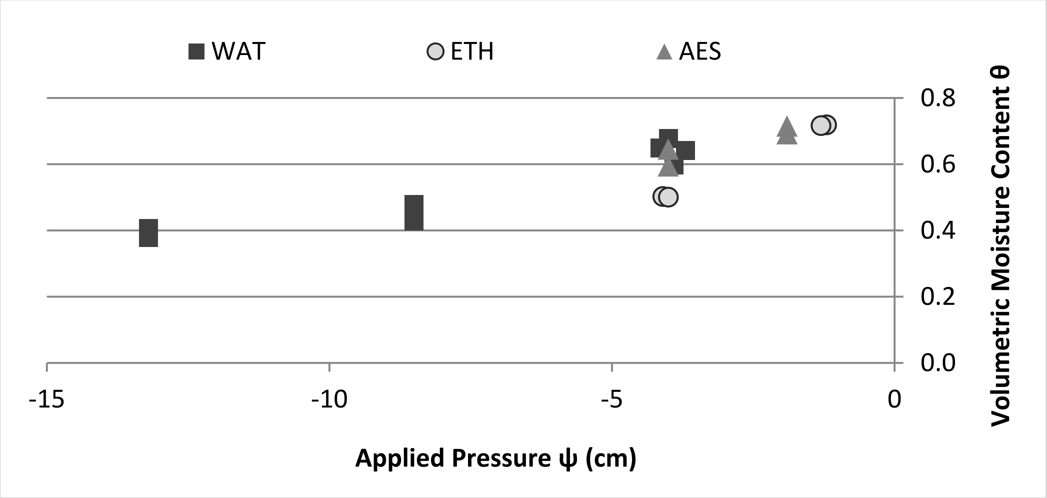

Figure 5.6 Impermeable column organic material volumetric moisture content versus applied pressure (cm) at the infiltrometer disc

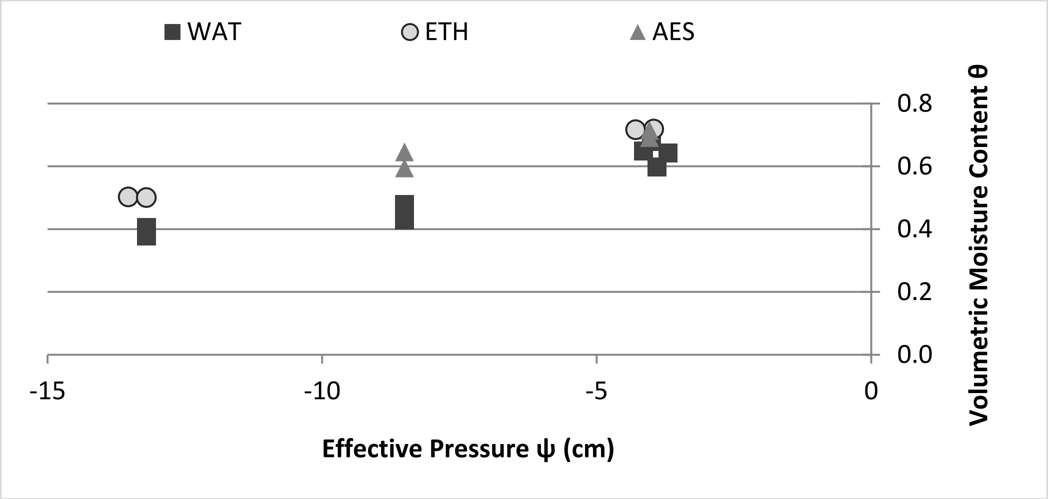

Figure 5.7 Impermeable column organic material volumetric moisture content versus effective pressure (cm) calculated using Equation 5.5 and listed in Table 5.1.

Figure 5.7 shows that for pore assemblages over the same size range ETH and AES fill more pores than WAT. For example at -13.2 cm effective pressure which for a perfectly wetted porous media fills "pores" of effective size 0.22 mm and smaller, ETH has a volumetric moisture content of 0.50 while WAT (applied and effective -13.2) has a volumetric moisture content of only 0.4. Assigning dynamic repellency as the primary cause leads to the conclusion that WAT is not filling about 20% of the pore spaces smaller than 0.22 mm, i.e., 20% of the pores smaller than 0.22 remain repellent to water under these conditions which included about 6 days duration of exposure to water in the WAT case. For AES and Wat at -8.2 cm effective pressure which for a perfectly wetted porous media fills "pores" of effective size 0.35 mm and smaller, AES has a volumetric moisture content of 0.62 while WAT (applied and effective -8.2) has a volumetric moisture content of only 0.45. That would be approximately 27% of the pores smaller than 0.35 mm effective size remaining repellent. Following this argument under these conditions, there is a larger proportion of pores expressing persistent repellency to water in the effective size range between 0.22 mm and 0.35 mm than pores smaller than 0.22 mm.

For ETH, AES and WAT at -4 cm effective pressure which for a perfectly wetted porous media fills "pores" of effective size 0.74 mm and smaller, ETH has a volumetric moisture content of 0.72 while AES has a similar volumetric moisture content of 0.70 and WAT (applied and effective -4) has a volumetric moisture content of only 0.64. That would be approximately 10% of the pores smaller than 0.74 mm effective size remaining repellent. At -4 cm effective pressure and corresponding pore size of 0.74 mm and smaller there is weak expression of ETH wetting better than AES which is significantly more wettable than WAT. This is consistent with the hypothesis that the 25% AES acts as an intermediate wetting fluid during drop tests and is not wetting all surfaces as effectively at ETH. This intermediate behaviour of AES in conjunction with tension infiltrometer shows promise for further studies on fractional wettability versus pore size assemblages.

5.4 Conclusions

Complimentary data sets that serve to isolate or target certain mechanisms are necessary for investigations in dynamic water repellent media. In this case, a systematic laboratory evaluation of water (WAT), ethanol (ETH), and an MED-derived aqueous ethanol solution (AES) of 25% ethanol by volume were used to generate greater insight into the nature of infiltration in dynamically repellent and fractionally wettable natural soil materials under -4 cm applied tension. WAT and AES solutions were used to preserve repellency and observe dynamics in varying amounts. ETH was used to effectively instantaneously eliminate repellency and dynamic behaviours.

Similar relational outcomes as those observed in the field were anticipated. In air-dried hydrophilic materials, the infiltration rate relationship trend of WAT > AES > ETH for non-wetting materials as observed in the presence of antecedent moisture content in the field was maintained and could be well defined by fluid properties alone. For the hydrophilic materials tested here, this relationship appears to be a stable one, with or without slow down effects caused by mixing of alcohols and water at the solute front. In contrast, the reverse relationship (of WAT < AES < ETH), as observed in the field, was not generated. This came as a consequence of slightly higher applied pressures than applied in the field and resultant effects on moisture contents and associated K_{unsat} in homogenized repellent materials, most notably in the case of ETH infiltrations.

The laboratory work reveals that only slight increases in the applied tension (to maintain negative pressures throughout repellent materials) can elicit complex infiltration behaviours driven largely by the activated or activate-able pore network. An applied -4 cm pressure head (vs. -2 cm) activates an operational pore space in ETH experiments equivalent to an effective tension of -13.2 cm for water wet conditions. Infiltration in these materials is substantially affected by the assemblage of pores over the -8.5 cm and -13.2 cm interval, even when wettable test fluids are applied. As a consequence, this generated similar overall infiltration rates between WAT and ETH infiltration test cases by slowing down ETH infiltration considerably.

Fluid properties, wettability, and the porous matrix all act in concert and can generate variability and difficult-to-explain non-uniqueness in infiltration responses. Attention should therefore be paid to the relationship between contact angle, pore sizes *and* applied pressures so specific insight can be expressed relative to the activated pore assemblage in any given experimental schema and resultant differences in the magnitude of rates can be compared and analysed in combination with wetting/non-wetting infiltration behaviours. Different surface tension fluids may be one approach to developing greater understanding of the expression of dynamic soil water repellency in different pore assemblages and resultant effects on K_{unsat} over a wider range of applied and effective tensions.

While clear characterization and quantification of the role of repellency is difficult in systems with non-uniqueness, comparison between infiltration behaviours and moisture contents provided useful relational information. In the wettable column configurations, WAT generated the highest moisture contents. In non-wettable column configurations, the AES solution elicited the highest moisture contents, even when a smaller operational pore space was activated (via relatively stronger (more negative) effective tension). Since AES accelerates contact angle changes in the repellent materials, it can be deduced that differences between final moisture contents of the WAT experiments and AES experiments reveals how much of the medium is remaining persistently repellent and the durations required to wet up the most persistent fractions found in the medium. While only one AES solution was used here, the sensitivity of the repellent layer to different test fluid situations indicates that using different ethanol solutions at varying effective pressures could be used further to discern which fractions of the medium are expressing resistance to contact angle change and consequently warrants further studies.

Acknowledgements

We would like to acknowledge the financial support of the Ontario Research Fund (PI: Dr. Beth Parker, University of Guelph), the Ontario Graduate Scholarship program (R. Edward Munn Award), and NSERC Discovery Grant program. This work was facilitated through the support of the Timmins, ON fire office and Chad St. Amant at Tembec Inc. Special thanks to Nicole Galambos, Joel Lagasy, and Tony Rachwalski for their assistance in data sharing, photos and knowledge transfer. We would also like to thank Jennie Kirby for her invaluable technical assistance in the lab.

References

Agriculture and Agri-Food Canada. 1986. [online] Soils of Gogama area Ontario. 1:250,000. Land Resource Research Institute, Agriculture Canada, Ottawa, Ontario. http://sis.agr.gc.ca/cansis/publications/surveys/on/on59/index.html (accessed 18.01.14).

Agriculture and Agri-Food Canada. 1978. [online] Soils of Timmins-Noranda-Rouyn area Ontario. Soil Survey Report no. 46. 1:250,000. Ottawa, Department of Energy, Mines and Resources. http://sis.agr.gc.ca/cansis/publications/surveys/on/on46/index.html (accessed 15.07.13).

Aelamanesh, P., M.R. Mosaddeghi, A.A. Mahoubi, B. Ahrens and A.A.S. Sinegani. 2014. Water repellency in calcareous soils under different land uses in western Iran. Pedosphere 24:378-390.

Bauters, T.W.J., T.S. Steenhuis, D.A. DiCarlo, J.L. Nieber, L.W. Dekker, C.J. Ritsema, J.-. Parlange and R. Haverkamp. 2000. Physics of water repellent soils. J. Hydrol. 231-232:233-243.

Bear, J. 1972. Dynamics of fluids in porous media. Dover Publications, Inc., New York.

Beatty, S.M. and J.E. Smith. 2014. Infiltration of water and ethanol solutions in water repellent post wildfire soils. J. Hydrol. 514:233-248.

Beatty, S.M. and J.E. Smith. 2013. Dynamic soil water repellency and infiltration in post-wildfire soils. Geoderma 192:160-172.

Beatty, S.M. and J.E. Smith. 2010. Fractional wettability and contact angle dynamics in burned water repellent soils. J. Hydrol. 391:97-108.

Bisdom, E.B.A., Dekker, L.W., Schoute, J.F.T., 1993. Water repellency of sieve fractions from sandy soils and relationships with organic material and soil structure. Geoderma 56, 105–118.

Buczko, U., O. Bens and R.F. Hüttl. 2006. Water infiltration and hydrophobicity in forest soils of a pine–beech transformation chronosequence. Journal of Hydrology 331:383-395.

Clothier, B.E., I. Vogeler and G.N. Magesan. 2000. The breakdown of water repellency and solute transport through a hydrophobic soil. J. Hydrol. 231-232:255-264.

Dekker, L.W. and C.J. Ritsema. 1994. How water moves in a water repellent sandy soil 1. Potential and actual water repellency. Water Resour. Res. 30:2507-2517.

Dekker, L.W., C.J. Ritsema, K. Oostindie, D. Moore and J.G. Wesseling. 2009. Methods for determining soil water repellency on field-moist samples. Water Resour. Res. 45, W00D33. http://dx.doi.org/10.1029/2008WR007070.

Diamantopoulos, E., W. Durner, A. Reszkowska and J. Bachmann. 2013. Effect of soil water repellency on soil hydraulic properties estimated under dynamic conditions. J. Hydrol. 486:175-186.

Diamantopoulos, E. and W. Durner. 2013. Physically-based model of soil hydraulic properties accounting for variable contact angle and its effect on hysteresis. Adv. Water Resour. 59:169-180.

Diehl, D. 2013. Soil water repellency: Dynamics of heterogeneous surfaces. Colloids Surf. Physicochem. Eng. Aspects 432:8-18.

Doerr, S.H. and A.D. Thomas. 2000. The role of soil moisture in controlling water repellency: New evidence from forest soils in Portugal. J. Hydrol. 231-232:134-147.

Doerr, S.H., Woods, S.W., Martin, D.A., Casimiro, M., 2009. Natural background soil water repellency in conifer forests of the north-western USA: its prediction and relationship to wildfire occurrence. J. Hydrol. 371, 12–21.

Feng, G.L., J. Letey and L. Wu. 2001. Water ponding depths affect temporal infiltration rates in a water-repellent sand. Soil Sci. Soc. Am. J. 65:315-320.

Feng, G., J. Letey and L. Wu. 2002. The influence of two surfactants on infiltration into a water-repellent soil. Soil Sci. Soc. Am. J. 66:361-367.

Gillespie, J.E., C.J. Acton and D.W. Hoffman. 1981. Soils of the Gogama map sheet, (41P) Ontario, report no. 59. [online]. Ontario Institute of Pedology, Guelph, Ontario. http://sis.agr.gc.ca/cansis/publications/surveys/on/on59/index.html (accessed 18.01.14).

Graber, E.R., S. Tagger and R. Wallach. 2007. Do surface active substances from water repellent soils aid wetting? Eur. J. Soil Sci. 58:1393-1399.

Hallin, I., P. Douglas, S.H. Doerr and R. Bryant. 2013. The role of drop volume and number on soil water repellency determination. Soil Sci. Soc. Am. J. 77:1732-1743.

Hardie, M.A., S. Lisson, R.B. Doyle and W.E. Cotching. 2013. Evaluation of rapid approaches for determining the soil water retention function and saturated hydraulic conductivity in a hydrologically complex soil. Soil Tillage Res. 130:99-108.

Imeson, A.C., J.M. Verstraten, E.J. van Mulligen and J. Sevink. 1992. The effects of fire and water repellency on infiltration and runoff under mediterranean type forest. Catena 19:345-361.

Jarvis, N., A. Etana and F. Stagnitti. 2008. Water repellency, near-saturated infiltration and preferential solute transport in a macroporous clay soil. Geoderma 143:223-230.

Jeyakumar, P., K. Mueller, M. Deurer, C. van den Dijssel, K. Mason, G. Le Mire and B. Clothier. 2014. A novel approach to quantify the impact of soil water repellency on run-off and solute loss. Geoderma 221:121-130.

Lamparter, A., J. Bachmann, M. Deurer and S.K. Woche. 2010. Applicability of ethanol for measuring intrinsic hydraulic properties of sand with various water repellency levels. Vadose Zone J. 9:445-450.

Leighton-Boyce, G., S.H. Doerr, R.A. Shakesby and R.P.D. Walsh. 2007. Quantifying the impact of soil water repellency on overland flow generation and erosion: A new approach using rainfall simulation and wetting agent on *in situ* soil. Hydrol. Process. 21:2337-2345.

Letey, J., M.L.K. Carrillo and X.P. Pang. 2000. Approaches to characterize the degree of water repellency. J. Hydrol. 231-232:61-65.

Leverett, M.A. 1941. Capillary behaviour in porous solids. Trans. of the AIME. 142: 159–172.

Lichner, L., P.D. Hallett, Z. Drongová, H. Czachor, L. Kovacik, J. Mataix-Solera and M. Homolák. 2013. Algae influence the hydrophysical parameters of a sandy soil. Catena 108:58-68.

Meteorological Service of Canada. 2015-02-11. [online] Timmins Victor Power A. Canadian Climate Normals 1971-2000 Station Data. <http://climate.weather.gc.ca/climate_normals> (accessed 20.05.15).

Ministry of Northern Development. 2005. Northern Ontario Engineering Geology Terrain Study (NOEGTS) – Polygons. [Shapefile geospatial data]. Scholars GeoPortal. Last updated, 2005.

Moody, J.A., Shakesby, R.A., Robichaud, P.R., Cannon, S.H., Martin, D.A., 2013. Current research issues related to post-wildfire runoff and erosion processes. Earth-Sci. Rev. 122, 10–37.

Moody, J.A., D.A. Kinner and X. Úbeda. 2009. Linking hydraulic properties of fire-affected soils to infiltration and water repellency. J. Hydrol. 379:291-303.

Nyman, P., Sheridan, G. J., Smith, H. G., Lane, P. N. J. 2014. Modeling the effects of surface storage, macropore flow and water repellency on infiltration after wildfire. Journal of Hydrology, 513(MAY), 301–313. doi:10.1016/j.jhydrol.2014.02.044

O'Carroll, D.M., L.M. Abriola, C.A. Polityka, S.A. Bradford and A.H. Demond. 2005. Prediction of two-phase capillary pressure-saturation relationships in fractional wettability systems. J. Contam. Hydrol. 77:247-270.

Oostindie, K., L.W. Dekker, J.G. Wesseling, C.J. Ritsema and V. Geissen. 2013. Development of actual water repellency in a grass-covered dune sand during a dehydration experiment. Geoderma 204:23-30.

Reszkowska, A., J. Bachmann, A. Lamparter, E. Diamantopoulos and W. Durner. 2014. The effect of temperature-induced soil water repellency on transient capillary pressure-water content relations during capillary rise. Eur. J. Soil Sci. 65:369-376.

Roy, J.L. and W.B. McGill. 2002. Assessing soil water repellency using the molarity of ethanol droplet (med) test. Soil Sci. 167:83-97.

Soil Measurement Systems (SMS). 2006. Tension Infiltrometer user manual. [online] Available: http://www.soilmeasurement.com/tension_infil.html. (Accessed: May, 2009).

Taumer, K., H. Stoffregen and G. Wessolek. 2005. Determination of repellency distribution using soil organic matter and water content. Geoderma 125:107-115.

Vogelmann, E.S., J.M. Reichert, J. Prevedello, C.O.B. Consensa, A.É. Oliveira, G.O. Awe and J. Mataix-Solera. 2013. Threshold water content beyond which hydrophobic soils become hydrophilic: The role of soil texture and organic matter content. Geoderma 209–210:177-187.

Wallach, R. and E.R. Graber. 2007. Infiltration into effluent irrigation-induced repellent soils and the dependence of repellency on ambient relative humidity. Hydrol. Process. 21:2346-2355.

Wang, Z., L. Wu and Wu, Q.J. 2000. Water-entry value as an alternative indicator of soil water-repellency and wettability. J. Hydrol. 231-232:76-83.

CHAPTER 6 - CONCLUSIONS AND CONTRIBUTIONS

6.1 Conclusions and contributions

In most soils, fractional wettability and how proportions of a porous medium change over time due to contact angle dynamics is rarely measured or discussed. In the pursuit of enhanced understanding and greater quantification of these fundamental drivers of infiltration in soils, this dissertation reports on a number of new conceptual, measurement and analysis approaches and observations generated through these new approaches. Conclusions from this investigation follow.

We conclude that the complex interplay between the relative fractions of wettable and non-wettable materials and how those proportions shift over time with dynamic contact angles is the fundamental nature of these systems. This conceptual framework was developed through a series of small column (4.5 cm diameter) laboratory experiments using tension infiltrometers which maintained a negative pressure through water repellent materials to remove the competing mechanism of flow caused by positive pore pressures or internal ponding. This work was the first to show how in non-wetting materials, contact angle dynamics and wettability act prior to other capillary controls during infiltration and that gravity is a primary driver at the onset of an infiltration event in non-wettable media relative to steep hydraulic gradients which are used to described monotonic infiltration rate behaviours in hydrophilic media. In the presence of contact angle dynamics and fractional wettability, a range of increasing and decreasing infiltration rates can be observed over the course of infiltration depending on which mechanisms are most activated. The new conceptual models presented in this work provide a mechanistic explanation of various drivers (hydraulic gradients, unsaturated hydraulic conductivities, capillarity, gravity) at various points in time in the presence of fractional wettability and contact angle dynamics, and provide a robust and flexible framework for understanding infiltration and moisture contents in dynamic systems. Further, we emphasise the mechanistic limitations of describing infiltration in non-wettable media using static and /or hydrophilic assumptions and draw caution to measurement techniques that rely on these assumptions in media expressing fractional wettability and contact angle dynamics.

While at this time there is limited practicality of using benchtop X-ray tomography (μXCT) to track moving interfaces caused by changes in fractional wettability and contact angles, proof of concept images generated further insight into dynamic soil water repellency through the filling and observation of different pore assemblages and particle structures in five post-wildfire soils. Low phase contrast, scanning artefacts, subresolvable features, and imperfect registration between wet and dry scans impeded quantitative analysis. However, substantial structural information, which facilitated qualitative analysis, was available through this approach. Halfway Lake Provincial Park (Brown) materials, which were evaluated in Chapter 2, showed quicker wetting at the pore scale (<2 hrs) under the application of small positive pressures than when observed in small laboratory column experiments under tension. No qualitatively discernable differences between these ‘quicker-to-wet-up’ materials and hydrophilic wetting could be observed within 3D scans generated through μXCT, in large part because of the relatively long duration of data capture in a benchtop scanning environment. However, in ‘longer-to-wet-up’ post wildfire materials, these scans are the first proof of concept evidence to show that at a given moisture content, changes in wettability cause a local shift in the size of physical pores occurred by water versus the air. This was best shown in the pore scale movement of water from larger pores and along column walls into smaller pores when a small volume of ethanol was added to a predominantly repellent sample already containing water. That is, ethanol changed the nature of filled pores within the column, by increasing entrapped air, draining pores through redistribution, and enhancing sorption into previously persistently non-wettable materials.

Field investigations of soil water repellency often generate robust characterizations of repellency in field materials typically in the form of drop penetration testing, but such data are rarely, if ever directly related to larger scale hydrologic processes and/or characterizations of fractional wettability and contact angle dynamics. Here, using data captured using tension infiltrometers filled with water, ethanol, and aqueous ethanol mixtures, a number of new measurement and analysis approaches were developed that relate MED/WDPT data, dynamic soil water repellency, and hydrologic process. For water infiltration, we modified the Time to First Bubble (TFB) method developed by Lewis and Robichaud (2006) to Time to First Five Bubbles (TFFB). The TFFB method uses a similar volume of water applied in water drop penetration time tests, is less sensitive to the initial condition of the tension infiltrometer (than TFB), and can be compared directly to early time and late time infiltration rate behaviours using the tension disk infiltrometer. Molarity of Ethanol Drop (MED) – derived aqueous ethanol solutions provided additional insights into the nature of infiltration in dynamically repellent soils (and MED as a classification tool) by showing responses intermediate between water and ethanol and threshold infiltration responses. These solutions provided additional trend information in fluid behaviours in a new analysis method which compared early- vs. late-time slopes of cumulative infiltration versus time (for water, aqueous solution, and ethanol). This analysis provided robust characterization of intra/inter-material and cross site comparisons in five different materials expressing variable spatial and temporal repellency characteristics. Additional analysis using averaged late time infiltration rates with water, ethanol, and MED-derived aqueous solutions further enhanced characterizations of long duration repellency and differences in fractional wettability. While ethanol is becoming more commonly used in repellency investigations and in measures such as Repellency Index (RI), this work is also the first reported consideration of what we term as the ‘sludge effect’ or a slowdown of the wetting front of ethanol in the presence of antecedent moisture content in the field due to the highly nonlinear combined effects of concentration-dependent viscosities and densities on fluid mobilities.

During investigations of infiltration in water repellent media, it is advantageous to maintain tension (negative pressures) in repellent soils to exclude the mechanism of internal ponding and associated positive pore water pressures or pushing water as a non-wetting fluid into repellent pore spaces. This facilitates the observance of changing wettability through associated changes in infiltration rate behaviours which, as a mechanism, can be masked by flow driven by positive pore water pressures. This however, can be challenging in the presence of large pore spaces where even relatively weak tensions can de-activate a significant portion of the bulk matrix. Fluid properties, wettability, and applied pressures work in concert to generate complex behaviours in water repellent media.

This work developed moisture content – pore water pressure head relationships and insights into infiltration behaviours in the field materials investigated and reported in Chapter 4 over a range of slightly higher applied tensions than used in the field. The tension disc infiltrometer method was used to maintain constant pressures within short 3cm deep laboratory columns with impermeable sides and bottom to generate moisture content pressure head data points for water, AES, and ethanol. The comparison of the measured moisture content data to applied pressures and effective pressures scaled by the interfacial tensions showed that even after multiple days of contact time a proportion of the material remained repellent to water whereas the AES and ethanol wetted the material more quickly and to higher moisture contents. This approach holds promise for further studies evaluating dynamic wettability. For example, results showed there was a larger proportion of pores expressing persistent repellency in the effective size range between 0.22 mm and 0.35 mm than in pores smaller than 0.22 mm. This type of data can better inform continuum based models which require scaling the storage properties through manipulation of the moisture characteristics curves, or given sufficient data, through a table lookup method.

While consideration of effective pore sizes relative to fluids of differing interfacial tensions is relatively easy to incorporate through scaling capillary pressures, this approach is more problematic in media with larger pore sizes as was the case for the homogenized duff used here. The large pore spaces in these hydrophobic materials were especially sensitive to small changes in applied tensions, which was most visible during ethanol infiltration. For example, applying -1.3 cm pressure to achieve a desired effective pressure of -4 cm can generate positive pressures in short (3 cm) columns which induces an undesirable positive pore liquid pressure condition in the lower section of the column. Conversely, applying -4 cm pressure generates an effective pressure of -13.2 cm which deactivated a portion of the overall medium and resulted in a significant reduction of Kunsat for ethanol. We therefore conclude that air entry values are an important consideration when using ethanol in water repellency investigations, particularly for comparisons to water infiltration as would be the case in Repellency Index (RI) calculations in materials such as this. Notably, however, MED-derived aqueous solutions were much more robust as a comparative measure in these materials. Increasing wettability through lowered contact angles accelerated infiltration rate and less sensitivity to pore assemblage effects provided the most reliable comparison to water based infiltration responses. This basic approach, particularly in conjunction with μXCT imaging, holds promise for evaluating dynamic repellency by pore size fraction. Future work with additional fluids and a range of materials could generate a comprehensive data set for testing and validation of scaled hydraulic functions and flow/infiltration models.

There is considerable literature that applies wettable soils theory and associated parameters to repellent soils. An example of this is presented in Chapter 4 wherein sorptivity and saturated hydraulic conductivity are calculated following the methods presented by Moody et al. (2009). Such approaches have been used “successfully” in weakly repellent soils with apparently short duration dynamic changes. In this dissertation, it is concluded the use S and Kf values for hydrologic simulations of repellent soils using standard hydrologic models is not recommended and not well justified. Specifically, the infiltration theory for wettable soils does not include any consideration for dynamic contact angles, i.e. changing repellency with time. A large proportion of physically impossible negative values of S (46.7% for water; 38.8% for all fluids) and Kf (33.3% for water; 34.7% for all fluids) found in this work demonstrates the questionable and limited utility of this approach. Furthermore, any positive values of S (53.3% for water; 61.2% for all fluids) and Kf (6.7% for water; 22.4% for all fluids) calculated and reported in Table 5.2 are subject to errors caused by the primary role changing repellency plays over time. That is, the sensitivity of wettable infiltration theory methods to dynamic repellency is not known and a first order process related to dynamic wettability is lacking.

APPENDIX A – GENERAL HYPOTHESIS OF WETTING IN THE PRESENCE OF DYNAMIC SOIL WATER REPELLENCY

The following description of water infiltration applies to wetting in fractionally wettable and dynamically repellent soils. In this context, it may be useful to think of fractional wettability as the spatial heterogeneity of repellency on solid surfaces at and below the pore scale and contact angle dynamics as the time dependent repellency where the wettability of soil surfaces change over time. Here, these ideas/concepts are discussed and explained in the context of pore scale wetting processes during an infiltration event. On the macroscopic-scale of a representative elementary volume (REV), the material is homogeneous with material properties of varying volumetric water contents, soil water pressure, and unsaturated hydraulic conductivities. The nature of and limitations of macroscopic values relative to common usage in wettable soils will be highlighted. Note that while this conceptual description is presented here at small scales, it links to and is up-scalable above the REV and has direct implications for catchment-scale wetting, draining, and retention processes.

In fractionally wettable porous media some of the particles or particle surfaces exhibit a resistance to wetting, and others exhibit a more wettable characteristic. However, fundamental hydrologic processes still govern flow during an infiltration event. The additional condition of dynamic soil water repellency affects the timing, activation and relative importance of particular hydraulic parameters during infiltration. During an infiltration event, in the presence of fractional wettability and contact angle dynamics, capillary forces, gravity, and hydraulic conductivity become activated in different ways and at different times than is commonly conceptualized. This has meaningful implications on infiltration and moisture contents.

For example, during an infiltration event in fully wettable systems, capillarity is a primary driver of infiltration at the outset of an infiltration event. Pores fill preferentially according to pore water pressures in the pores, with smaller spaces having lower (more negative) relative water pressures, which elicit steeper capillary gradients and preferentially fills smaller pore spaces by capillarity. These fluid / material interactions result in infiltration rates that drops monotonically over time as hydraulic gradients decrease exponentially and gravity becomes the primary driver of infiltration as the infiltration front moves deeper into the soil.

In contrast, fractionally wettable (spatially heterogeneous) and dynamically changing (temporally dependent) systems, fractional wettability and contact angle dynamics establish different mechanistic conditions that can be observed throughout an infiltration event. So much so, that the role of capillarity switches according to the wettability of a particular surface or pore. When pores are wettable, capillarity is a primary driver of infiltration. When pores exhibit substantially reduced or repellent wettability, gravity is the primary driver with capillarity acting to resist infiltration and hydraulic gradients are only tenuously related to pore sizes. These conditions result in complex infiltration behaviours that include both increasing and decreasing infiltration rates over time. This can occur at any time throughout an infiltration event and changes can be rapid or slow. Wetting processes and pore network development in such a system is conceptualized in Figure A.1.

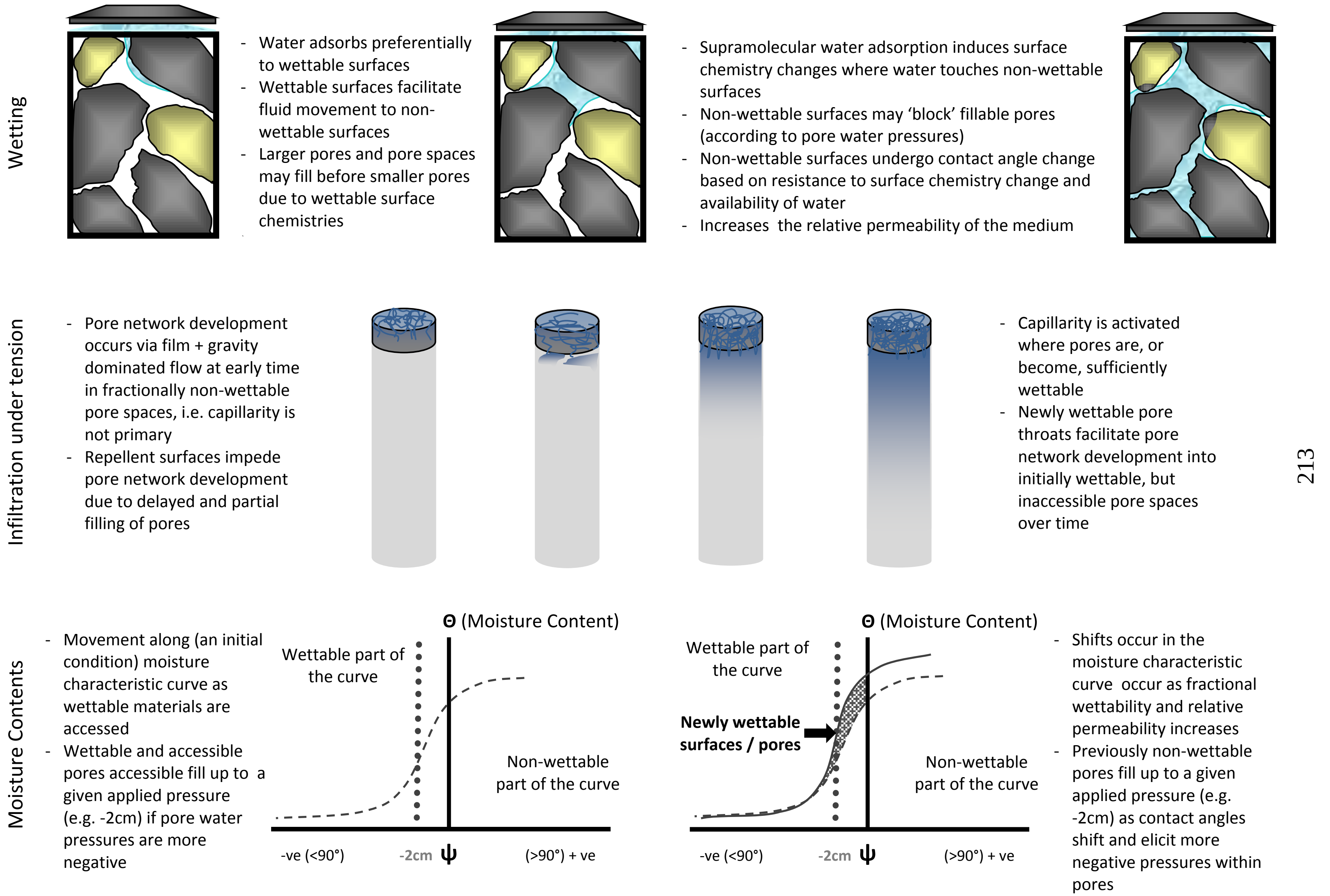

- Water adsorbs preferentially to wettable surfaces
- Wettable surfaces facilitate fluid movement to non-wettable surfaces
- Larger pores and pore spaces may fill before smaller pores due to wettable surface chemistries

- Supramolecular water adsorption induces surface chemistry changes where water touches non-wettable surfaces
- Non-wettable surfaces may ‘block’ fillable pores (according to pore water pressures)
- Non-wettable surfaces undergo contact angle change based on resistance to surface chemistry change and availability of water
- Increases the relative permeability of the medium

- Pore network development occurs via film + gravity dominated flow at early time in fractionally non-wettable pore spaces, i.e. capillarity is not primary
- Repellent surfaces impede pore network development due to delayed and partial filling of pores

- Capillarity is activated where pores are, or become, sufficiently wettable
- Newly wettable pore throats facilitate pore network development into initially wettable, but inaccessible pore spaces over time

- Movement along (an initial condition) moisture characteristic curve as wettable materials are accessed
- Wettable and accessible pores accessible fill up to a given applied pressure (e.g. -2cm) if pore water pressures are more negative

- Shifts occur in the moisture characteristic curve occur as fractional wettability and relative permeability increases
- Previously non-wettable pores fill up to a given applied pressure (e.g. -2cm) as contact angles shift and elicit more negative pressures within pores

Figure A.1 – General hypothesis of wetting in the presence of dynamic soil water repellency